C.D.I. Report No. 06-27

Stress Analysis of the Hope Creek Unit 1 Steam Dryer at EPU Conditions Using 1/8th Scale Model Pressure Measurement Data

Revision 2

Prepared by

Continuum Dynamics, Inc.
34 Lexington Avenue
Ewing, NJ 08618

Prepared under Purchase Order No. 4500366543 for

Nuclear Business Unit, PSEG Nuclear LLC
Materials Center, Alloway Creek Neck Road
Hancocks Bridge, NJ 08038

Approved by

Alan J. Bilanin

Reviewed by

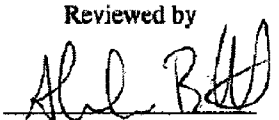

Alexander H. Boschitsch

February 2007

Executive Summary

In this analysis, stresses induced by the flow of steam through the steam dryer at Hope Creek Unit 1 are calculated and evaluated using 1/8th scale pressure measurement data at Extended Power Uprate (EPU) nominal frequency conditions and with frequencies scaled both up and down by up to 10%. EPU is 115% of Current Licensed Thermal Power (CLTP). The fluctuating pressure loads induced by the flowing steam were predicted by a separate acoustic circuit analysis of the steam dome and main steam lines [1]. These loads were then applied to the steam dryer structure for 2 seconds at 115% CLTP conditions and the resulting stresses calculated by performing a time history structural dynamics analysis using the commercial finite element model, ANSYS 10.0. Rev 1

Assessment of the stress results for compliance with the ASME B&PV Code, Section III, subsection NG, was carried out for the load combination corresponding to normal operation (the Level A Service Condition). This combination consists of the fluctuating pressure loads and weight. The evaluation is done for both maximum (peak) and alternating (fatigue type) stresses. Level B service conditions, which include seismic loads, are not included in this evaluation.

The results show that on the basis of these 1/8th scale pressure measurements at 115% CLTP conditions the minimum stress ratio (allowable stress divided by the computed stress with appropriate adjustments made for stress type and weld factors) is 1.53, which corresponds to a peak stress and occurs at the welded junction of the thin closure plate and inner hood. A virtually identical peak stress ratio, SR-P = 1.54, is also found on the weld where the skirt joins the upper support ring. The minimum stress ratio associated with alternating stresses is 1.96 and occurs at the bottom of the drain channel where it joins the skirt. All stress ratios are greater than unity and so do not exceed the allowables. Rev 1

The EPU load conditions with the frequencies scaled by ±2.5%, ±5%, ±7.5% and ±10% are also examined. The minimum stress ratio encountered for any of these frequency shift is 1.33, is due to alternating stress and occurs at the +10% frequency shift on the weld between the reinforcement strip and middle hood near the end plate. This stress ratio indicates that all stresses, both peak and alternating, are within allowable levels at all frequency shifts considered. The smallest stress ratio identified with a peak stress is 1.46 and occurs at the +2.5% frequency shift on the weld where the skirt joins the upper support ring. Stress ratios for specific locations on the steam dryer are tabulated in the report in Table 7. It is emphasized that no additional adjustments associated with modeling uncertainty, correlations with plant data and uncertainty in measurements are reflected in these stress ratios. Rev 1

The data shows that the minimum alternating stress ratio, SR-a=1.33 is clearly an outlier and occurs only at one weld location and only at the +10% frequency shift. If the -10% to +7.5% range of frequency shifts is considered then the minimum alternating stress ratio increases to SR-a=1.62 so that the overall minimum stress ratio is now associated with a peak stress, SR-P=1.46.

This analysis includes all Hope Creek Unit 1 dryer modifications done prior to commercial operations and accounts for the proposed power uprate, 115% CLTP. To evaluate additional Rev 1

dryer modifications and/or power uprates, the stresses should be recomputed using appropriately modified structural models to account for steam dryer modifications, and main steam line strain gage measurements taken during power uprate and processed by a separate acoustic circuit analysis. Rev 1

Revision Summary

Revision 0 provided the stress reports for the HCGS steam dryer which used the loads predicted by the 1/8th scale model test. Revision 0 indicated that the stress ratios at EPU conditions had, in some cases, low margins. Subsequently, Tech Evaluation 80090626, dated October 7, 2006, submitted to the NRC, demonstrated that there was significant conservatism in the load predicted by the 1/8th scale model test (SMT). This conservatism was primarily shown by benchmarking at CLTP the SMT load against the plant data load. In addition, it was apparent that the 1/8th SMT was prematurely predicting the onset of SRV acoustic resonance since it predicted onset well below 90% CLTP whereas plant data and the 1/5th SMT (CDI 05-31) showed that SRV onset was not present at CLTP. Rev 1

Continuum Dynamics, Inc. (C.D.I.) performed additional benchmarking efforts which showed that the loads used for CLTP and EPU in Revision 0 were actually 115% and 133% of CLTP, respectively (Appendix B). Because of this effort, the finite element analyses prepared from SMT data are revised as follows: Rev 2

- The nominal frequency analysis in Revision 0 labeled "CLTP" is representative of 116% CLTP. Since it is slightly above the proposed power uprate, 115% CLTP, it is retained in Revision 1 but it is relabeled "115% CLTP". No changes were required to the text/tables/figures for this analysis other than changing "CLTP" to "115% CLTP".

- The analysis for the nominal frequency analysis in Revision 0 labeled as "EPU" was representative of 133% CLTP. It is replaced by 'worst case' results for 115% CLTP which, at any given node, are the highest stresses and lowest stress ratios encountered for 115% CLTP at any of the frequency shifts considered.

- The frequency variation (+/-10%) analyses in Revision 0 was representative of 133% CLTP. It is replaced with similar analyses in Revision 1 for the loading calculated for 115% CLTP. Rev 1

Subsequent to Revision 0, confirmation was found on a back-weld reinforcement done to the welds between the middle and inner hoods to their respective end plates prior to plant commercial operation. The details and impact of the added, back-welds are discussed in Appendix A. It results in a significant reduction in the stresses at that weld joint.

As a result of the above, the discussions in the Executive Summary and Conclusion sections reflect the new stress ratios. In addition, they discuss separately the stress ratio (SR) for the peak stress (SR-P) and the SR for alternating stress (SR-a).

The discussion in Section 4.4 was expanded to include full penetration welds. The previous discussion was focused on fillet welds.

New and revised paragraphs are shown by a revision bar to the side of the revised text. However, a revision bar is not used when the only change is "CLTP" to "115% CLTP".

Table of Contents

1. Introduction and Purpose

Recent inspections of the steam dryers in Mark I plants have shown cracks in the fillet welds and nearby structures. The industry has addressed this problem with physical modifications to the dryers, as well as a program to define steam dryer loads and their resulting stresses. Hope Creek Unit 1 (HC1) is part of this program and the purpose of the stress analysis discussed here is to calculate the peak and alternating stresses generated during EPU conditions and determine whether these stresses are within the acceptance criteria dictated by the ASME Code. This step establishes whether the modifications done prior to commercial operations are adequate for sustaining structural integrity and preventing future weld cracking under planned (EPU) operating conditions. Rev 1

The damaging steam dryer loads are due to pressure fluctuations, induced by steam flow through the dryer. Over a long period of time, cyclic stresses from these loads can produce fatigue cracking if loads are sufficiently high. Since fillet welds are the structural features most susceptible to fatigue failure, most of the failures have been found in these areas.

The fluctuating pressure loads, induced by the flowing steam, were previously predicted by a separate acoustic circuit analysis of the steam dome and main steam lines [1]. In the present analysis, these loads are applied to the steam dryer structure and the resulting stresses are calculated using a finite element model (the ANSYS 10.0 computer code). The loads are applied to the structure at 1.422×10^{-3} sec intervals for 2.0 sec (1405 time steps), and the equations representing the structural dynamics solved using time history dynamic analysis.

One way to evaluate the sensitivity of the stress results to modeling approximations and perturbations in the applied loading is to perturb the frequencies in the applied load history and determine whether this produces significant changes in the structural response. In the context of the transient simulations performed here, this frequency scaling is easily effected and is tantamount to modifying the time step (a 10% reduction in the time step corresponds to a 10% increase of all frequencies). Thus, eight additional cases are considered here where the dryer structural model is subjected to the same EPU load history, but with the frequency altered by: ±2.5%, ±5%, ±7.5% and ±10%. Results are reported for the ±10% shifts as well as the non-shifted case. In addition, worst case results obtained by recording the highest stress encountered at any frequency shift, are presented. Rev 1

The load combination considered here corresponds to normal operation (the Level A Service Condition) and consists almost entirely of the fluctuating pressure loads and weight. The resulting stresses are examined for compliance with the ASME B&PV Code, Section III, subsection NG. Both maximum and cyclic (fatigue type) stresses are considered in this evaluation. Level B service conditions, which include seismic, are not addressed here.

2. Model Description

A description of the ANSYS model of the HC1 steam dryer follows.

2.1 Steam Dryer Geometry

A geometry model of the HC1 steam dryer was developed from available drawings, as well as from field measurements taken by C.D.I. on an identical spare dryer for the cancelled Hope Creek Unit 2. The completed model is shown in Figure 1.

This model includes modifications made to the HC1 steam dryer on-site, prior to commercial operation. These are:

- Tie bars, outer hoods, and center end plates were replaced on the original dryer (FDI-041-79450).
- Reinforcement bars were added to the middle and inner hoods (HCI-KTI-415-7)
- Back-welding of the middle and inner hoods weld joint to their end plates (HCI-KTI-415-3 and -5)

Rev 1

The externally modified areas are shown in Figure 2. Appendix A details the back-welds.

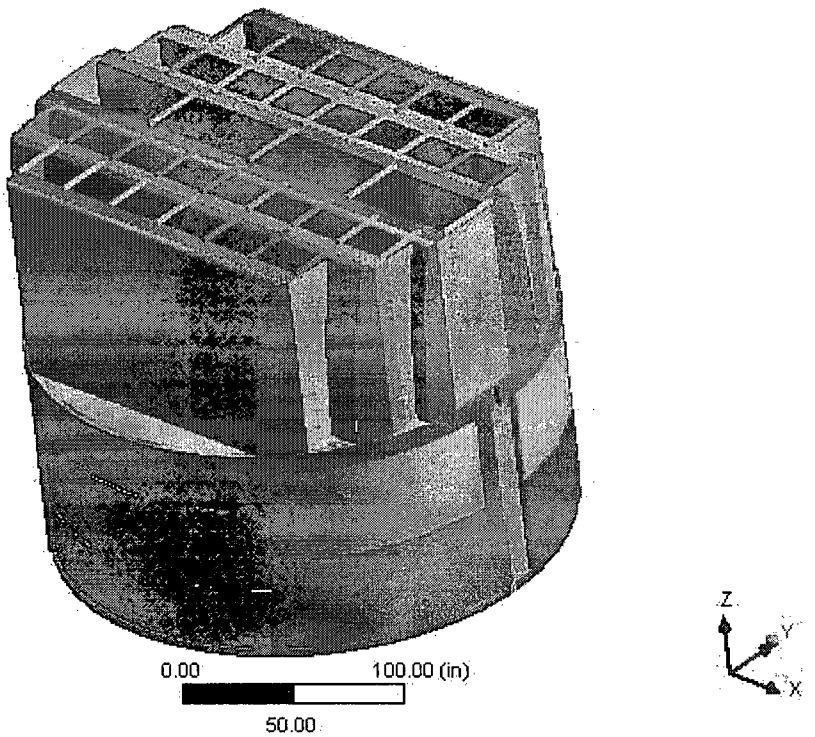

Figure 1. Overall geometry of the HC1 steam dryer model.

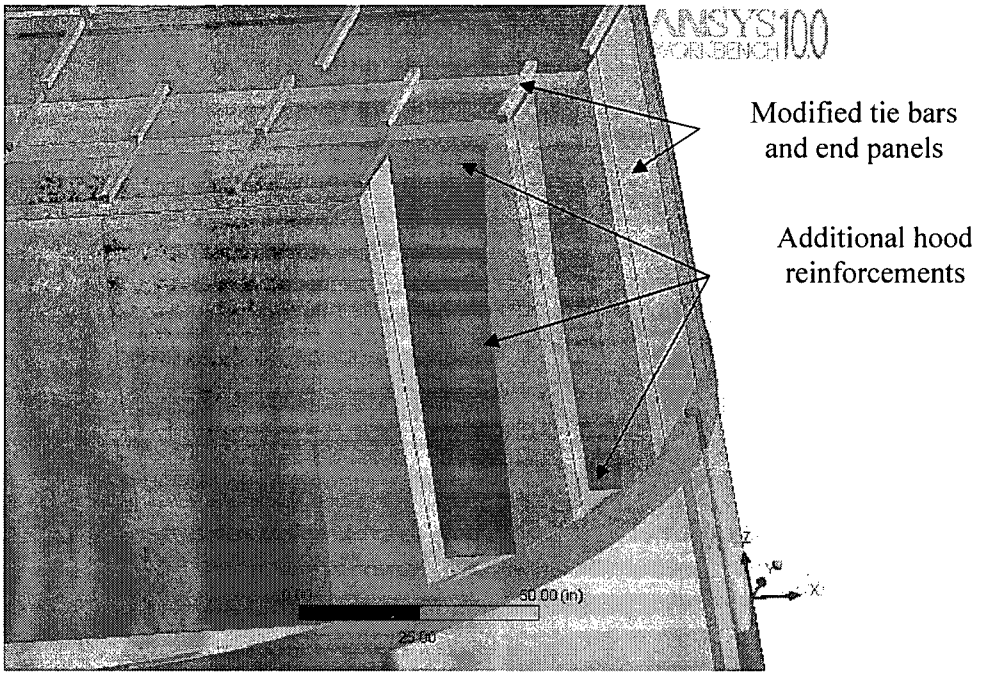

Figure 2. On-site modifications accounted for in the model.

Rev 1

2.2 Material Properties

The steam dryer is constructed from Type 304 stainless steel and has an operating temperature of 550°F. Properties used in the analysis are summarized below in Table 1.

Table 1. Material properties.

	Young's Modulus (10^6 psi)	Density (lbm/in^3)	Poisson Ratio
Structural Steel	25.55	0.284	0.3
Structural Steel for Perforated Plates	15.33	0.227	0.3
Structural Steel with Added Water Inertia Effect	25.55	1.183	0.3

The structural steel modulus is taken from Appendix A of the ASME Code for Type 304 Stainless Steel at an operating temperature 550°F. The effective properties of perforated plates and submerged parts are discussed in Section 3.

2.3 Pressure Loading

The transient loads are produced by the unsteady pressures acting on the exposed surfaces of steam dryer. The pressure time history loading was obtained from an acoustic circuit model of the HC1 steam dryer, performed by C.D.I. using data obtained from a 1/8th scale rig and detailed in [1]. This loading was provided over the steam dryer surface on a three-inch grid, at a total of 10,963 locations. The time interval spanned the 2.0 sec of data during which the pressure ranges (i.e., the maximum pressure minus the minimum pressure during the 2 sec. interval) summed over the nodes of a low-resolution grid of the dryer (including only corners and edges, a total of 104 locations) achieved a maximum. The pressure time history is shown in Figure 3, at a location on the outer bank hood opposite the A and B main steam lines. Rev 1

These results were interpolated onto the detailed structural grid of the HC1 steam dryer, and the ANSYS calculation was then undertaken. The program was developed to properly convert the data into a format recognizable by the ANSYS software. Inspection of the resulting pressures at selected nodes shows that these pressures vary in a well-behaved manner between the nodes with prescribed pressures. Graphical depictions of the resulting pressures, comparisons between the peak pressures in the original nodal histories and those in the final surface load distributions produced in ANSYS, and comparison of the pressure histories at randomly selected nodes in the original pressure history data files and the ANSYS loading arrays, all confirm that the load data are interpolated accurately and transferred correctly to ANSYS.

The fluctuating pressure loads were applied to surfaces above the water level, as indicated in Figure 4. In addition to the fluctuating pressure load, the static loading by the weight of the steam dryer is analyzed separately. The resulting static and transient stresses are linearly combined to obtain total values which are then processed to calculate peak and alternating stress intensities for assessment in Section 5.

To evaluate the sensitivity of the stress results to approximations in the structural modeling and applied loads, the EPU loads were modified by rescaling the frequencies over the range ±10% and the stress response recomputed. In the context of the transient simulations performed here, this frequency scaling is easily effected and is tantamount to modifying the time step. The EPU load was modified by rescaling the frequencies ±2.5%, ±5%, ±7.5% and ±10%, and applied to the structure for the 2 second interval. The peak and alternating stress intensities for each rescaled frequency were then calculated and compared to identify the case producing the highest increase in stresses. Rev 1

The unsteady pressure loads applied to the dryer contain a strong 80 Hz component which has been shown to be fictitious [2]. Specifically, the signal arises from the interaction between sensors used to record the unsteady pressures. Therefore the stress ratios were calculated with the 80 Hz signal removed. For frequencies scaled up by 10%, the 88 Hz component corresponds to the 80 Hz signal in the original EPU loading and was therefore removed. Similarly, for the case with frequencies scaled down by 10% the 72 Hz component was filtered out. Due to linearity of the model, the relevant component can be removed during post-processing of the results. The power spectrum density (PSD) of the pressure loading at a location on the outer bank hood is shown on Figure 5 where the curves both with and without the 80 Hz signal are compared. The next peak about 120 Hz appears to be associated with a standpipe. The time pressure loading time histories with and without the 80 Hz component removed are compared in Figure 6. All stress results and stress ratios are obtained with the 80 Hz signal removed.

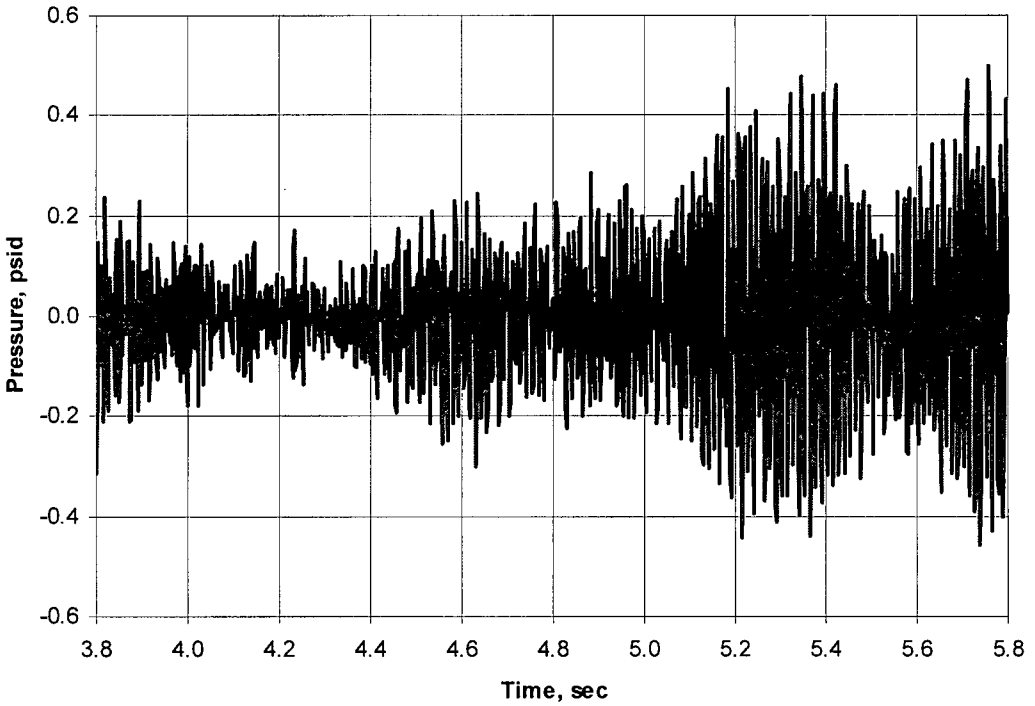

Figure 3. Pressure time history applied to the ANSYS model at the bottom of the outer hood (side MSL AB) at 115% CLTP loading.

Rev 1

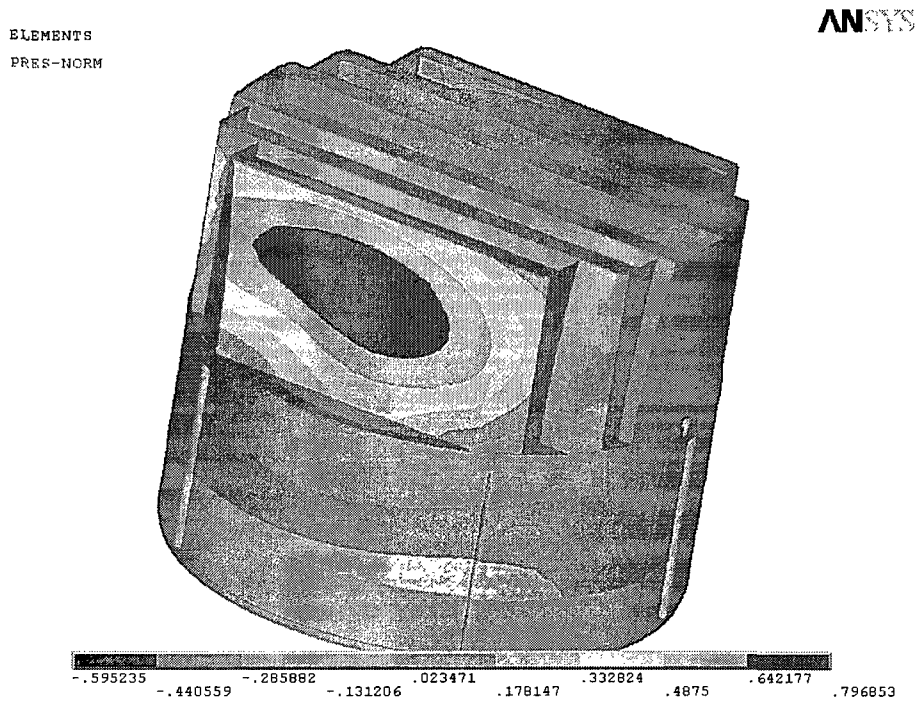

t=0.711s (500 time steps)

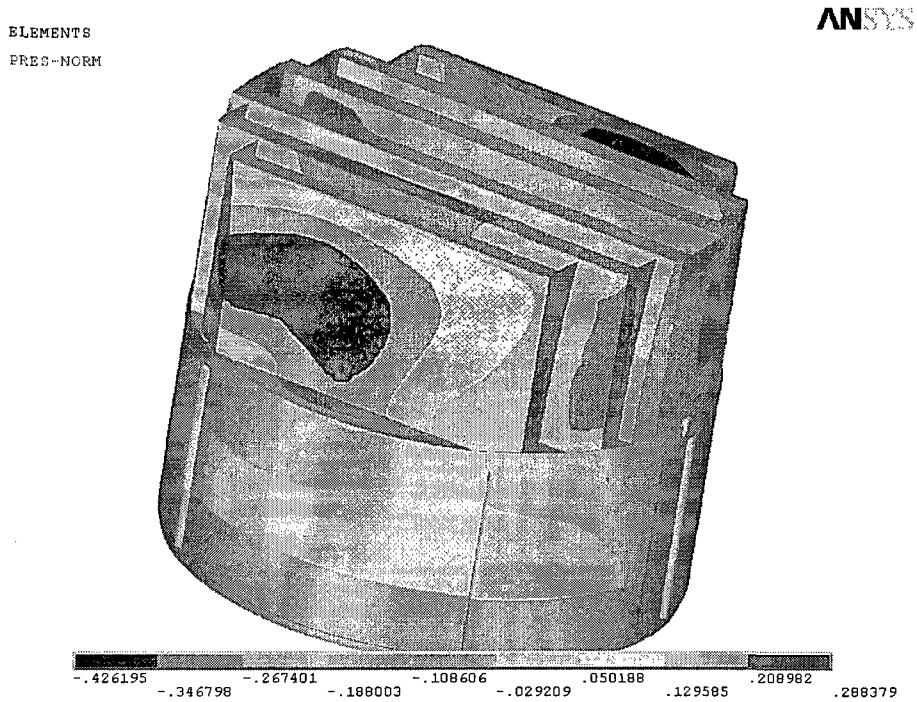

t=1.422s (1000 time steps)

Figure 4. 115% CLTP pressure loading (in psid) on the steam dryer at different time steps. No loading is applied to the submerged light blue surface. | Rev 1

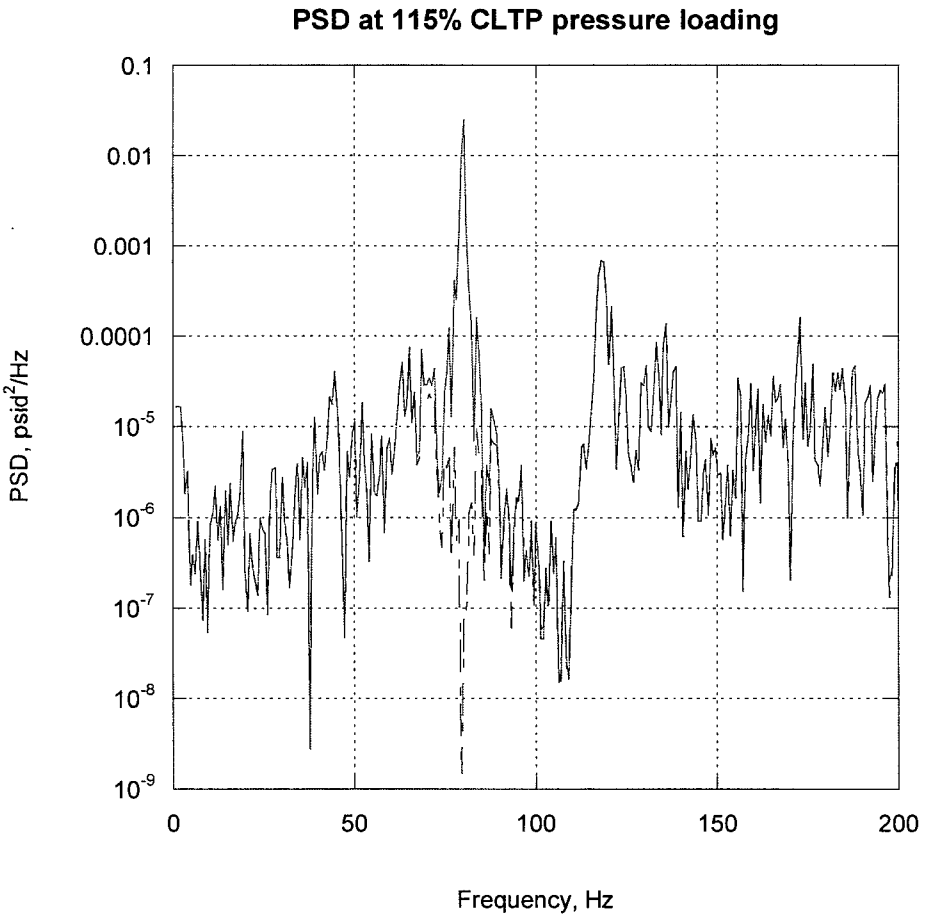

Rev 1

Figure 5. PSD of pressure loading on the outer hood. The red curve corresponds to the original pressure loading; the blue curve corresponds to the loading with the 80 Hz component removed.

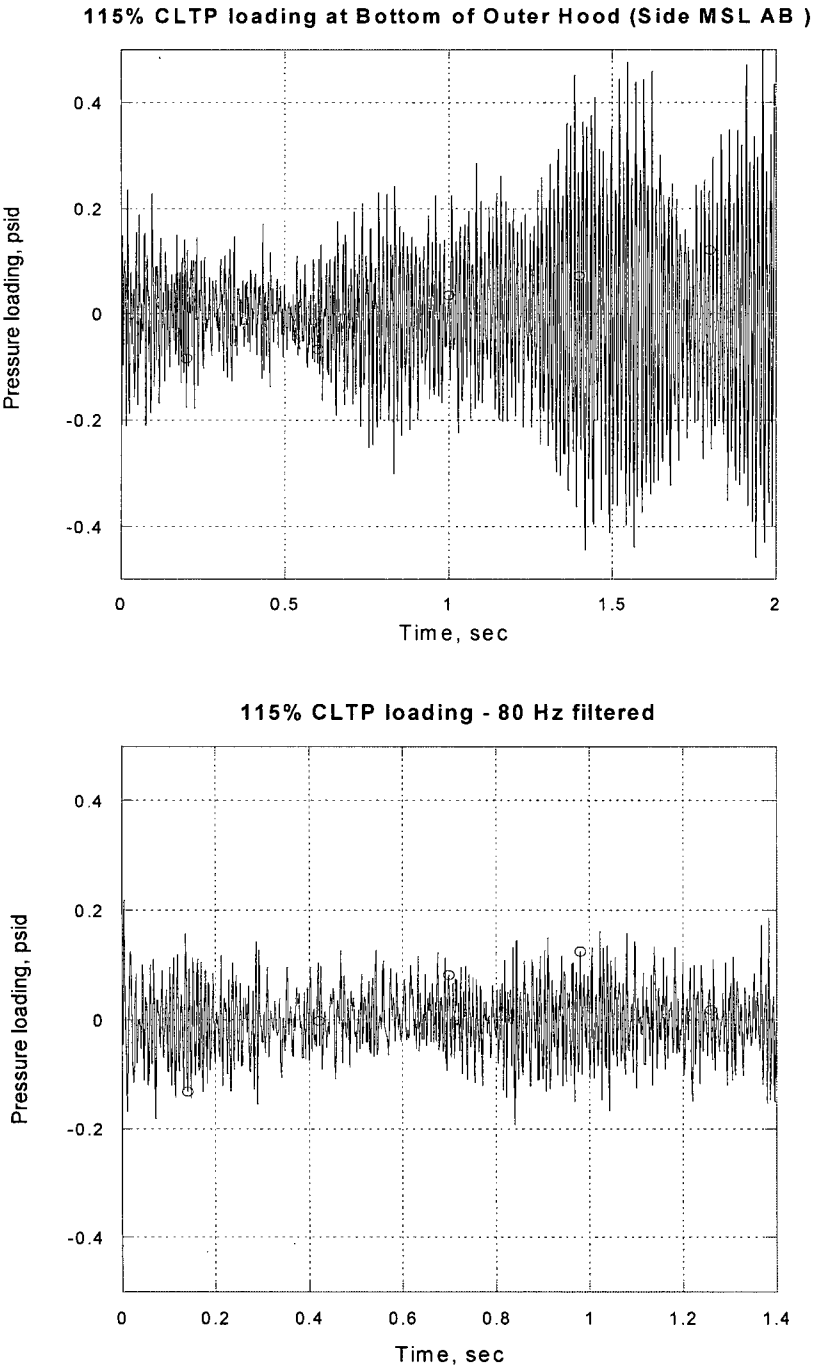

Figure 6. Comparison of the time histories at the 115% CLTP condition with and without the 80 Hz component.

Rev 1

3. Finite Element Model

The dynamics of the steam dryer were modeled using the ANSYS computer code.

3.1 Model Simplifications

The following simplifications were made in order to reduce model size while retaining key structural properties:

- Most welds were replaced by node-to-node connections; interconnected parts share the common nodes along the welds. In other locations the constraint equations between nodal degrees of freedom were introduced.

- The drying vanes were replaced by point masses, attached to the corresponding trough bottom plates and vane bank top covers (Figure 7). The bounding perforated plates, vane bank end plates, and vane bank top covers were explicitly modeled.

- The lower part of the skirt and drain channels are below the reactor water level. An analysis was used to calculate the effective mass of this water and thus account for its interaction with the structure. This added water mass was included in the ANSYS model by appropriately modifying the density of the submerged structural elements when computing transient loads.

- Fixed constraints were imposed at the underside of the steam dryer upper support ring where it makes contact with the four steam dryer support brackets that are located on the reactor vessel and spaced at 90° intervals (Figure 8). No credit was taken for the constraints from the reactor vessel lift lugs.

3.2 Perforated Plate Model

The perforated plates were modeled as solid plates with adjusted elastic and dynamic properties. Properties of the perforated plates were assigned according to the type and size of perforation. Based on [3], for an equilateral triangular pattern with given hole size and spacing the effective modulus of elasticity was found to be a factor of 0.6 times the original modulus, while the effective density was a factor of 0.8 times the original steel density. These adjusted properties were shown in Table 1.

3.3 Vane Bank Model

The vanes were modeled as point masses, located at the center of mass for each vane bank. The following approximate masses were used for the vanes, based on data found on drawings supplied by PSE&G: inner banks, 6,545 lbm; middle banks, 5,970 lbm; and outer banks, 4,685 lbm. These weights were applied to the base plates and vane top covers using the standard ANSYS point mass modeling option, element MASS21. ANSYS automatically distributes the point mass inertial loads to the nodes of the selected structure. The distribution algorithm minimizes the sum of the squares of the nodal inertial forces, while ensuring that the net forces and moments are conserved. Vane banks are not exposed to main steam lines directly, but rather shielded by the hoods. Thus, compared to the hoods, less motion is anticipated on the vane banks

so that approximating their inertial properties with equivalent point masses is justified. Nevertheless, the bounding parts, such as perforated plates, side panels, and top covers, are retained in the model.

3.4 Water Inertia Effect on Submerged Panels

Water inertia was modeled by an increase in density of the submerged structure. The added mass was found by a separate analysis to be 0.225 lbm/in^2 of submerged skirt area.

3.5 Structural Damping

Time history analysis in the ANSYS program requires that the damping be specified in terms of mass and stiffness Raleigh damping (i.e., the damping parameters, α and β, defined in Section 5.9.3 of the ANSYS 10.0 documentation). These material constants can be defined from the damping ratio over the range of frequencies examined. For the calculation presented here, a damping ratio of 1% was assumed over the range of frequencies from 10 to 150 Hz. This assumption leads to the following values used in the analysis: α=1.18 and $\beta=2\times10^{-5}$. For the calculation with +10% frequency shift, the 1% damping was assumed over the range 10 to 118 Hz (frequency where the maximum alternating stress occurred) resulting in the values: α=1.16 and $\beta=2.5\times10^{-5}$. This damping is consistent with guidance given in NUREG-1.61. Rev 1

3.6 Mesh Details and Element Types

Shell elements were employed to model the skirt, hoods, perforated plates, side and end plates, trough bottom plates, reinforcements, and cover plates. Specifically, the four-node, Shell Element 63, was selected to model most of these structural components. This element models bending and membrane stresses, but omits transverse shear. Compared to the default shell element in ANSYS, Shell Element 181, the Shell Element 63 is more sensitive to warping and requires higher resolution of curved regions. Care was taken to ensure that adequate resolution was provided on the curved hoods (one element per 15° arc). Shell Element 181 was used only for modeling submerged parts of the drain channels. This is due to less number of elements needed to adequately resolve curved regions, also, more accurate stresses are computed as considerable shear components develop in these areas. All other parts, including tie bars and the upper and lower support rings, were modeled with solid brick elements. The elements SURF154 are used to assure proper application of pressure loading to the structure. Mesh details and element types are shown in Table 2 and Table 3. Details of the finite element mesh are shown in Figure 9.

3.7 Connections between Structural Components

Most connections between parts were modeled as node-to-node connections. However, in several places, such as connections between shell and solid elements or dissimilarly meshed parts, constraint equations were used to connect adjacent structures. Basically, all such constraints express the deflection (and rotation for shell elements) of a node, $\mathbf{R}_1$, on one structural component in terms of the deflections/rotations of the corresponding point, $\mathbf{P}_2$, on the other connected component. Specifically, the element containing $\mathbf{P}_2$ is identified and the deformations at $\mathbf{P}_2$ determined by interpolation between the element nodes. Several types of connections arose in the steam dryer model including the following:

1. Shell edge to shell edge connections with dissimilar meshes.

2. Connections of shell faces to solid faces (Figure 10a). While only displacement degrees of freedom are explicitly constrained, this approach also implicitly constrains the rotational degrees of freedom when multiple shell nodes on a sufficiently dense grid are connected to the same solid face.
3. Connections of shell edges to solids (e.g., connection of the bottom of closure plates with the upper ring). Since solid elements do not have rotational degrees of freedom, the coupling approach consisted of having the shell penetrate into the solid by one shell thickness and then constraining both the embedded shell element nodes (inside the solid) and the ones located on the surface of the solid structure (see Figure 10b). Numerical tests involving simple structures showed that this approach reproduces both the deflections and stresses of the same structure modeled using only solid elements or ANSYS' bonded contact technology. Continuity of rotations and displacements is achieved as illustrated in Figure 11 in the vicinity of the junction between inlet end plate and upper support ring.
4. Connections of solid elements to shells, e.g., connections of the tie bars to the vane covers.

The use of constraint conditions rather than the bonded contacts advocated by ANSYS for connecting independently meshed structural components, confers two useful numerical advantages to the structural analysis of the steam dryer. First it results in better conditioned and smaller matrices. The smaller size results from the fact that equations and degrees of freedom are eliminated rather than augmented (in Lagrange multiplier-based methods) by additional degrees of freedom. Also, the implementation of contact elements relies on the use of very high stiffness elements (in penalty function-based implementations) or results in indefinite matrices (Lagrange multiplier implementations) with poorer convergence behavior compared to positive definite matrices. Secondly, elimination of contact elements allows ANSYS to reuse the decomposed solution matrix so that only a single (expensive) LU-decomposition is required at the start of the calculation. In subsequent steps only inexpensive back-substitutions are required to update the structural state. This results in faster simulation times than models employing contact elements which require an LU decomposition at every time step.

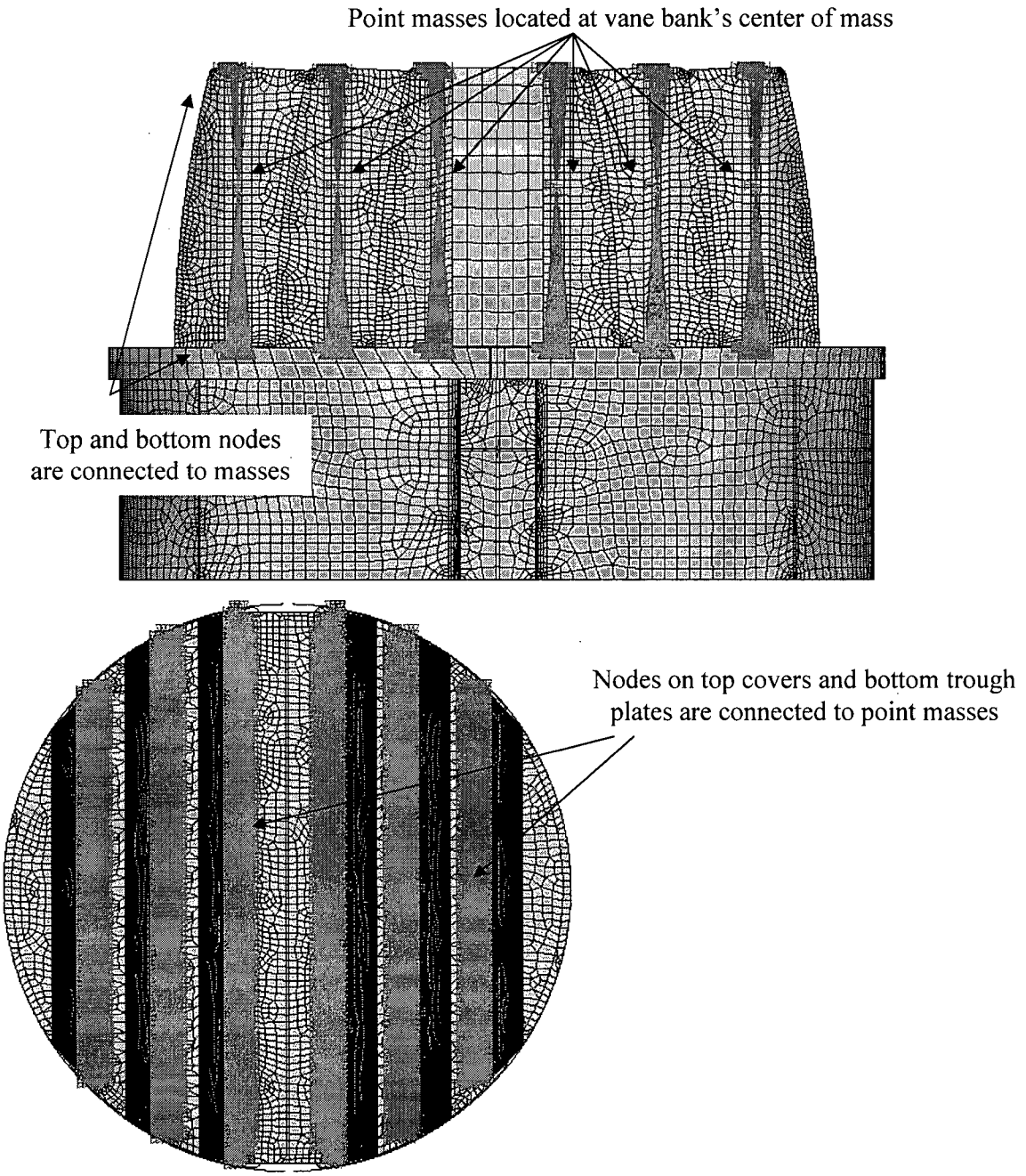

Figure 7. Point masses representing the vanes. The pink shading represents where constraint equations between nodes are applied in the point mass implementation.

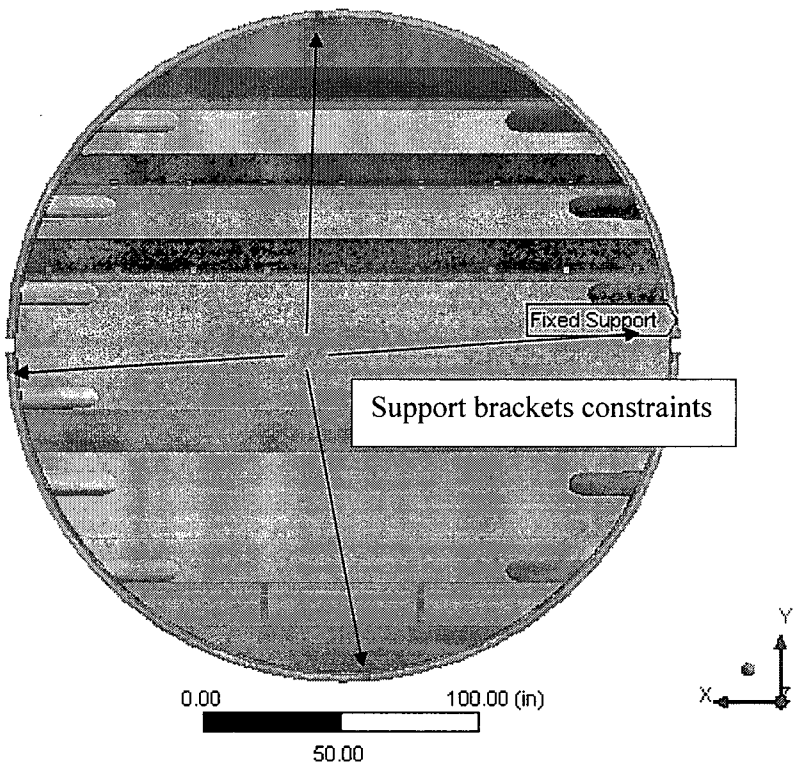

Figure 8. Fixed support constraints.

Table 2. FE Model Summary.

Description	Quantity
Total Nodes	93,951
Total Structural Elements	126,322
Element Types	5
Materials	3

Table 3. Listing of Element Types.

Generic Element Type Name	Element Name	ANSYS Name
20-Node Quadratic Hexahedron	SOLID186	20-Node Hexahedral Structural Solid
4-Node Elastic Shell	SHELL63	4-Node Elastic Shell
4-Node Linear Quadrilateral Shell	SHELL181	4-Node Finite Strain Shell
Mass Element	MASS21	Structural Mass
Pressure Surface Definition	SURF154	3D Structural Surface Effect

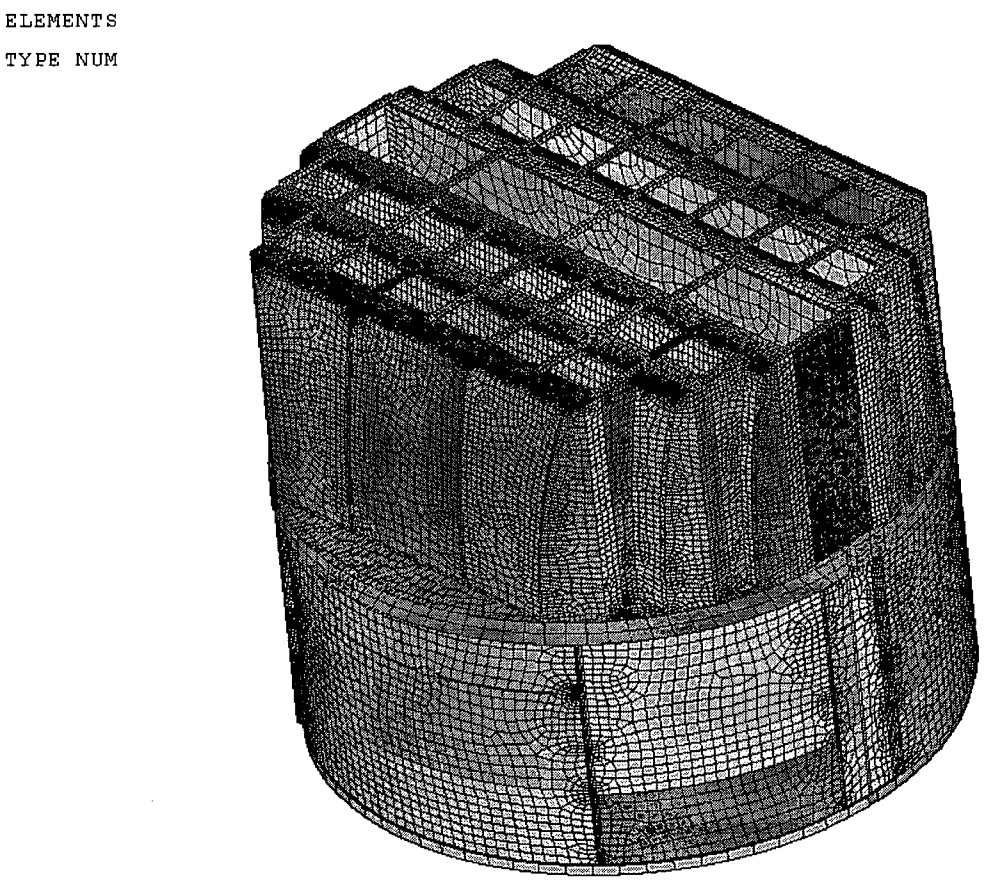

Figure 9a. Mesh overview. The colors emphasize element type.

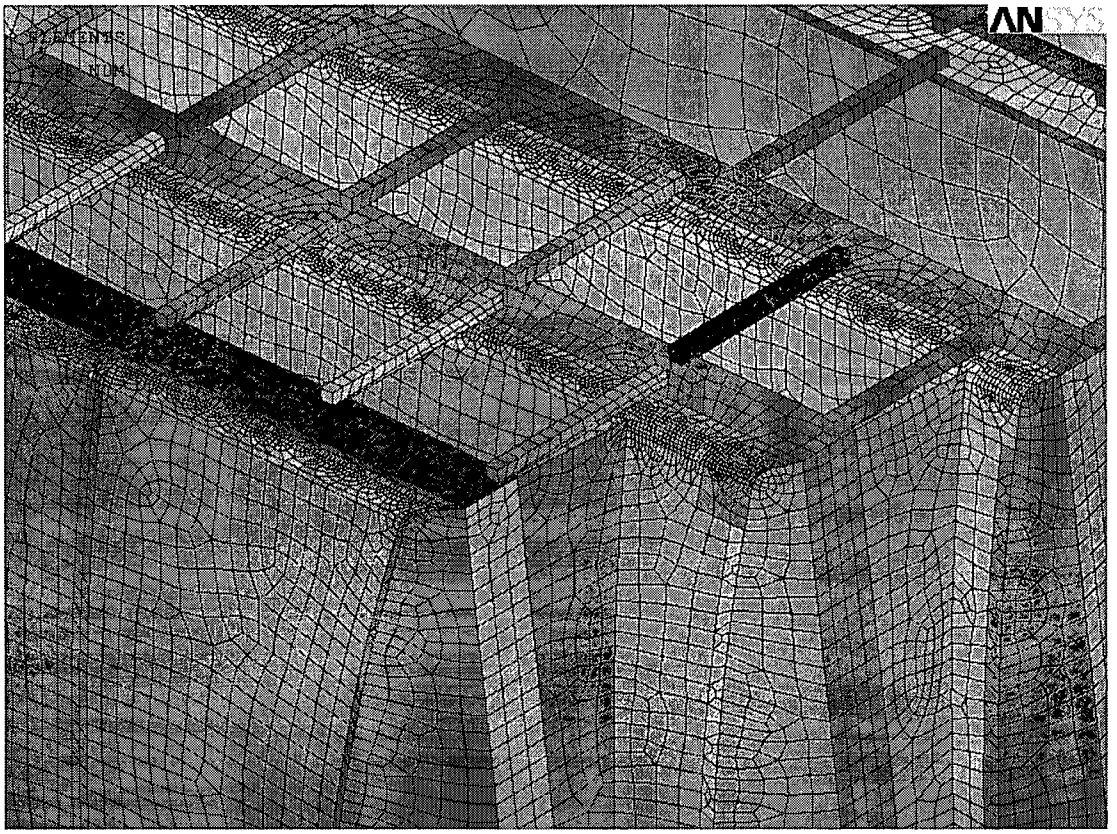

Figure 9b. Close up of mesh showing hoods, reinforcement panels, and tie bars. The colors emphasize element type.

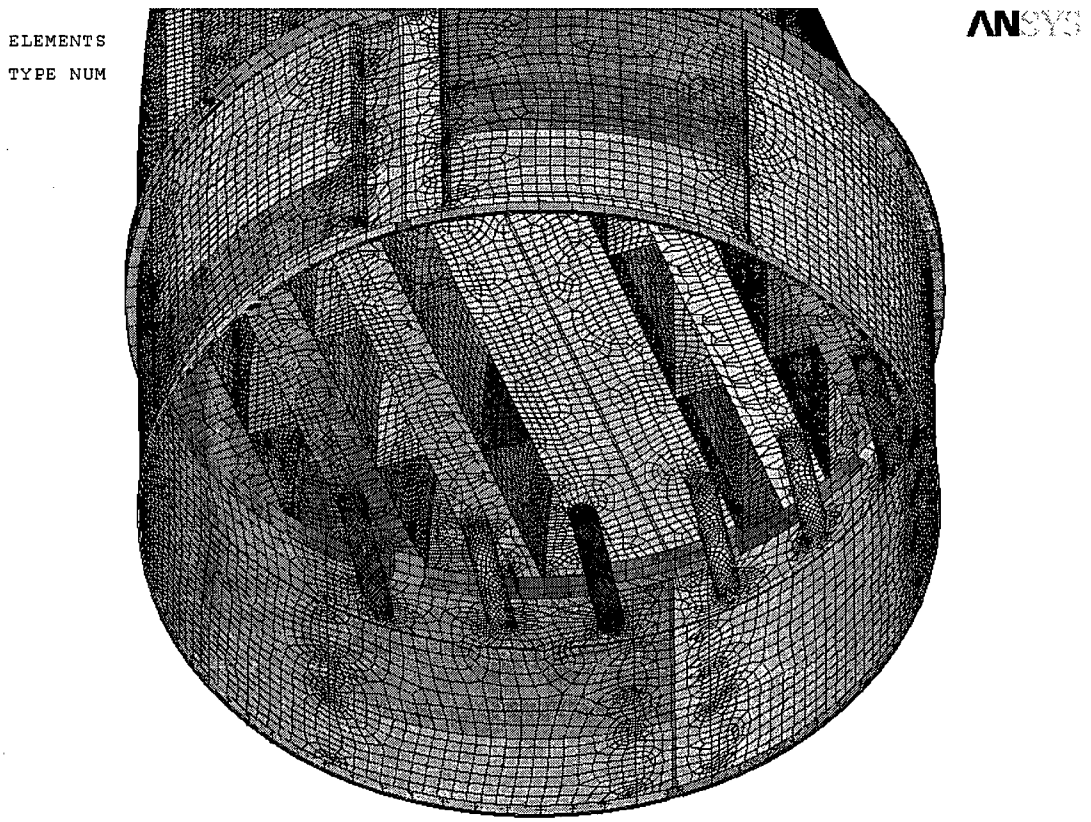

Figure 9c. Close up of mesh showing drain pipes and hood supports. The colors emphasize element type.

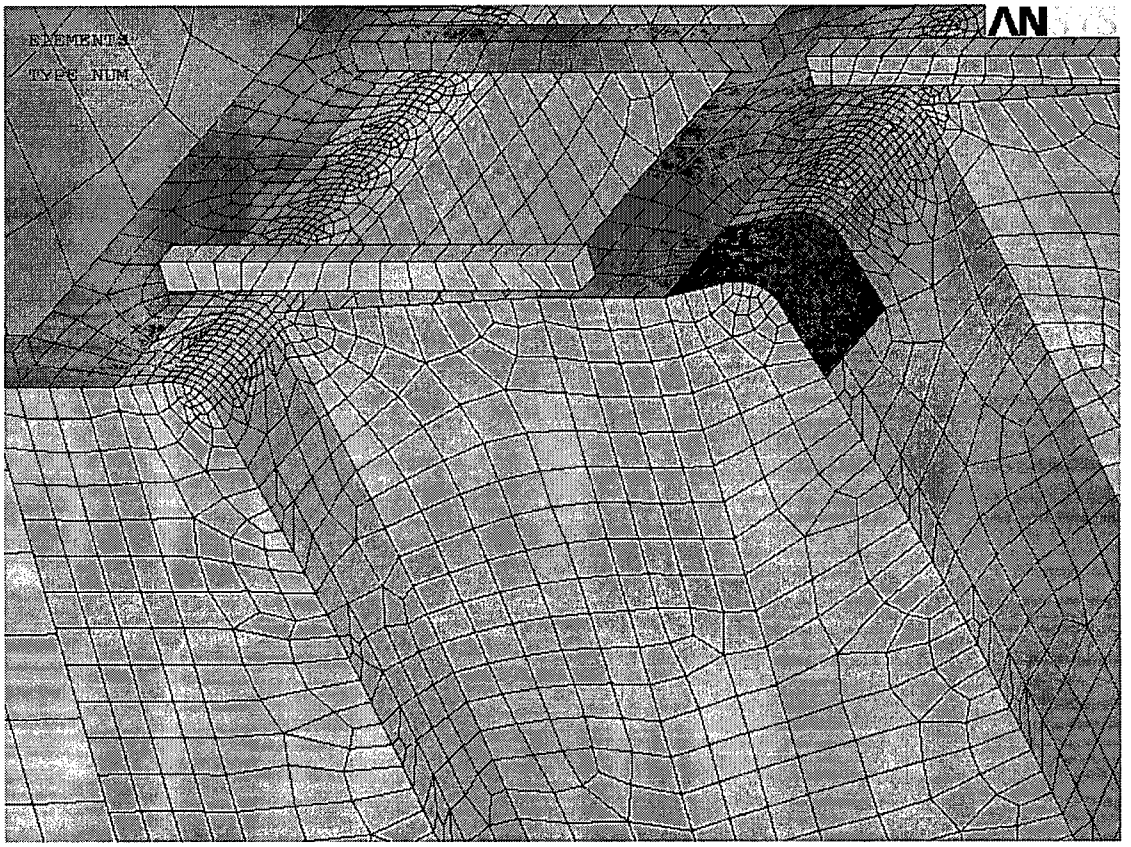

Figure 9d. Close up of mesh showing node-to-node connections between closure plates, end plates, and hoods. The colors emphasize element types.

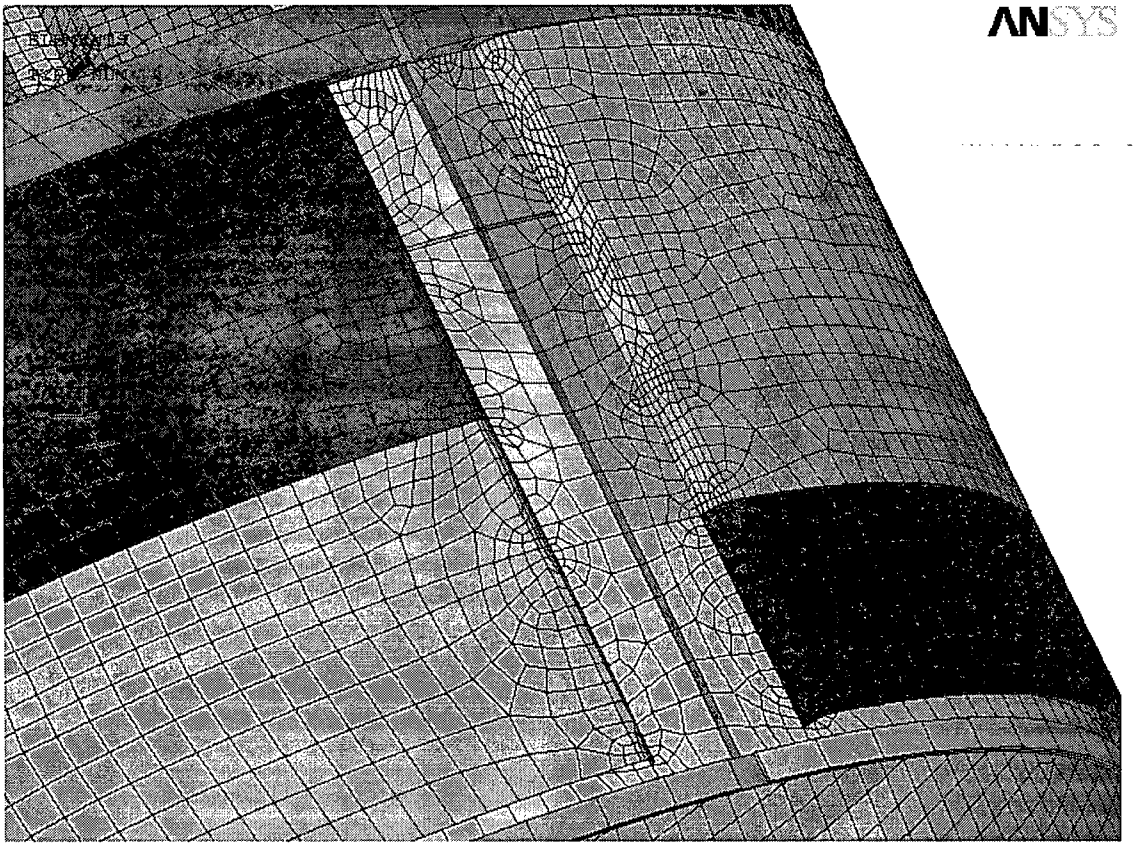

Figure 9e. Close up of mesh showing node-to-node connections between the skirt and drain channels. The colors emphasize element type.

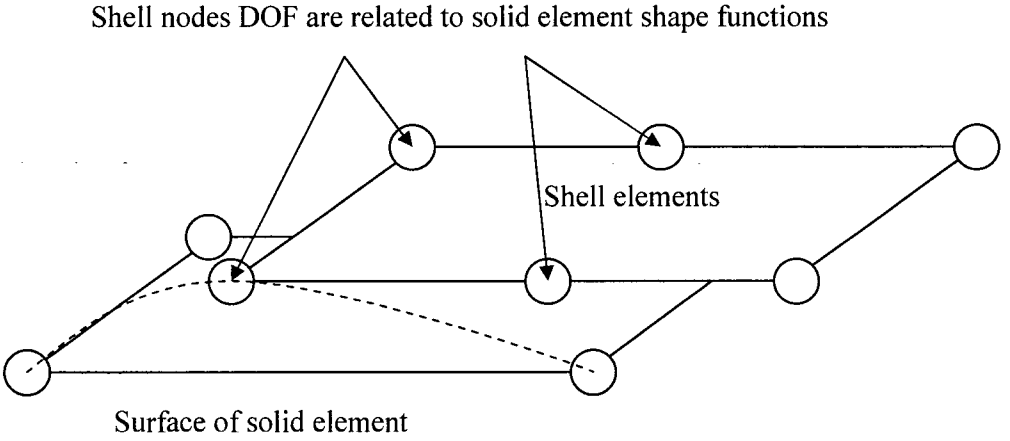

Figure 10a. Face-to-face shell to solid connection.

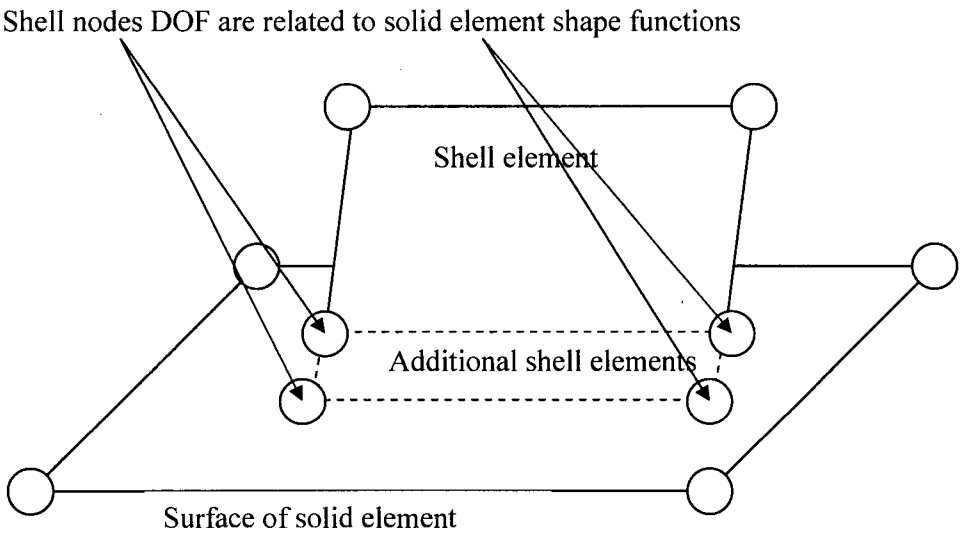

Figure 10b. Shell edge-to-solid face connection.

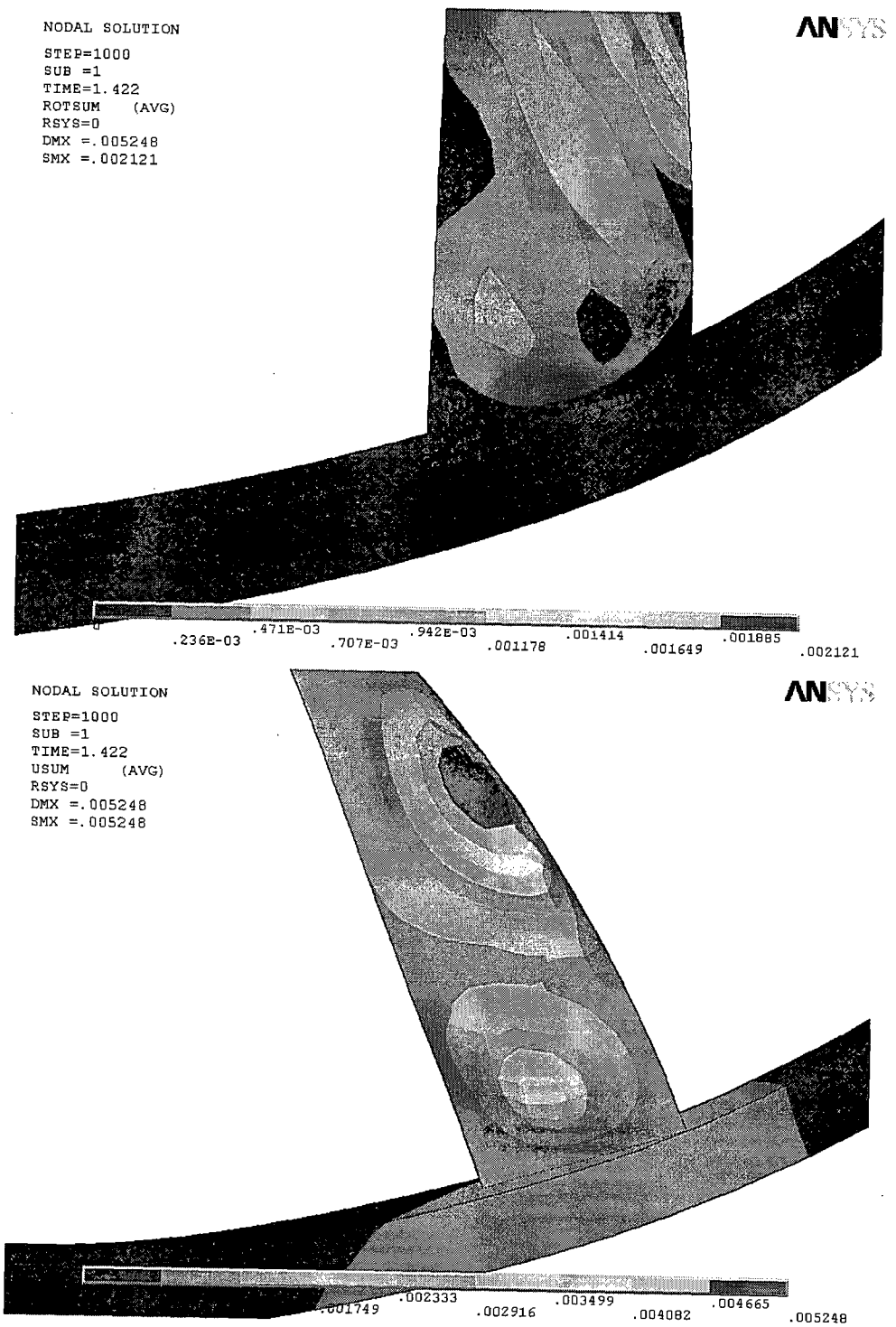

Figure 11. Shell edge-to-solid face connection between hood end plate and upper support ring. Rotations (top) and displacements (bottom). Time t=1.422 sec.

4. Structural Analysis

The solution is decomposed into static and transient parts. The static solution produces the stress field induced by the supported structure subjected to its own weight, whereas the transient solution accounts for the unsteady stress field due to the acoustic loads acting on the dryer. The two solutions are linearly combined to obtain the final displacement and stress histories. This decomposition facilitates prescription of the added mass model accounting for hydrodynamic interaction and allows one to compare the stress contributions arising from static and unsteady loads separately. Alternating stresses are independent of static loads and thus can be obtained using only the transient response due to pressure loads. Proper evaluation of the peak membrane and membrane+bending stresses, however, requires that the static loads due to weight be accounted for. Hence both static and transient analyses must be carried out.

4.1 Static Analysis

The results of the static analysis are shown on Figure 12. Only a few locations exhibited high stress intensity levels. These locations include the skirt/upper support ring connection with stress intensity 8,775 psi, the trough thin section/vane bank end plate/thick closure plate junction with stress intensity 5,416 psi and the thin closure plate/inner hood junction with stress intensity 8,133 psi. All locations are near the steam dryer support brackets. The locations with high static stress intensity are shown in Figure 13. Note that these locations have high stress intensity also when static and transient runs are combined, primarily due to static loading.

4.2 Transient Analysis

The fluctuating pressure loads were applied to the structural model at all surface nodes described in Section 2.3. The pressures were varied at increments of 1.422×10^{-3} sec for 1405 time steps both for CLTP and EPU loadings – a total time of 2 sec. For the EPU cases with frequency shift the same 1405 steps of EPU loading were used, but with different time steps: 1.28×10^{-3} sec with total time 1.8 sec for scaling 10% up, and 1.564×10^{-3} sec with total time 2.2 sec for scaling 10% down. These stress results are discussed in Section 5. Typical stress intensity distributions over the structure are shown in Figure 14.

To evaluate peak stresses, the static and transient stresses were combined and peak stress intensities during the response, evaluated. According to ASME B&PV Code, Section III, Subsection NG-3216.2 the following procedure was established to calculate alternating stresses. For every node, the stress difference tensors, $\boldsymbol{\sigma}'_{nm} = \boldsymbol{\sigma}_n - \boldsymbol{\sigma}_m$, were considered for all possible pairs of the stresses σ_n and σ_m at different time levels, t_n and t_m. Note that all possible pairs require consideration since there are no 'obvious' extrema in the stress responses. For each stress difference tensor, the principal stresses S_1, S_2, S_3 were computed and the maximum absolute value among principal stress differences, $S_{nm} = \max\{|S_1 - S_2|, |S_1 - S_3|, |S_2 - S_3|\}$, obtained. The alternating stress at the node was then one-half the maximum value of S_{nm} taken over all combinations (n,m), i.e., $S_{alt} = \frac{1}{2}\max_{n,m}\{S_{nm}\}$. This alternating stress was compared against allowable values, depending on the node location with respect to welds.

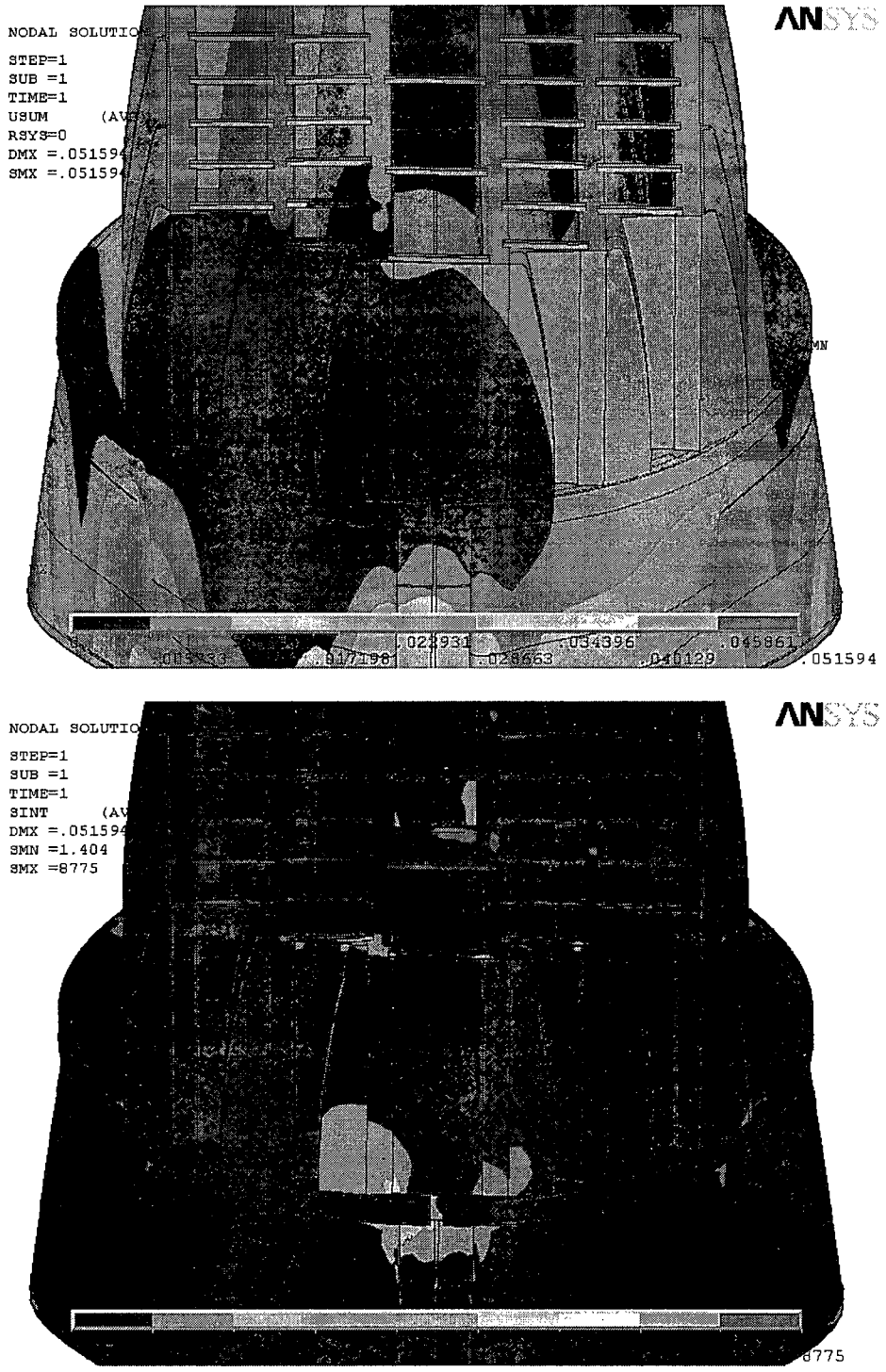

Figure 12. Overview of static calculations showing displacements (top, in inches) and stress intensities (bottom, in psi). Maximum displacement (DMX) is 0.052"; maximum stress intensity (SMX) is 8,775 psi.

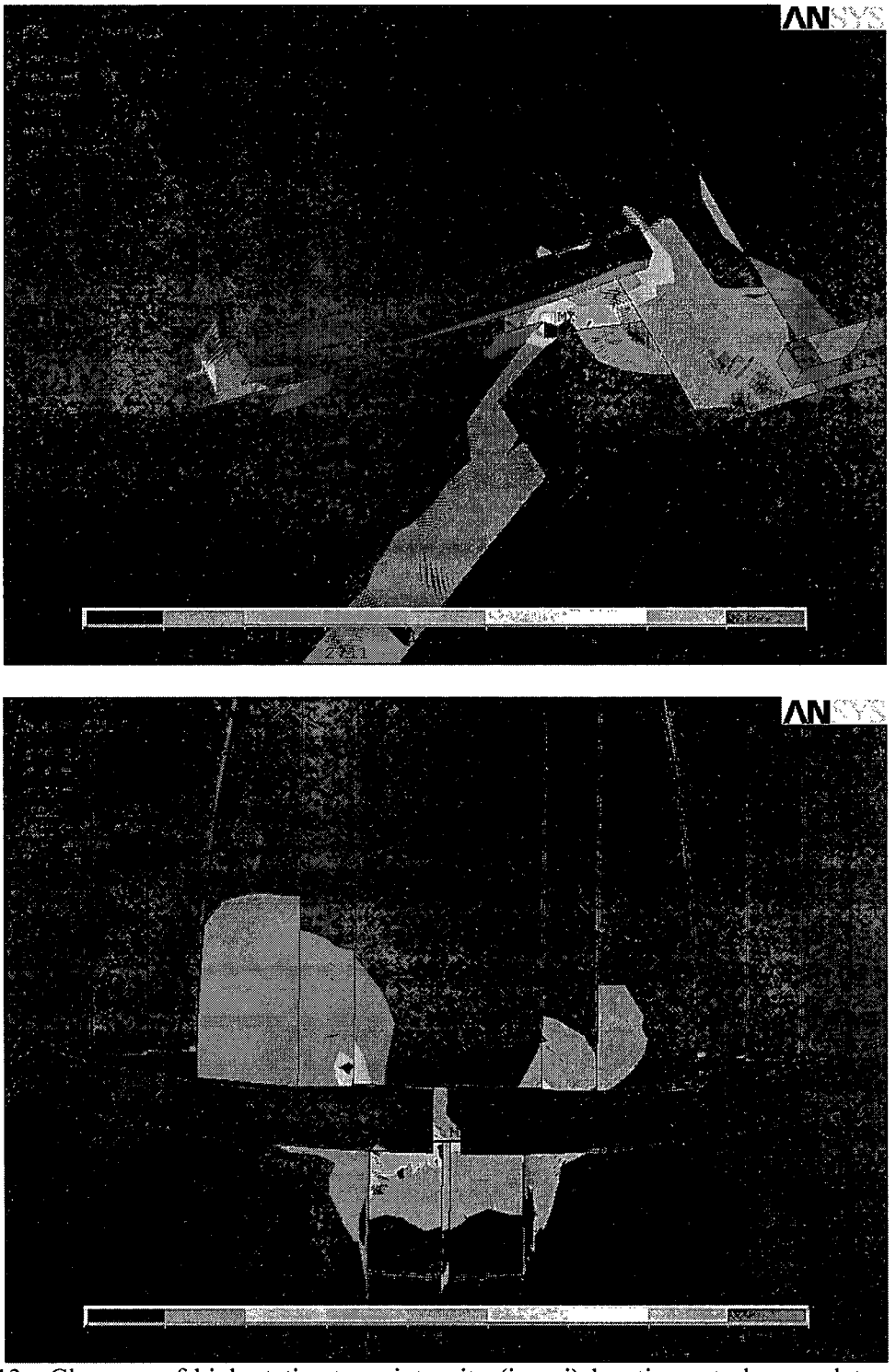

Figure 13. Close up of high static stress intensity (in psi) locations at closure plates and near support brackets.

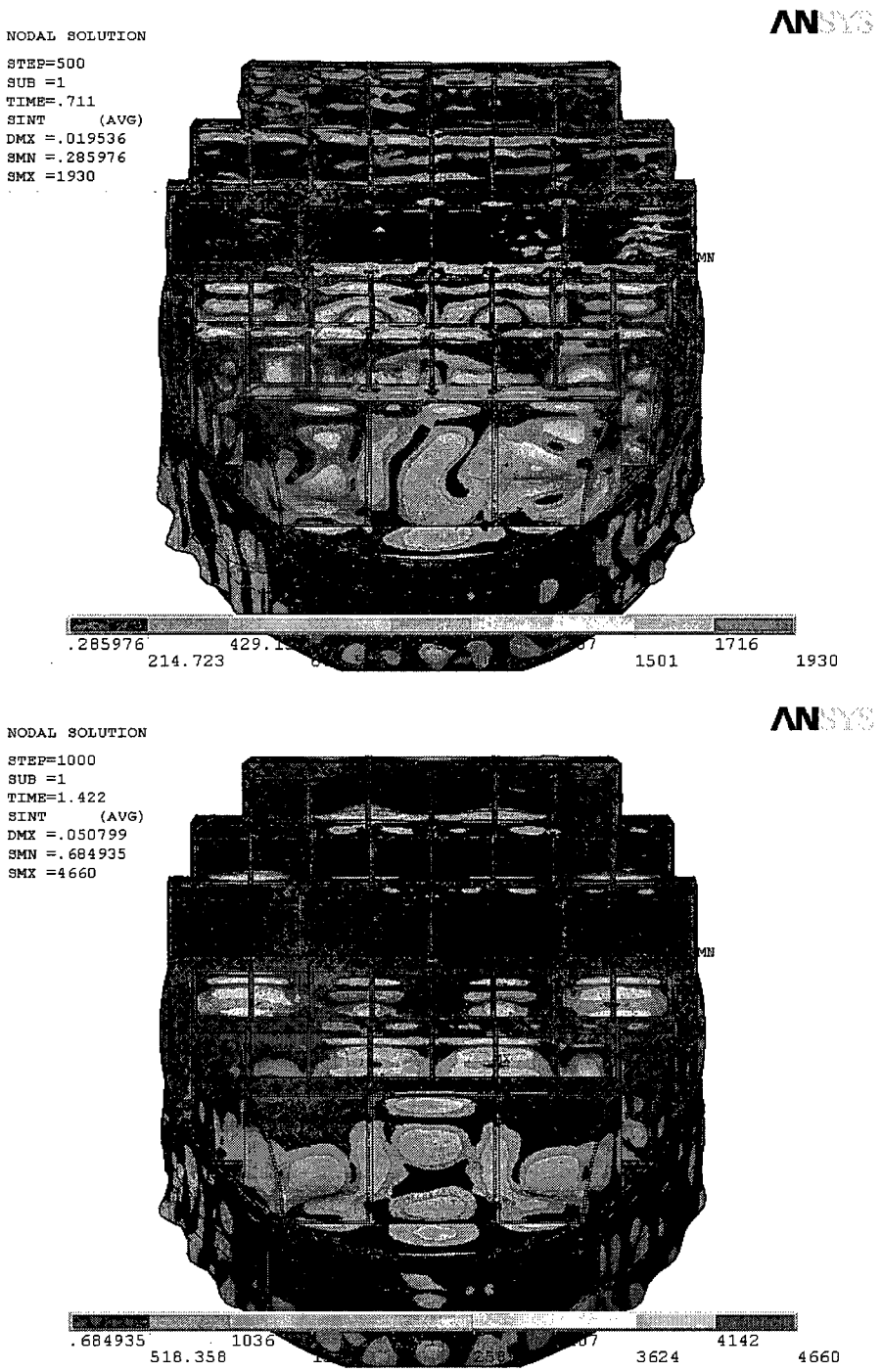

Figure 14a. Overview of transient calculations for 115% CLTP loading showing stress intensities (in psi) along with displacements. Time step 500 (top) and 1000 (bottom). | Rev 1

Rev 1

Figure 14b. [DELETED]

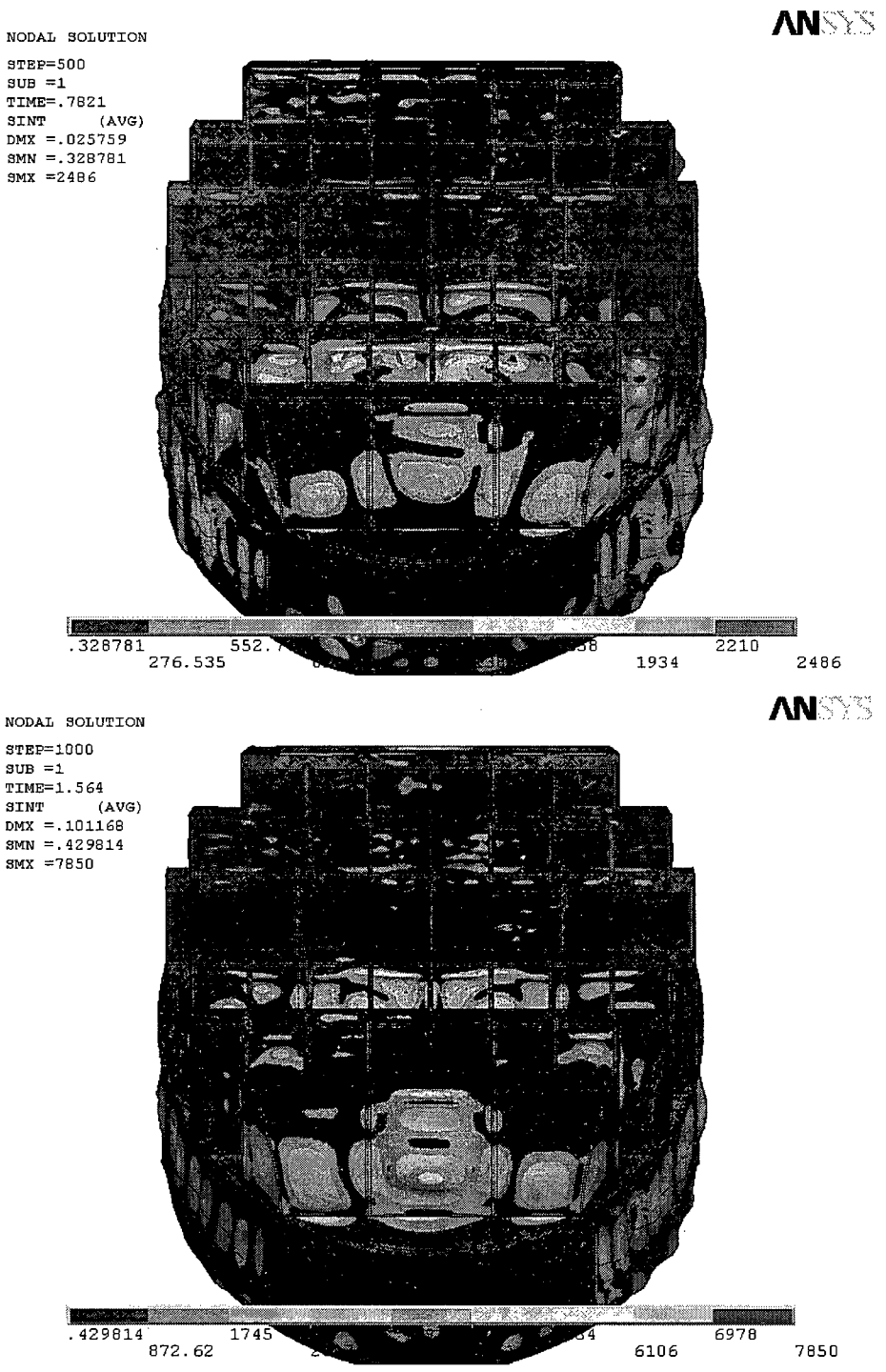

Rev 1

Figure 14c. Overview of transient calculations for 115% CLTP loading with -10% frequency shift showing stress intensities (in psi) along with displacements. Time step 500 (top) and 1000 (bottom).

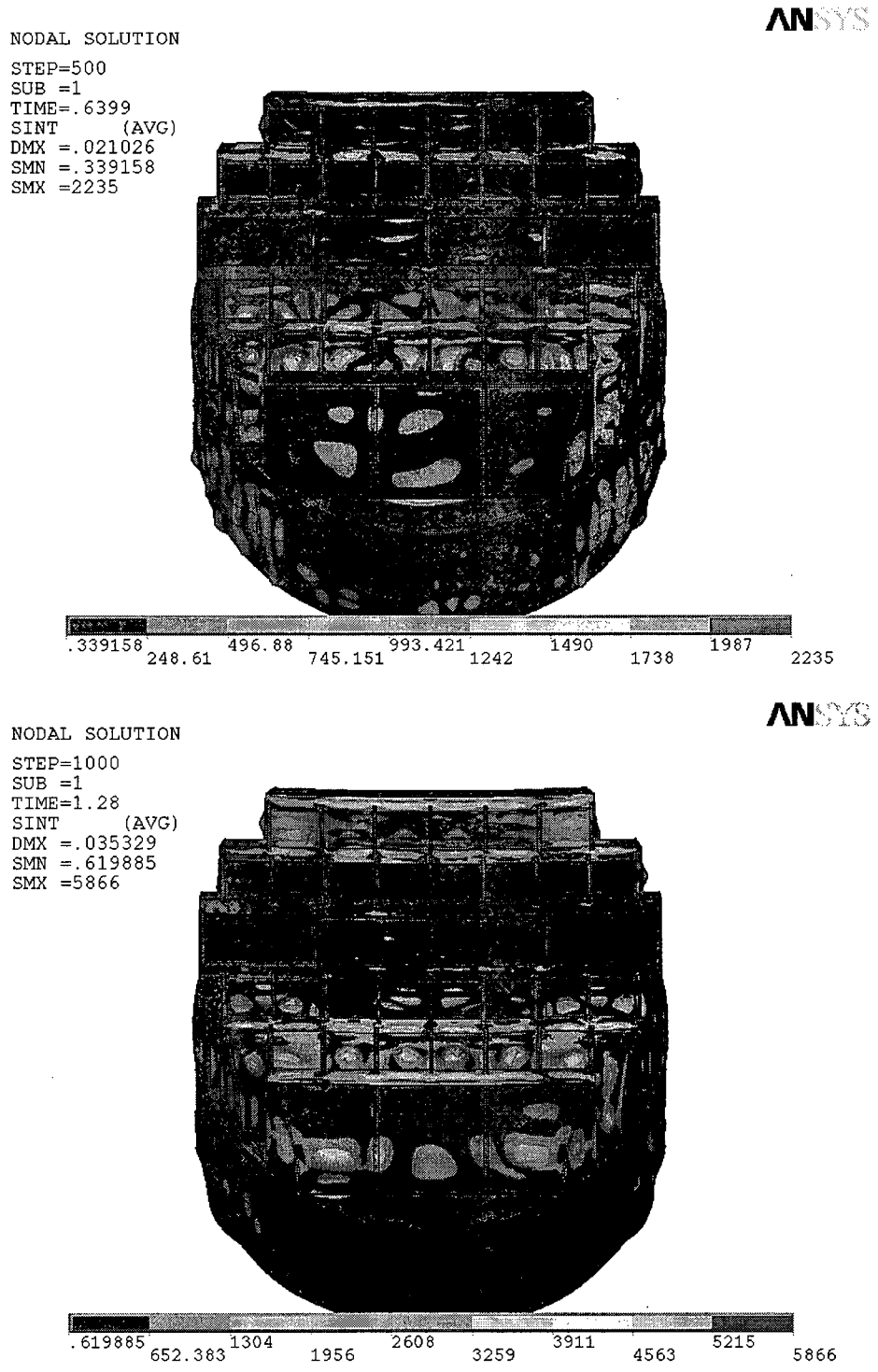

Rev 1

Figure 14d. Overview of transient calculations for 115% CLTP loading with +10% frequency shift showing stress intensities (in psi) along with displacements. Time step 500 (top) and 1000 (bottom).

4.3 Post-Processing

The static and transient stresses computed at every node with the ANSYS program were exported into files for subsequent post-processing. These files were then read in with separate customized software to compute the peak and alternating stresses at every node. The peak stress was defined for each node as the largest stress intensity occurring during the time history. Alternating stresses were calculated according to the ASME standard described above. For shell elements the peak stresses were calculated separately at the mid-plane, where only membrane stress is present, and at top/bottom of the shell, where bending stresses are also present.

For nodes that are shared between several structural components or lie on junctions, the peak and alternating stress intensities are calculated as follows. First the nodal stress tensor is computed separately for each individual component by averaging over all finite elements meeting at the node and belonging to the same structural component. The time histories of these stress tensors are then processed to deduce the peak and alternating stress intensities for each structural component. Finally for nodes shared across multiple components the maximum of the peak and alternating stresses is recorded as the 'nodal' stress. This approach prevents averaging of stresses across components and thus yields conservative estimates for nodal stresses at the weld locations where several components are joined together.

The peak stresses are compared against allowables values which depend upon the stress type (membrane, membrane+bending, alternating – Pm, Pm+Pb, S_{alt}) and location (at a weld or away from welds). These allowables are specified in the following section. For solid elements the most conservative allowable, Pm for membrane stress, is used, although bending stresses are nearly always present also. The structure is then assessed in terms of stress ratios formed by dividing allowables by the computed stresses at every node. Stress ratios less than unity imply that the associated peak and/or alternating stress intensities exceed the allowable levels. Post-processing tools calculate the stress ratios, identifying the nodes with low stress ratios and generating files formatted for input to the 3D graphics program, TecPlot, which provides more general and sophisticated plotting options than currently available in ANSYS.

The unsteady pressure loads applied to the dryer contain a strong 80Hz component (see Figure 5) which is not present in the plant. The erroneous signal is caused by the interaction between sensors used to record the unsteady pressures. The stress assessment was therefore performed with the 80Hz signal removed. Since the problem is linear, forcing the structure at a given frequency produces a steady state response at the same frequency. Therefore, attenuating the 80Hz signal is equivalent to attenuating the resulting stress response. Thus, rather than repeating the structural dynamics calculation, the 80Hz signal was simply filtered from the existing stress histories prior to calculating the peak and alternating stresses. For EPU cases with frequency shift 10% up and down, the components 88 Hz and 72 Hz respectively were removed.

4.4 Computation of Stress Ratios for Structural Assessment

The ASME B&PV Code, Section III, subsection NG provides different allowable stresses for different load combinations and plant conditions. The stress levels of interest in this analysis are for the normal operating condition, which is the Level A service condition. The load combination for this condition is:

Normal Operating Load Combination = Weight + Pressure + Thermal

The weight and fluctuating pressure contributions have been calculated in this analysis and are included in the stress results. The static pressure differences and thermal expansion stresses are small, since the entire steam dryer is suspended inside the reactor vessel and all surfaces are exposed to the same conditions. Seismic loads only occur in Level B and C cases, and are not considered in this analysis.

Allowable Stress Intensities

The ASME B&PV Code, Section III, subsection NG shows the following (Table 4) for the maximum allowable stress intensity (Sm) and alternating stress intensity (Sa) for the Level A service condition. The allowable stress intensity values for type 304 stainless steel at operating temperature 550°F are taken from Table I-1.2 and Fig. I-9.2.2 of Appendix I of Section III, the ASME B&PV Code. The calculation for different stress categories is performed in accordance with Fig. NG-3221-1 of Division I, Section III, subsection NG.

Table 4. Maximum Allowable Stress Intensity and Alternating Stress Intensity for all areas other than welds. The notation Pm represents membrane stress; Pb represents stress due to bending; Q represents secondary stresses (from thermal effects and gross structural discontinuities, for example); and F represents peak stresses (due to local structural discontinuities, for example).

Type	Notation	Calculation	Allowable Value (psi)
Peak Stress Allowables:			
General Membrane	Pm	Sm	18,300
Membrane + Bending	Pm + Pb	1.5 Sm	27,450
Primary + Secondary	Pm + Pb + Q	3.0 Sm	54,900
Alternating Stress Allowable:			
Primary + Secondary + Peak	S_{alt}	Sa	13,600

When evaluating welds, either the calculated or allowable stress was adjusted, to account for a stress concentration factor. Specifically:

- For maximum allowable stress intensity, the allowable value is decreased by multiplying its value in Table 6.1 by 0.55.

- For alternating stress intensity, the calculated weld stress intensity is multiplied by a weld stress intensity (fatigue) factor of 1.8, before comparison to the Sa value given above.

The factors of 0.55 and 1.8 were selected based on the observable quality of the shop welds and NDE testing of all welds (excluding tack and intermittent welds) during fabrication. GE Purchase Specification for the HCGS Steam Dryer (21A9355 Section 9.2) called for liquid penetrant testing of all welds (excluding tack and intermittent welds) along the entire length or circumference, using the guidance of ASME Boiler and Pressure Code, Paragraph N-6127.3. In addition, critical welds are subject to periodical visual inspections in accordance with the

requirements of GE SIL 644. Therefore, for weld stress intensities, the allowable values are shown in Table 5.

These factors (0.55 and 1.8) also conservatively presume that the structure is joined using fillet welds unless specified otherwise. Since fillet welds correspond to larger stress concentration factors than other types of welds, this assumption is a conservative one. At some locations however (e.g., full penetration welds), this assumption is excessively conservative and more detailed consideration of the weld geometry is warranted. This is the case with the welds joining the curved hoods with the side panels which have been reinforced in the Hope Creek steam dryer. Appendix A presents the analysis of these welds and shows that a conservative treatment of these welds allows the stress concentration factor of these welds to be reduced by an additional factor, f_{sw}=1.25. Everywhere else, f_{sw}=1 indicating no reduction from the nominal fillet weld values. Rev 1

Table 5. Weld Stress Intensities.

Type	Notation	Calculation	Allowable Value (psi)
Peak Stress Allowables:			
General Membrane	Pm	0.55 Sm	10,065
Membrane + Bending	Pm + Pb	0.825 Sm	15,098
Primary + Secondary	Pm + Pb + Q	1.65 Sm	30,195
Alternating Stress Allowables:			
Primary + Secondary + Peak	S_{alt}	Sa	13,600

Comparison of Calculated and Allowable Stress Intensities

The classification of stresses into general membrane or membrane + bending types was made according to the exact location, where the stress intensity was calculated; namely, general membrane, Pm, for middle surface of shell element, and membrane + bending, Pm + Pb, for other locations. For solid elements the most conservative, general membrane, Pm, allowable is used.

The structural assessment is carried out by computing stress ratios between the computed peak and alternating stress intensities, and the allowable levels. Locations where any of the stresses exceed allowable levels will have stress ratios less than unity. Since computation of stress ratios and related quantities within ANSYS is time-consuming and awkward, a separate FORTRAN code was developed to compute the necessary peak and alternating stress intensities, Pm, Pm+Pb, and S_{alt}, and then compare it to allowables. Specifically, the following quantities were computed at every node:

1. The peak membrane stress intensity, Pm (evaluated at the mid-thickness location for shells),
2. The peak stress intensity, Pm+Pb, (taken as the maximum of the peak stress intensity values at the bottom, top, and mid thickness locations, for shells),

3. The peak alternating stress, S_{alt}, (the maximum value over the three thickness locations is taken).
4. The minimum peak stress ratio assuming the node lies at a non-weld location:
   SR-P(nw) = min{ Sm/Pm, 1.5 * Sm/(Pm+Pb) }.
5. The alternating stress ratio assuming the node lies at a non-weld location,
   SR-a(nw) = Sa / (1.1 * S_{alt}),
6. The same as 4, but assuming the node lies on a weld,
   SR-P(w)=SR-P(nw) * f_{sw} * 0.55 Rev 1
7. The same as 5, but assuming the node lies on a weld,
   SR-a(w)=SR-a(nw) * f_{sw} / 1.8.

where f_{sw}=1 at all welds except for the lengths of welds connecting the inner and middle curved hoods to the side plates and lying less than 60" above the bottom plates; for these welds f_{sw}=1.25. Note that in steps 4 and 6, the minimum of the stress ratios based on Pm and Pm+Pb, is taken. Rev 1 The allowables listed in Table 4, Sm=18,300 psi and Sa=13,600 psi. The factors, 0.55 and 1.8, are the weld factors discussed above. The factor of 1.1 accounts for the differences in Young's moduli for the steel used in the steam dryer and the values assumed in alternating stress allowable. According to NG-3222.4 the effect of elastic modulus upon alternating stresses is taken into account by multiplying alternating stress S_{alt} at all locations by the ratio, E/E_{model}=1.1, where:

E = 28.3 10^6 psi, as shown on Fig. I-9.2.2. ASME BP&V Code
E_{model} = 25.55 10^6 psi (Table 2.1)

The nodes with stress ratios lower than 4 are plotted in TecPlot to establish whether they lie on a weld or not. The appropriate peak and alternating stress ratios, SR-P and SR-a, are thus determined and a final listing of nodes having minimum stress ratios is generated. Nodes identified as having the smallest stress ratios are listed below, in Table 7. The corresponding locations are depicted in Figure 19 to Figure 22.

5. Results

5.1 General Stress Distribution and Maximum Stress Locations

The maximum stress intensities obtained by post-processing the ANSYS stress histories for 115% CLTP at nominal frequency and with frequency shift operating conditions are listed in Table 6. Contour plots of the peak and alternating stress intensities over the steam dryer structure are shown on Figure 15 (nominal frequency), Figure 16 (max. stress over all frequency shifts), Figure 17 (-10% frequency shift), and Figure 18 (+10% frequency shift). The figures are oriented to emphasize the maximum stress regions. Note that these stress intensities *do not* account for weld factors. Further, it should be noted that since the allowable stresses vary with location, peak stress intensities do not necessarily correspond to regions of primary structural concern. Instead, structural evaluation is more accurately made in terms of the stress ratios which compare the computed stresses to allowable levels with due account made for stress type and weld factors. Comparisons on the basis of stress ratios are made in Section 5.2. Rev 1

The tabulated stresses are obtained by computing the relevant stress intensities at every node and then sorting the nodes according to stress levels. The maximum stress node is noted and all neighboring nodes within 10 inches of the maximum stress node and its symmetric images (i.e., reflections across the x=0 and y=0 planes) are 'blanked' (i.e., excluded from the search for subsequent peak stress locations). Of the remaining nodes, the next highest stress node is identified and its neighbors (closer than 10 inches) blanked. The third highest stress node is similarly located and the search continued in this fashion until all nodes are either blanked or have stresses less than half the peak value on the structure or stress ratios lower than 4. The blanking of neighboring nodes is intended to prevent extracting peak stress nodes from essentially the same location on the structure.

Even under EPU conditions the maximum stress intensities in most areas are low (less than 500 psi, or 5% of the most conservative critical stress). For the membrane stresses (Pm) the high stress regions tend to occur in the following regions: (i) Near the dryer support mounts where the static load component tends to dominate. (ii) At the junctions of the hoods with adjoining structures – tie bars, closure plates and cover plates These regions are more localized and are more critical from a structural assessment perspective because they contain welds and in some cases (tie bars and closure plates) also support significant static loads. (iii) On the inner and middle curved hoods outside the thin closure plates. The latter stresses appear to be the result of acoustic loading rather than static forces since the same region experiences comparatively high alternating stresses. While the outer hoods generally carry the brunt of the unsteady loading, the middle and inner hoods are also subjected to unsteady loads and, because they are thinner, they experience higher stresses. Rev 1

The membrane + bending stress (Pm+Pb) distributions are quite different and show evidence of significant modal response in all cases. Modal excitations are most pronounced for the nominal frequency (Figure 16b) and +10% frequency shift (Figure 18b) where vibrations are most evident in the drain channels and the middle hoods outside of the thin closure plates. Again stress concentrations are also observed, particularly where the thin closure plates connect to the hoods or vane bank end plates, along the skirt/drain channel welds and where the curved hoods join to the vane end plates.

The alternating stress, S_{alt}, distributions are qualitatively similar to those for Pm+Pb. The modal excitations in the skirt region and inner and middle curved hoods are now even more pronounced. The outer hoods also exhibit significant response. The skirt response occurs at approximately 120Hz and leads to high stresses in the submerged portion. Similar drain channel response modes and accompanying high stresses have appeared here in other calculations using alternate element types, mesh sizes, connection methods (bonded contacts) and hydrodynamic mass models. Since the submerged skirt is not subjected to pressure loads it manifests a modal excitation which is not surprising since the drain channels and skirt are thin (and therefore easily excited) and of large dimension so that they support a significant number of response modes over the applied load frequency range. It appears therefore that the loading applied to the upper portion of the skirt above the waterline as well as to the structure above the upper support ring, incites one or more of the drain channel modes near resonance.

Rev 1

Shifting the frequencies has a relatively weak effect on the peak membrane (Pm) and membrane+bending (Pm+Pb) stresses, with ranges $Pm \in [6644,7209]$ psi and $Pm+Pb \in [9832,10329]$ psi (or ±4% and ±2% variations respectively about the median). The variations with frequency shift in the alternating stresses on the other hand are higher with $Salt \in [3663,5147]$ psi or a ±17% variation about the median value. The maximum alternating stress occurs at the +10% frequency shift. Examining Table 6b shows that most of the high stresses occur at positive frequency shifts (+2.5% and +10%). It is also interesting to note that the alternating stresses can fall off at markedly different rates at the various frequency shifts. Thus, at nominal frequencies the top five alternating stresses differ by less than 10%. At the +10% shift however, this difference rises to 90%. This isolation of peak stress locations is further evidence of the excitation of only a small number of modes at the 115% CLTP conditions.

Table 6a. Locations with highest predicted stress intensities for 1/8th scale 115% CLTP conditions with no frequency shift.

Stress Category	Location		Location (in)				Stress Intensities (psi)		
		Weld	x	y	z	node	Pm	Pm+Pb	S_{alt}
Pm	1. Inner hood (top) near closure plate	No	109.0	-27.6	95.3	44886	7017	10033	1908
"	2. Upper ring / thick closure plate / vane end plate	Yes	-118.8	14.4	7.5	85994	4317	5915	465
"	3. Skirt / upper support ring	Yes	118.7	-5.9	-2.0	91960	4177	6002	707
"	4. Inner hood (bottom) / closure plate	Yes	-108.4	38.4	8.1	87035	4177	4354	956
"	5. Middle vane bank / closure plate (top)	Yes	-108.4	45.9	95.9	85891	4169	5237	1367
Pm+Pb	1. Inner hood (top) near closure plate	No	109.0	-27.6	95.3	44886	7017	10033	1908
"	2. Skirt / upper support ring	Yes	-118.8	-0.6	-2.0	79487	2556	9778	1276
"	3. Outer hood bottom / cover plate	Yes	59.1	101.4	7.5	93493	1793	7688	3431
"	4. Skirt / 45° drain pipe	Yes	88.2	79.6	-20.5	91083	2297	6663	1511
"	5. Upper ring / thick closure plate / vane end plate	Yes	-118.8	14.4	7.5	85994	4317	5915	465
S_{alt}	1. Lower inner hood	No	27.9	36.0	50.5	42098	1609	4015	3549
"	2. Drain channel (bottom) / skirt	Yes	118.2	-12.0	-94.3	93818	2219	3705	3496
"	3. Outer hood bottom / cover plate	Yes	59.1	101.4	7.5	93493	1793	7688	3431
"	4. Lower middle hood	No	25.6	69.3	29.9	37254	608	3838	3253
"	5. Middle hood (half-height)	No	-25.2	67.1	53.3	37915	817	3642	3230

Node numbers are retained for further reference.
Spatial coordinate are in the coordinate system, defined by the origin at the centerline of steam dryer 7.5" below bottom plates. The x-axis is parallel to the hoods, y-axis is normal to the hoods pointing from MSL AB to MSL CD, z-axis is vertical, positive up.
Thin closure plates - the 3/16 inch plates on the steam outlet side of the outer and middle vane banks. The straight vertical edge is welded to the vane bank end plate and on curved vertical edge is welded to the outside of the curved hood. These plates ensure that the steam exiting the vane banks is directed upward into the dome.
Thick closure plate - this 1/2 inch plate performs the same function as the thin closure plate, but it spans the steam outlet space between two inner hoods vane banks.
Supports - the vertical stiffeners on the inside of the hoods. The straight vertical edge is welded to the inlet of the vane bank assembly. The curved vertical edge is welded to the inside of the hood.

Table 6b. Locations with highest predicted stress intensities taken over all frequency shifts for 1/8th scale at 115% CLTP conditions.

Stress Category	Location	Weld	Freq. Shift	Location (in)				Stress Intensities (psi)		
				x	y	z	node	Pm	Pm+Pb	S_{alt}
Pm	1. Inner hood (top) near closure plate	No	+2.5%	109.0	-27.6	95.3	44886	7209	10277	2151
"	2. Inner bottom plate / vane bank side plate	Yes	-10%	118.8	-14.4	7.5	86577	4576	6339	908
"	3. Skirt / upper support ring	Yes	-10%	118.7	-5.9	-2.0	91960	4434	6325	937
"	4. Middle vane bank / closure plate (top)	Yes	+2.5%	-108.4	45.9	95.9	85891	4291	6369	2648
"	5. Inner hood (bottom) / closure plate	Yes	+10%	-108.4	38.4	8.1	87035	4177	4373	1137
Pm+Pb	1. Skirt / upper support ring	Yes	+2.5%	-118.8	-0.6	-2.0	79487	2689	10329	1661
"	2. Inner hood (top) near closure plate	No	+2.5%	109.0	-27.6	95.3	44886	7209	10277	2151
"	3. Outer hood bottom / cover plate	Yes	+2.5%	59.1	101.4	7.5	93493	1836	8525	3807
"	4. Skirt / 45° drain pipe	Yes	+7.5%	88.2	79.6	-20.5	91083	2328	6666	1511
"	5. Middle vane bank / closure plate (top)	Yes	-10%	-108.4	45.9	95.9	85891	4291	6369	2648
S_{alt}	1. Middle hood and reinforcement strip	Yes	+10%	-98.0	69.3	29.9	84521	1411	5345	5147
"	2. Drain channel (bottom) / skirt	Yes	+2.5%	118.2	-12.0	-94.2	93818	2507	4444	4246
"	3. Thin closure plate, top/middle hood	Yes	-10%	-84.7	-59.3	95.0	85091	3724	5937	3912
"	4. Outer hood bottom / cover plate	Yes	+2.5%	59.1	101.4	7.5	93493	1836	8525	3807
"	5. Inner hood / thin closure plate	Yes	-10%	-108.4	-28.2	94.5	88253	1977	4910	3701

Rev 1

See Table 6a for locations nomenclature.

Table 6c. Locations with highest predicted stress intensities for 1/8th scale at 115% CLTP conditions with -10% frequency shift.

Stress Category	Location		Location (in)				Stress Intensities (psi)		
		Weld	x	y	z	node	Pm	Pm+Pb	S_{alt}
Pm	1. Inner hood near thin closure plate	No	109.0	-27.6	95.3	44886	6815	9784	1439
"	2. Inner bottom plate /vane bank side plate	Yes	118.8	-14.4	7.5	86577	4576	6339	908
"	3. Skirt / upper support ring	Yes	118.7	-5.9	-2.0	91960	4434	6325	937
"	4. Middle vane bank / closure plate (top)	Yes	-108.4	45.9	95.9	85891	4118	6369	2648
"	5. Inner hood (bottom) / closure plate	Yes	-108.4	38.4	8.1	87035	4003	4260	951
Pm+Pb	1. Skirt / upper support ring	Yes	118.8	0.6	-2.0	88325	2550	10312	1517
"	2. Inner hood near thin closure plate	No	109.0	-27.6	95.3	44886	6815	9784	1439
"	3. Middle vane bank / closure plate (top)	Yes	-108.4	45.9	95.9	85891	4118	6369	2648
"	4. Inner bottom plate /vane bank side plate	Yes	118.8	-14.4	7.5	86577	4576	6339	908
"	5. Outer hood bottom / cover plate	Yes	59.1	101.4	7.5	93493	1644	6010	1405
S_{alt}	1. Middle hood / thin closure plate	Yes	-84.7	-59.3	95.0	85091	3724	5937	3912
"	2. Inner hood / thin closure plate	Yes	-108.4	-28.2	94.5	88253	1977	4910	3701
"	3. Thin closure plate, top cover / outer vane bank side plate	Yes	-84.7	77.4	94.6	92443	722	3726	3379
"	4. Drain channel (bottom) / skirt	Yes	73.8	-93.1	-94.2	93833	1191	5531	3221
"	5. Thin closure plate, top cover / middle vane bank side plate	Yes	-108.4	-45.9	94.4	90710	1327	4210	3172

Rev 1

See Table 6a for locations nomenclature.

Table 6d. Locations with highest predicted stress intensities for $1/8^{th}$ scale at 115% CLTP conditions with +10% frequency shift.

Stress Category	Location		Location (in)				Stress Intensities (psi)		
		Weld	x	y	z	node	Pm	Pm+Pb	S_{alt}
Pm	1. Inner hood near thin closure plate	No	109.0	-27.6	95.3	44886	6807	9640	1359
"	2. Upper ring / thick closure plate / vane end plate	Yes	-118.8	14.4	7.5	85994	4272	5850	439
"	3. Inner hood (bottom) / hood support	Yes	0.0	38.4	7.5	86960	4120	4153	1856
"	4. Skirt / upper support ring	Yes	118.7	-5.9	-2.0	91960	4069	5982	570
"	5. Inner hood (bottom) / closure plate	Yes	-108.4	38.4	8.1	87035	3952	4216	929
Pm+Pb	1. Skirt / upper support ring	Yes	-118.8	-0.6	-2.0	79487	2513	9832	1208
"	2. Inner hood near thin closure plate	No	109.0	-27.6	95.3	44886	6807	9640	1359
"	3. Outer hood bottom / cover plate	Yes	59.1	101.4	7.5	93493	1669	6737	2328
"	4. Skirt / 45° drain pipe	Yes	88.2	79.6	-20.5	91083	2168	6189	1171
"	5. Upper ring / thick closure plate / vane end plate	Yes	-118.8	14.4	7.5	85994	4272	5850	439
S_{alt}	1. Middle hood / reinforcement strip	Yes	-98.0	69.3	29.9	84521	1196	5345	5147
"	2. Middle hood / reinforcement strip	Yes	-98.4	-68.4	41.7	84399	843	3773	3496
"	3. Inner hood / thin closure plate	Yes	84.7	59.3	95.0	92526	3246	5038	3244
"	4. Middle hood (near bottom and bank side plate)	No	91.2	-69.7	21.6	47474	1211	3299	3151
"	5. Thin closure plate, top cover / outer vane bank side plate	Yes	-84.7	-77.4	96.1	82694	905	2847	2658

Rev 1

See Table 6a for locations nomenclature.

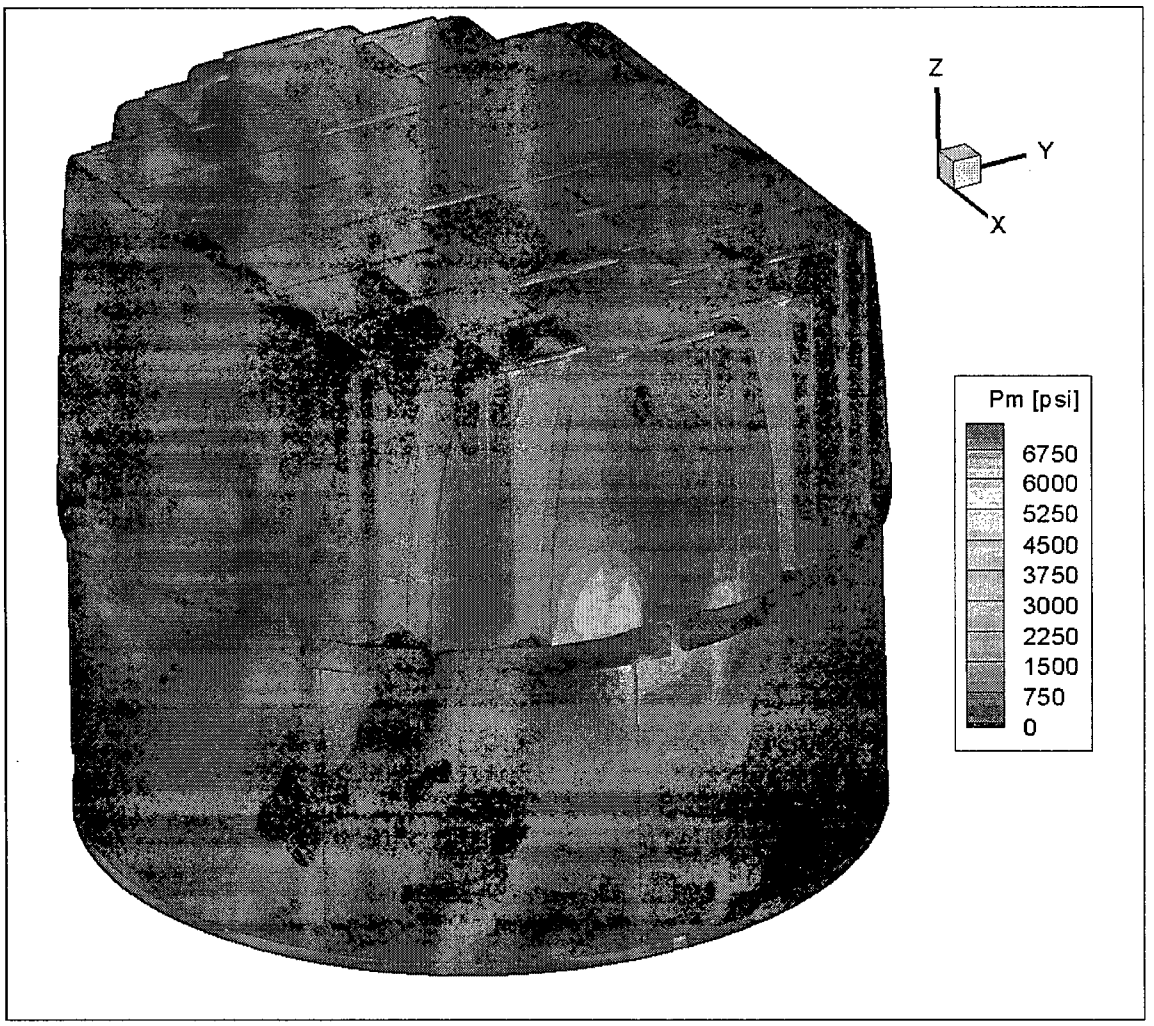

Figure 15a. Contour plot of peak membrane stress intensity, Pm, for $1/8^{th}$ scale 115% CLTP load. The maximum stress intensity is 7017 psi.

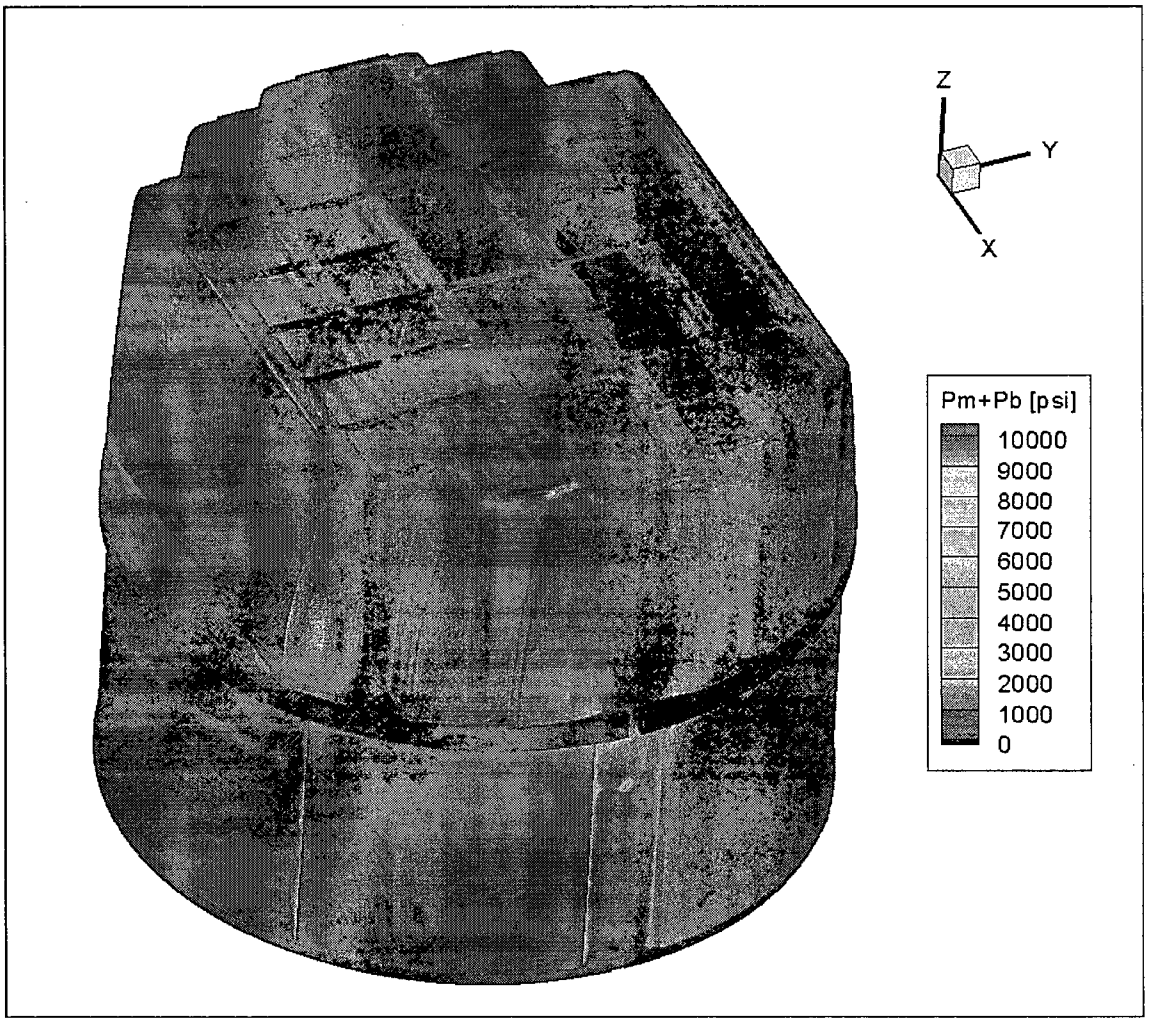

Figure 15b. Contour plot of peak membrane+bending stress intensity, Pm+Pb, for $1/8^{th}$ scale 115% CLTP load. The maximum stress intensity is 10033 psi.

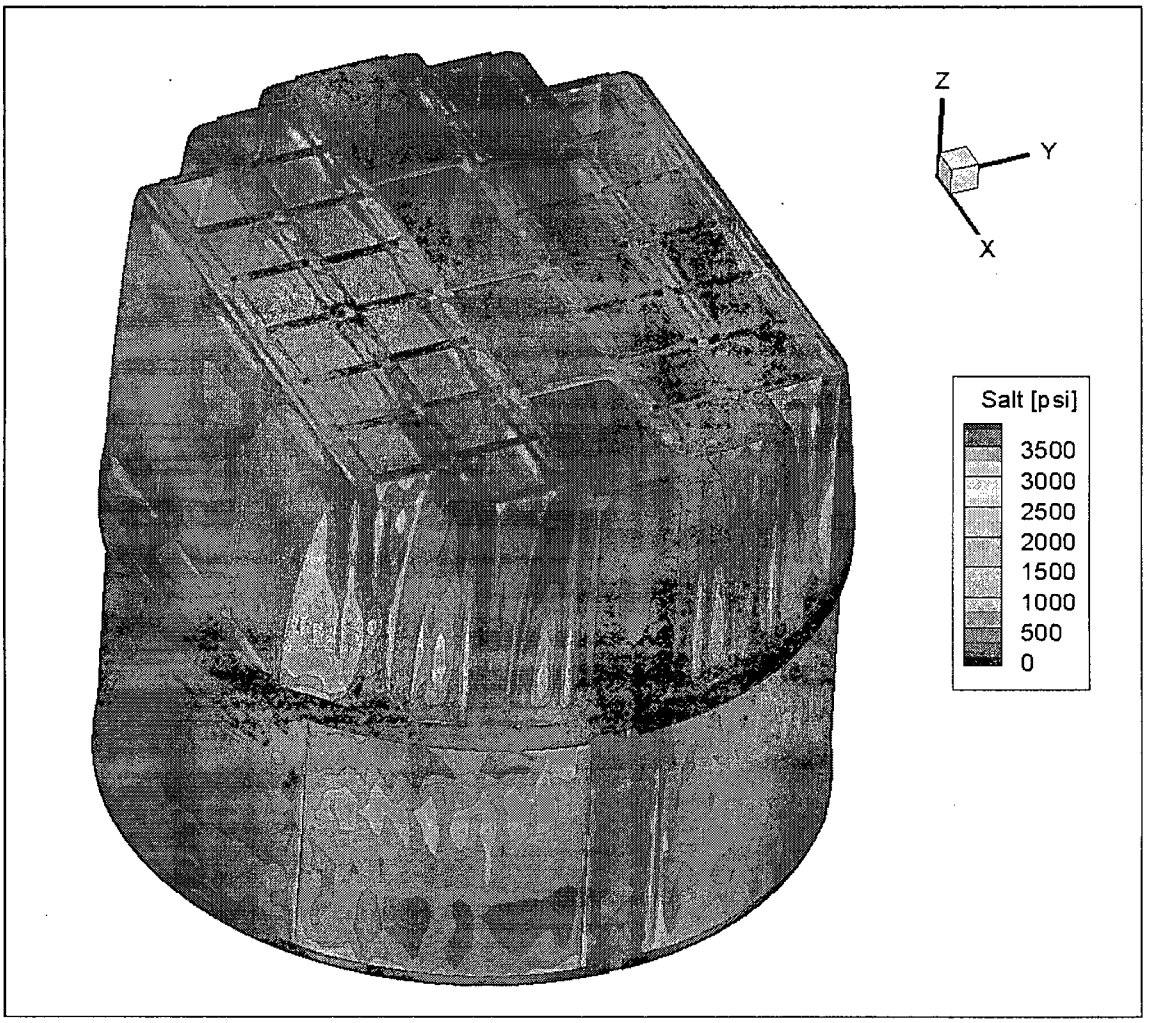

Figure 15c. Contour plot of alternating stress intensity, S_{alt}, for $1/8^{th}$ scale 115% CLTP load. The maximum stress intensity is 3549 psi.

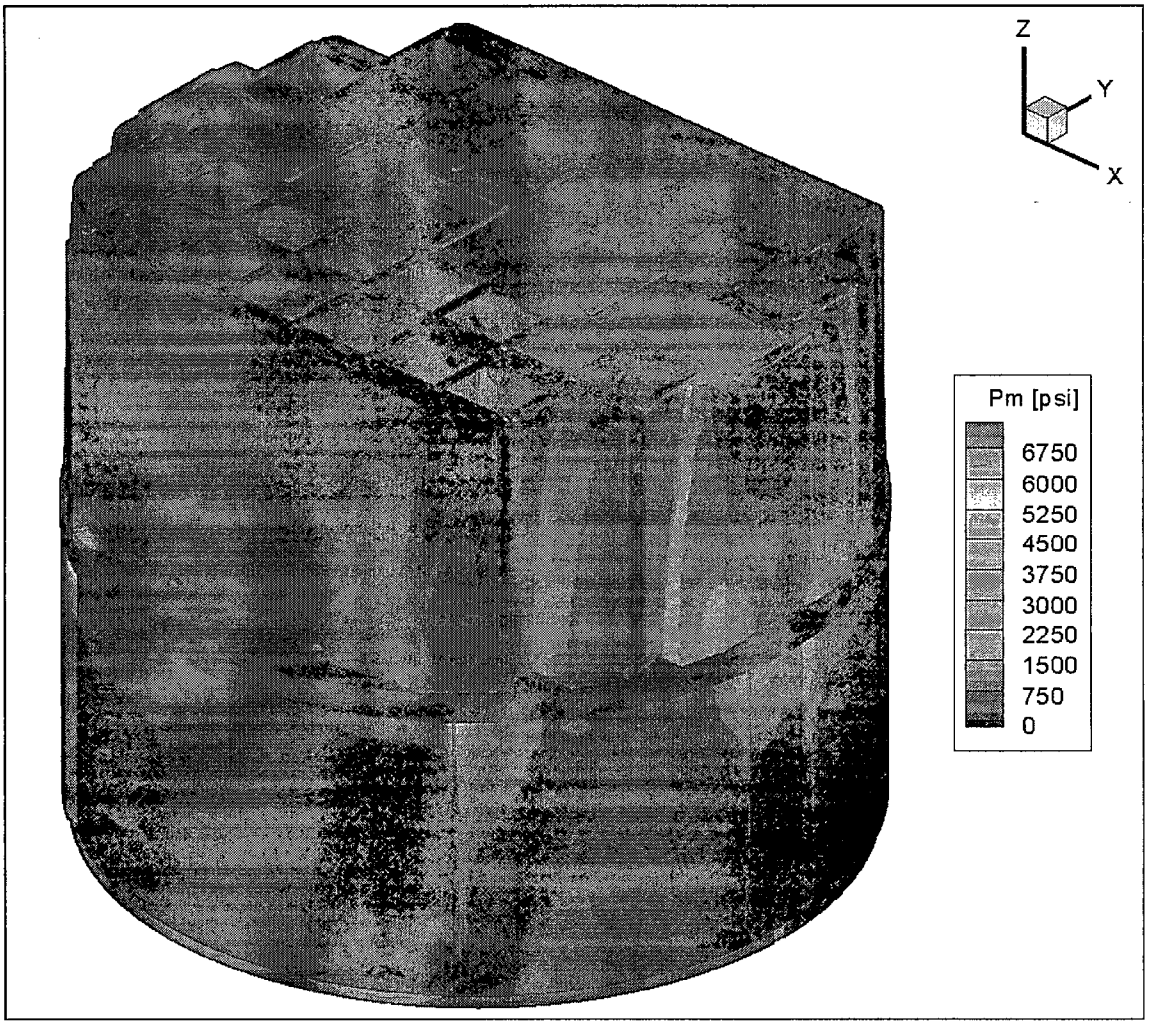

Rev 1

Figure 16a. Contour plot of peak membrane stress intensity, Pm, for 1/8th scale 115% CLTP operation with frequency shifts. The recorded stress at a node is the maximum value taken over all frequency shifts. The maximum stress intensity is 7209 psi.

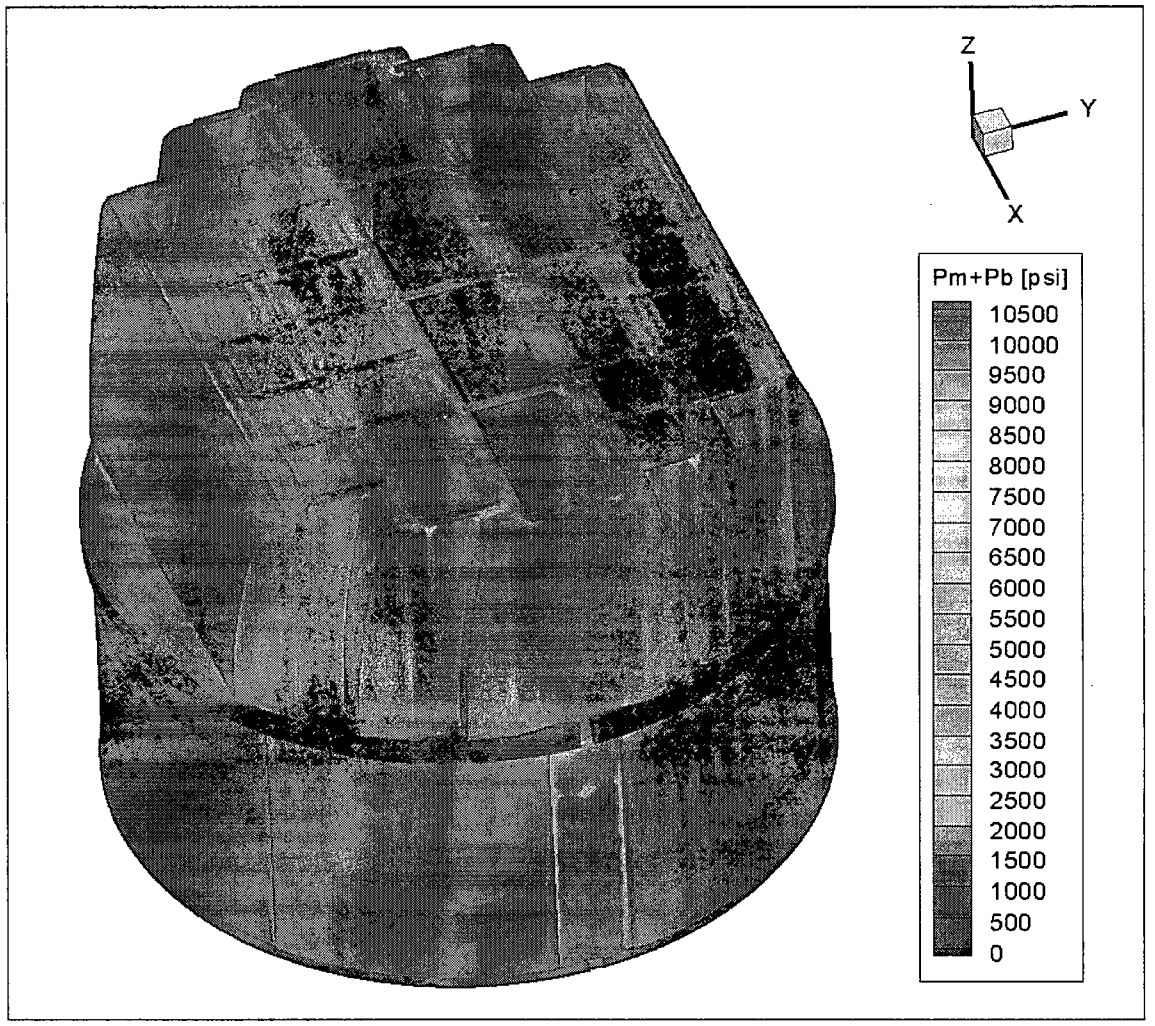

Rev 1

Figure 16b. Contour plot of peak membrane+bending stress intensity, Pm+Pb, for $1/8^{th}$ scale 115% CLTP operation with frequency shifts. The recorded stress at a node is the maximum value taken over all frequency shifts. The maximum stress intensity is 10329 psi.

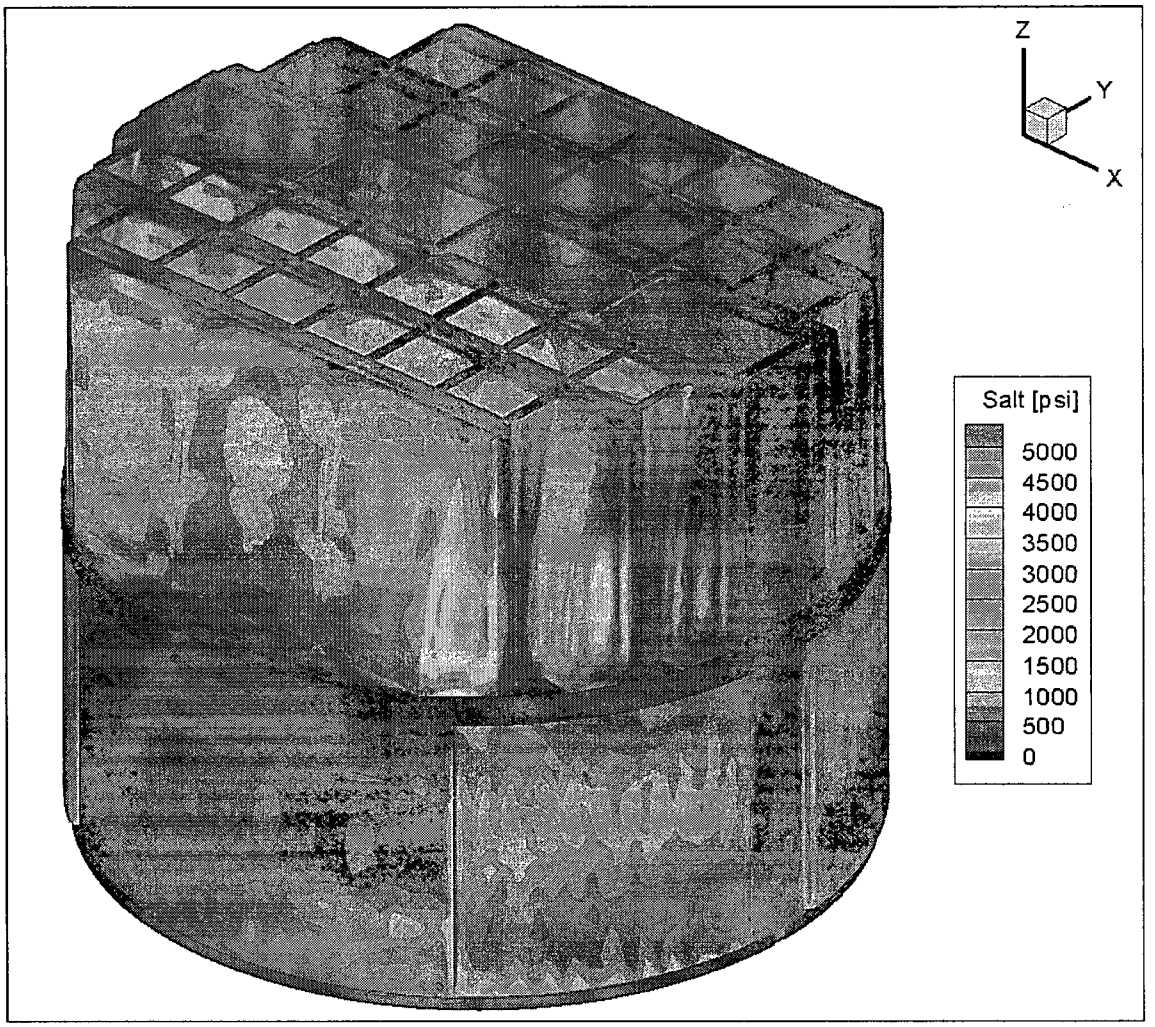

Rev 1

Figure 16c. Contour plot of alternating stress intensity, S_{alt}, for $1/8^{th}$ scale 115% CLTP operation with frequency shifts. The recorded stress at a node is the maximum value taken over all frequency shifts. The maximum stress intensity is 5147 psi.

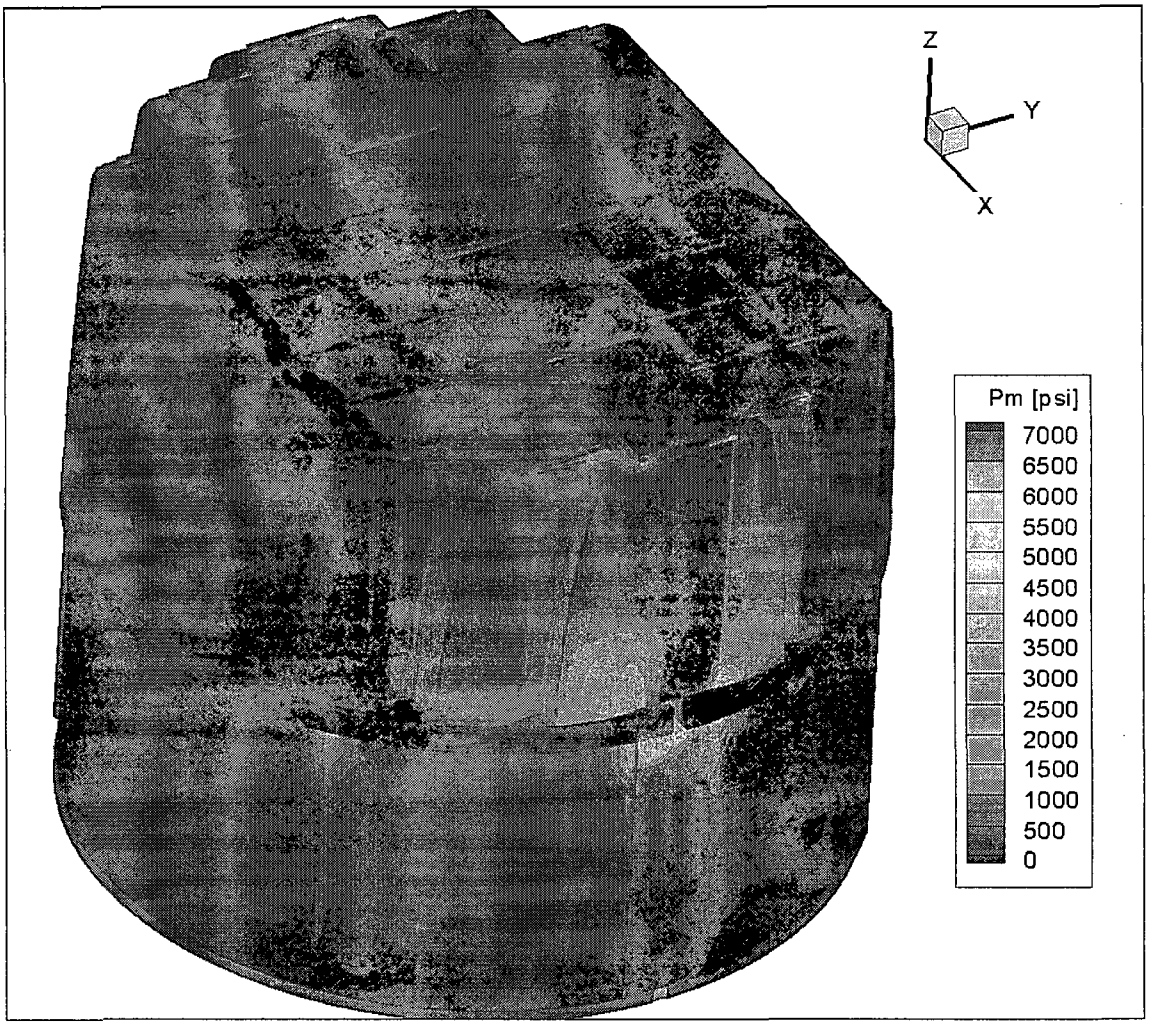

Rev 1

Figure 17a. Contour plot of peak membrane stress intensity, Pm, for $1/8^{th}$ scale 115% CLTP load with -10% frequency shift. The maximum stress intensity is 6815 psi.

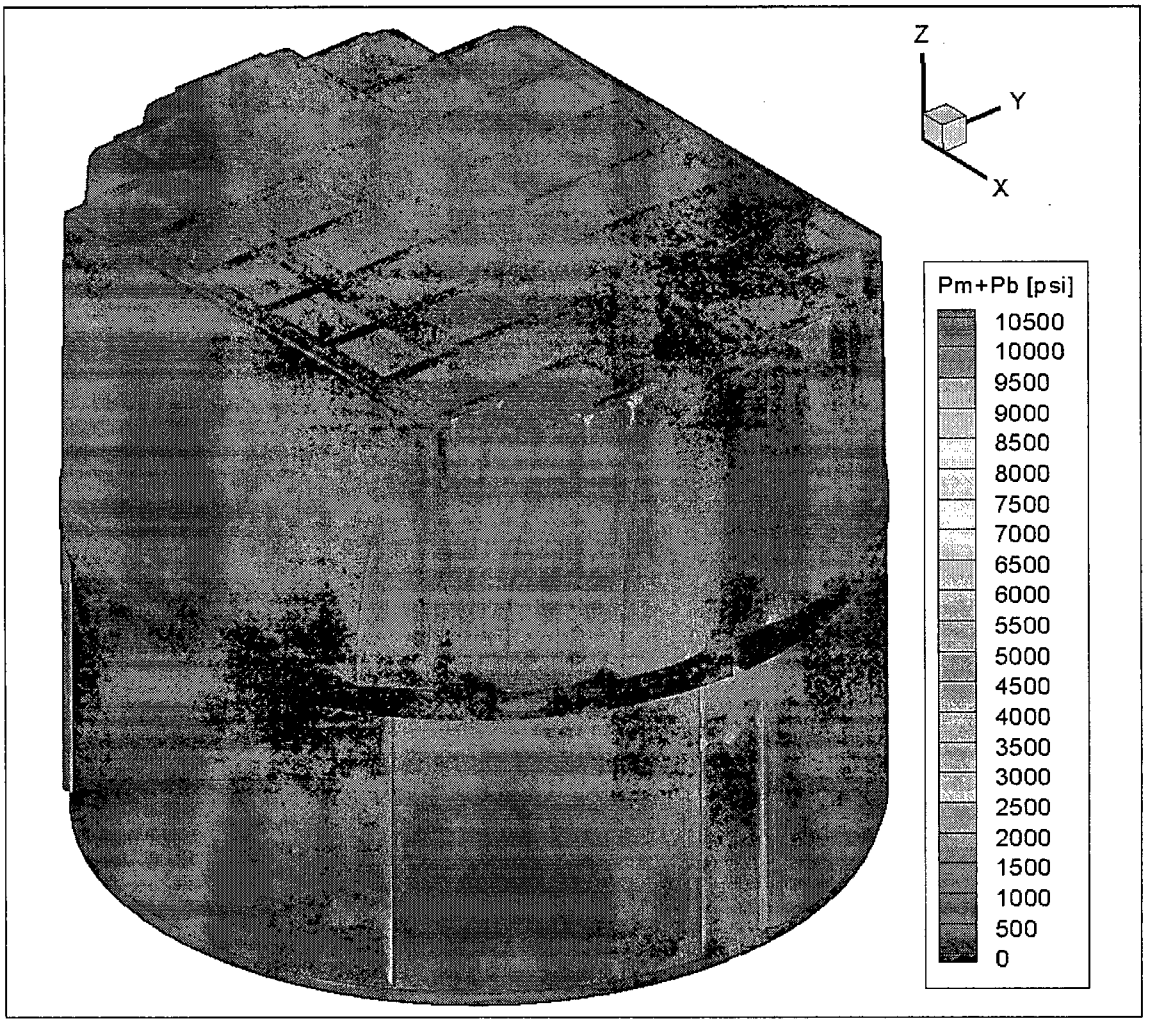

Rev 1

Figure 17b. Contour plot of peak membrane+bending stress intensity, Pm+Pb, for $1/8^{th}$ scale 115% CLTP load with -10% frequency shift. The maximum stress intensity is 10312 psi.

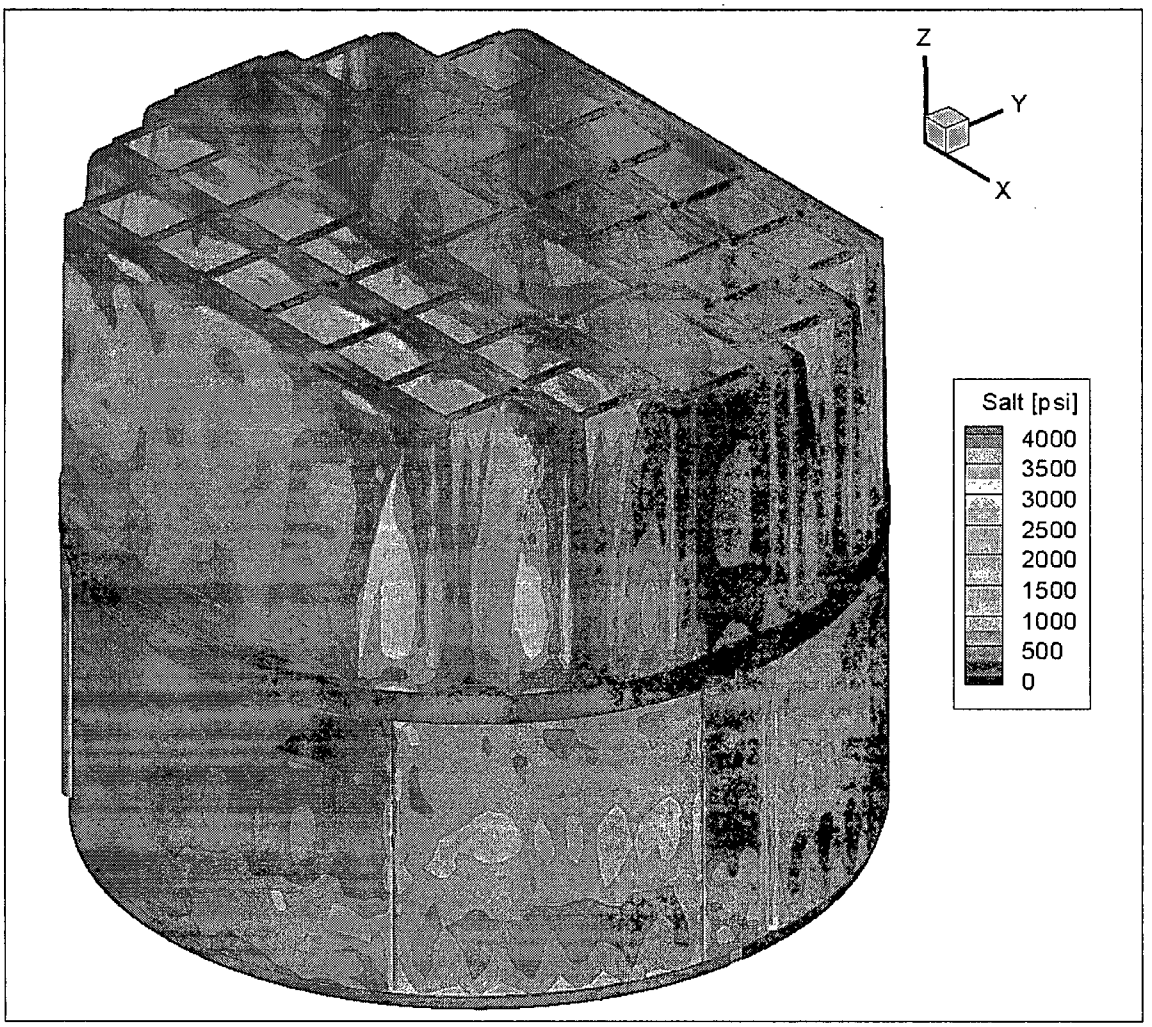

Rev 1

Figure 17c. Contour plot of alternating stress intensity, S_{alt}, for $1/8^{th}$ scale 115% CLTP load with -10% frequency shift. The maximum stress intensity is 3912 psi.

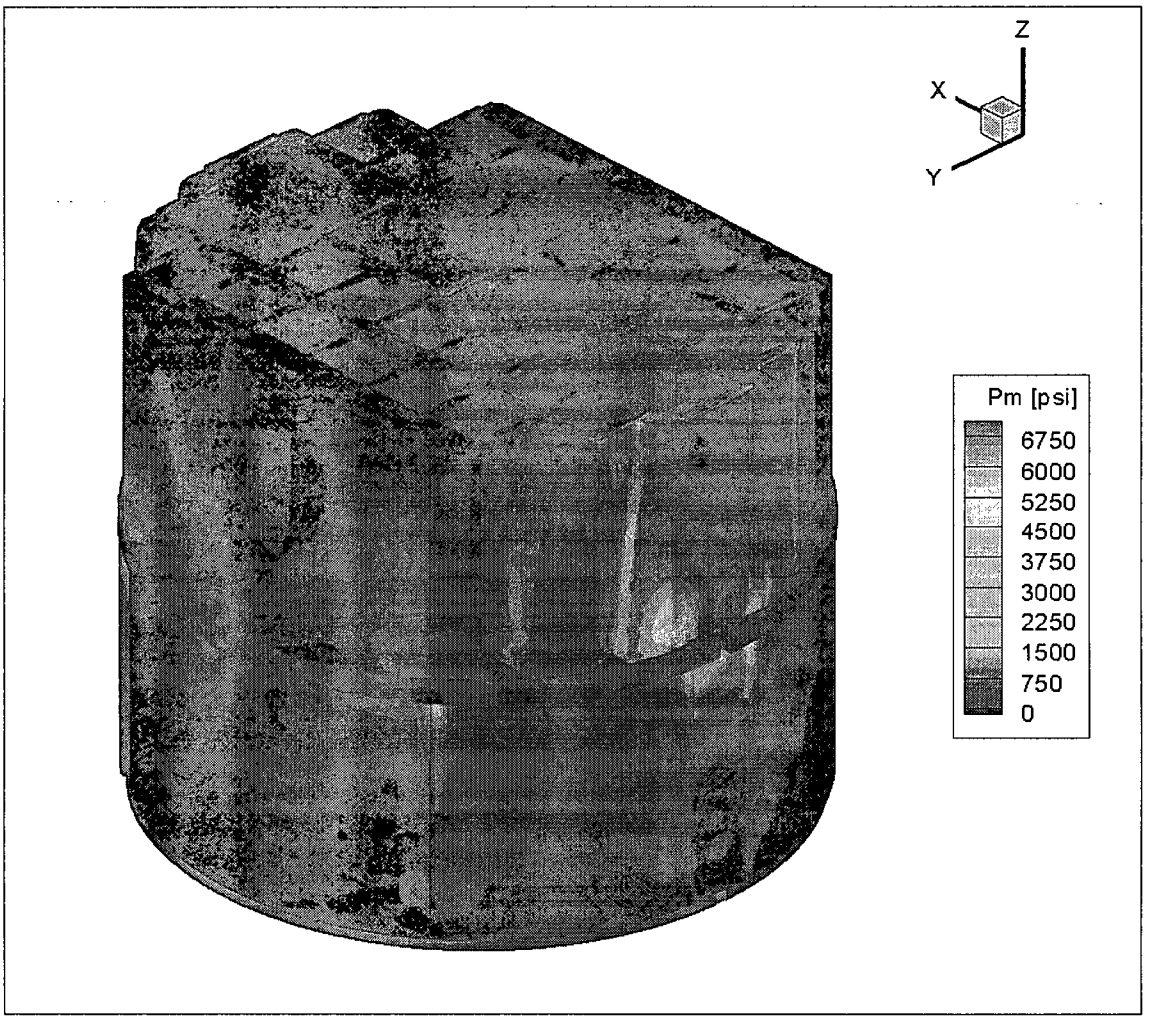

Rev 1

Figure 18a. Contour plot of peak membrane stress intensity, Pm, for 1/8th scale 115% CLTP load with +10% frequency shift. The maximum stress intensity is 6807 psi.

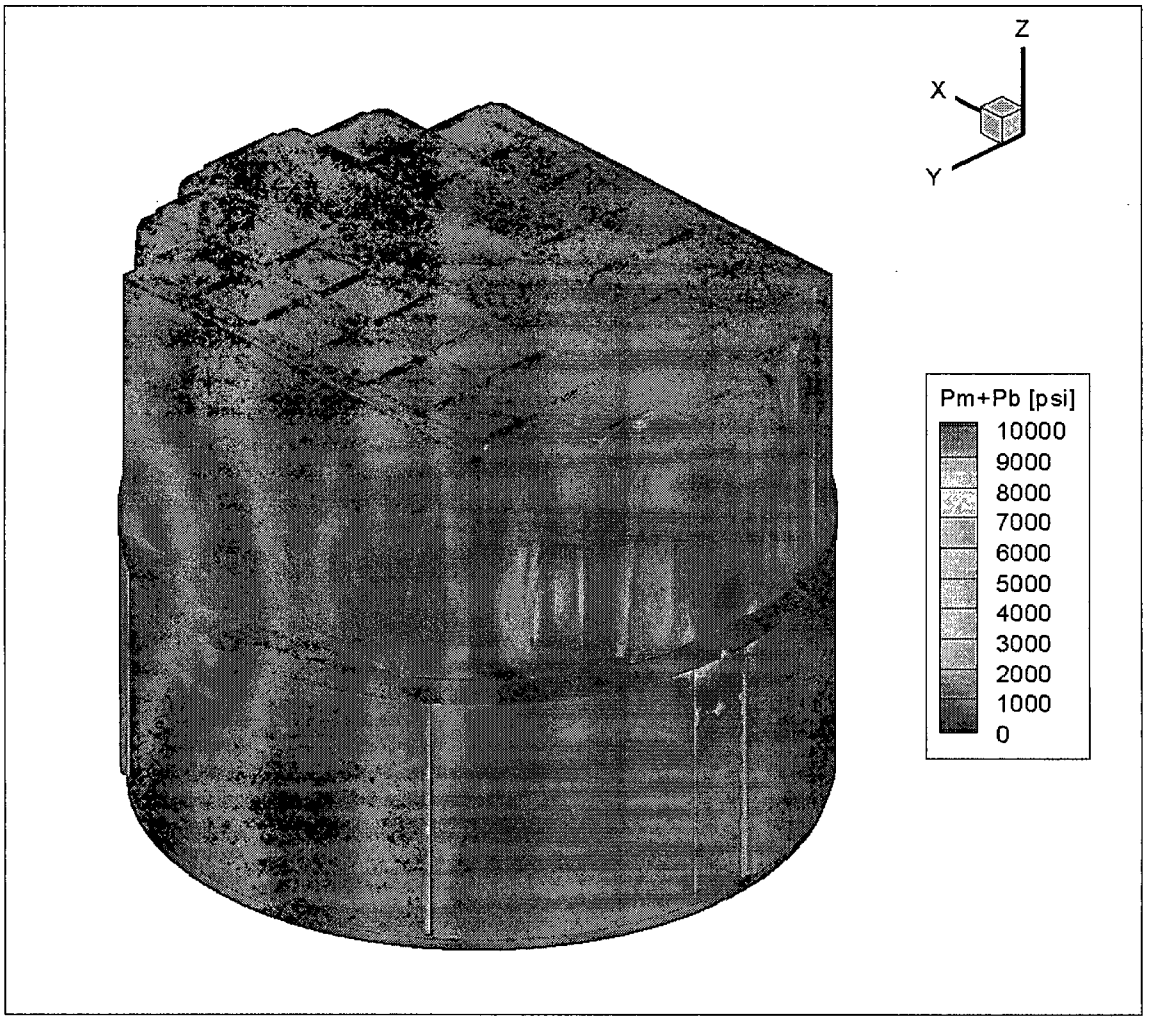

Rev 1

Figure 18b. Contour plot of peak membrane+bending stress intensity, Pm+Pb, for $1/8^{th}$ scale 115% CLTP load with +10% frequency shift. The maximum stress intensity is 9832 psi.

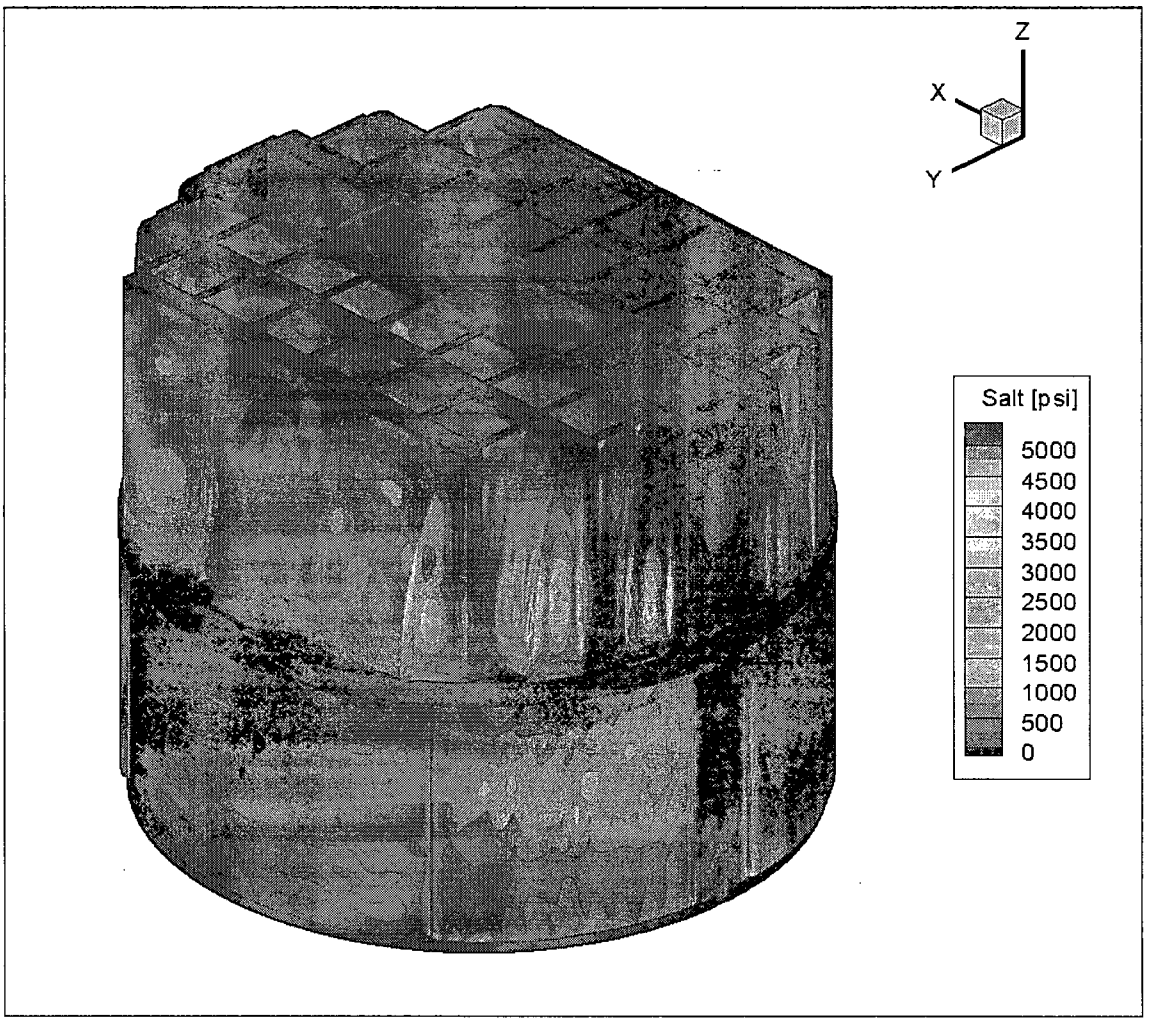

Rev 1

Figure 18c. Contour plot of alternating stress intensity, S_{alt}, for $1/8^{th}$ scale 115% CLTP load with +10% frequency shift. The maximum stress intensity is 5147 psi.

5.2 Load Combinations and Allowable Stress Intensities

The stress ratios computed for 115% CLTP at nominal frequency and with frequency shifting are listed in Table 7. The stress ratios are grouped according to type (SR-P for peak membrane and membrane+bending stress, SR-a for alternating stress) and location (away from welds or on a weld). Rev 1

In 115% CLTP operation at nominal frequency the minimum stress ratios are associated with peak stresses and occur at: (i) the junction of inner hood and thin closure plate (SR-P=1.53) and (ii) where the skirt attaches to the upper support ring (SR-P=1.54). Other critical regions with low stress ratios are the base of the outer hood where it meets the cover plate (SR-P=1.96) and where the drain channel joins the skirt (alternating stress ratio, SR-a=1.96). All of these locations lie on welds as summarized in Table 7a and the accompanying Figure 19. The minimum stress ratio at a non-weld, SR-P=2.61, is again identified with a peak stress and occurs on the inner hood near the thin closure plate. In this case, the minimum stress ratio location is near, but not on, a weld. If the stress ratio for a weld were applied then the value would drop to 1.44 which is still well within the allowable level.

The effects of frequency shifts can be conservatively accounted for by identifying the minimum stress ratio at every node, where the minimum is taken over all the frequency shifts considered (including the nominal or 0% shift case). The resulting stress ratios are then processed as before to identify the smallest stress ratios anywhere on the structure, categorized by stress type (peak or alternating) and location (on or away from a weld). The results are summarized in Table 7b and show that the minimum stress ratio, SR-a=1.33, is identified with an alternating stress and occurs at the weld joining the middle hood to the reinforcement strip used at the hood's junction with the hood's end plate. This is the smallest stress ratio encountered anywhere on the structure for any frequency shift at the 115% CLTP condition. The smallest stress ratio associated with a peak stress is SR-P=1.46 and occurs on the weld joining the skirt to the upper support ring. This stress ratio is only slightly smaller than the minimum peak stress ratio at the nominal frequency. Rev 1

It is important to note that the minimum stress ratio, SR-a=1.33 is an outlier and occurs only at one weld location and only at the +10% frequency shift. If only the -10% to +7.5% range of frequency shifts is considered then the minimum alternating stress ratio becomes SR-a=1.62 so that the minimum stress ratio is associated with a peak stress, SR-P=1.46.

Because the worst case stress ratios (i.e., the minimum stress ratio over all frequency shifts) are most important for conservative structural assessment, the locations of *all* nodes having SR<1.8 are plotted in Figure 20f-g (peak stresses) and Figure 20h-i (alternating stresses). Note that all plotted stress ratios occur on welds since all stress ratios at non-welds are 2.54 or higher. These plots differ from the preceding ones where (see discussion in Section 5.3), the smallest stress ratio in a 10" region is identified and all other nodes in this region excluded from display and tabulation. In the current plots, this blanking is not performed so that a more complete picture of where stress ratios are low, is conveyed. These plots show that all peak stress ratios, SR-P<1.8 occur where: (i) the skirt joins the upper support ring as shown; (ii) the inner hood is welded to the thin closure plate; and (iii) the bottom of the outer hood (one node only). All

alternating stress ratios, SR-a<1.8 occur at: (i) the weld joining the reinforcement strip to the middle hood; (ii) the connection between the middle hood and thin closure plates; and (iii) the weld between the skirt and drainage channels (towards the bottom). Rev 1

For the -10% shift (Table 7c) the minimum stress ratio corresponds to a peak stress and is SR-P=1.46. This occurs on the weld connecting the skirt and upper support ring which was one of the lowest stress ratio locations at nominal frequency. The other location with low peak stress ratio in the nominal frequency case, namely the junction between the inner hood and thin closure plate, now has a somewhat higher stress ratio (SR-P=1.72). Finally, the minimum alternating stress ratio, SR-a=1.76 and occurs at the junction between the middle hood and thin closure plate. Rev 1

For the +10% frequency shift (Table 7d), the minimum stress ratio is now identified with an alternating stress and assumes a significantly smaller value, SR-a=1.33. This is a localized peak since the next smallest alternating stress ratio is much higher, SR-a=1.96. Both stress ratios occur on the weld fixing the reinforcement strip to the middle hood in the vicinity of the hood / side panel junction. The peak stress ratios and locations do not change as much, with the value at the skirt/upper support ring weld remaining essentially unchanged (SR-P=1.54) and the one at the inner hood / thin closure plate junction increasing to SR-P=1.82. Rev 1

In summary, the general picture that emerges is that at 115% CLTP loads the frequency shifts significantly affect the minimum stress ratios and reposition the peak stress locations to different parts of the structure. These indicate that the dryer has a rich modal structure so that shifting load frequencies results in the excitation of different modes.

Table 7a. Locations with minimum stress ratios for 1/8th scale at 115% CLTP conditions. Stress ratios are grouped according to stress type (peak – SR-P; or alternating – SR-a) and location (away from a weld or at a weld). Bold text indicates minimum stress ratio of any type on the structure. Locations are depicted in Figure 19.

Stress Ratio	Location	Weld	Location (in.)				Stress Intensity (psi)			Stress Ratio	
			x	y	z	node	Pm	Pm+Pb	S_{alt}	SR-P	SR-a
SR-P	1. Inner hood near thin closure plate	No	109.0	-27.6	95.3	44886	7017	10033	1908	2.61	6.48
SR-P	**1. Inner hood / thin closure plate**	**Yes**	**-108.4**	**-27.9**	**94.9**	**88252**	**6595**	**9778**	**2907**	**1.53**	**2.36**
"	2. Skirt / upper support ring	"	-118.8	-0.6	-2.0	79487	2556	9778	1276	1.54	5.38
"	3. Outer hood bottom / cover plate	"	59.1	101.4	7.5	93493	1793	7688	3431	1.96	2.00
SR-a	1. Inner hood (half-height)	No	27.9	36.0	50.5	42098	1609	4015	3549	6.84	3.48
"	2. Middle hood (1/3 height)	"	25.6	69.3	29.9	37254	608	3838	3253	7.15	3.80
"	3. Middle hood (half-height)	"	-25.2	67.1	53.3	37915	817	3642	3230	7.54	3.83
SR-a	1. Drain channel (bottom) / skirt	Yes	118.2	-12.0	-94.3	93818	2219	3705	3496	4.07	1.96
"	2. Outer hood bottom / cover plate	"	59.1	101.4	7.5	93493	1793	7688	3431	1.96	2.00
"	3. Middle hood / thin closure plate	"	-84.7	59.3	95.0	87837	3004	4328	3151	3.35	2.18

See Table 6a for locations nomenclature.

Table 7b. Locations with minimum stress ratios for 1/8th scale at 115% CLTP conditions with frequency shifts. Stress ratios at every node are recorded as the lowest stress ratio identified during the frequency shifts. Stress ratios are grouped according to stress type (peak – SR-P; or alternating – SR-a) and location (away from a weld or at a weld). Bold text indicates minimum stress ratio of any type on the structure. Locations are depicted in Figure 20.

Stress Ratio	Location	Weld	Freq. Shift	Location (in.)				Stress Intensity (psi)			Stress Ratio	
				x	y	z	node	Pm	Pm+Pb	S_{alt}	SR-P	SR-a
SR-P	1. Inner hood near thin closure plate	No	+2.5%	109.0	-27.6	95.3	44886	7209	10277	2151	2.54	5.75
SR-P	1. Skirt / upper support ring	Yes	+2.5%	-118.8	-0.6	-2.0	79487	2689	10329	1661	1.46	4.14
"	2. Inner hood / thin closure plate	"	0%	-108.4	-27.9	94.9	88252	6595	9778	3440	1.53	2.00
"	3. Outer hood bottom / cover plate	"	+2.5%	59.1	101.4	7.5	93493	1836	8525	3807	1.77	1.80
"	4. Inner bottom plate /vane bank side plate	"	-10%	118.8	-14.4	7.5	86577	4576	6339	908	2.20	7.56
SR-a	1. Middle hood, mid-section	No	-5%	-91.7	67.6	49.6	36637	1242	3958	3582	6.94	3.45
"	2. Inner hood (half-height)	"	0%	27.9	36.0	50.5	42098	1609	4015	3549	6.84	3.48
SR-a	**1. Middle hood / reinforcement strip**	**Yes**	**+10%**	**-98.0**	**69.3**	**29.9**	**84521**	**1411**	**5345**	**5147**	**2.82**	**1.33**
"	2. Drain channel (bottom) / skirt	"	+2.5%	118.2	-12.0	-94.2	93818	2507	4444	4246	3.40	1.62
"	3. Middle hood / thin closure plate	"	-10%	-84.7	-59.3	95.0	85091	3724	5937	3912	2.54	1.76
	4. Outer hood bottom / cover plate	"	+2.5%	59.1	101.4	7.5	93493	1836	8525	3807	1.77	1.80
	5. Inner hood / thin closure plate	"	-10%	-108.4	-28.2	94.5	88253	2195	4910	3701	3.07	1.86
	6. Middle hood / reinforcement strip	"	-5%	-98.8	67.7	48.8	84518	1234	3845	3515	3.93	1.95
	7. Thin closure plate, top cover / outer vane bank side plate	"	-5%	-84.7	77.4	96.1	92445	1719	4188	3408	3.60	2.02

Rev 1

See Table 6a for locations nomenclature.

Table 7c. Locations with minimum stress ratios for 1/8th scale at 115% CLTP conditions with -10% frequency shift. Stress ratios are grouped according to stress type (peak – SR-P; or alternating – SR-a) and location (away from a weld or at a weld). Bold text indicates minimum stress ratio of any type on the structure. Locations are depicted in Figure 21.

Stress Ratio	Location	Weld	Location (in.)				Stress Intensity (psi)			Stress Ratio	
			x	y	z	node	Pm	Pm+Pb	S_{alt}	SR-P	SR-a
SR-P	1. Inner hood near thin closure plate	No	109.0	-27.6	95.3	44886	6815	9784	1439	2.69	8.59
SR-P	**1. Skirt / upper support ring**	**Yes**	**118.8**	**0.6**	**-2.0**	**88325**	**2550**	**10312**	**1517**	**1.46**	**4.53**
"	2. Inner hood / thin closure plate	"	108.4	27.9	94.9	85409	5845	8535	3594	1.72	1.91
"	3. Inner bottom plate /vane bank side plate	"	118.8	-14.4	7.5	86577	4576	6339	908	2.20	7.56
SR-a	1. Thin closure plate, near middle hood junction	No	-84.7	60.1	94.7	28598	714	3442	3106	7.97	3.98
SR-a	1. Middle hood / thin closure plate	Yes	-84.7	-59.3	95.0	85091	3724	5937	3912	2.54	1.76
"	2. Inner hood / thin closure plate	"	-108.4	-28.2	94.5	88253	1977	4910	3701	3.07	1.86
"	3. Thin closure plate, top cover / outer vane bank side plate	"	-84.7	77.4	94.6	92443	722	3726	3379	4.05	2.03
"	4. Drain channel (bottom) / skirt	"	73.8	-93.1	-94.2	93833	1191	5531	3221	2.73	2.13
"	5. Thin closure plate, top cover / middle vane bank side plate	"	-108.4	-45.9	94.4	90710	1327	4210	3172	3.59	2.17
"	6. Outer hood bottom / cover plate	"	-28.4	101.4	7.5	93390	3193	3399	3017	3.15	2.28

Rev 1

See Table 6a for locations nomenclature.

Table 7d. Locations with minimum stress ratios for 1/8th scale at 115% CLTP conditions with +10% frequency shift. Stress ratios are grouped according to stress type (peak – SR-P; or alternating – SR-a) and location (away from a weld or at a weld). Bold text indicates minimum stress ratio of any type on the structure. Locations are depicted in Figure 22.

Stress Ratio	Location	Weld	Location (in.)				Stress Intensity (psi)			Stress Ratio	
			x	y	z	node	Pm	Pm+Pb	S_{alt}	SR-P	SR-a
SR-P	1. Inner hood near thin closure plate	No	109.0	-27.6	95.3	44886	6807	9640	1359	2.69	9.09
SR-P	1. Skirt / upper support ring	Yes	-118.8	-0.6	-2.0	79487	2513	9832	1208	1.54	5.69
"	2. Inner hood / thin closure plate	"	108.4	27.9	94.9	85409	5541	8131	2272	1.82	3.02
"	3. Outer hood bottom / cover plate	"	59.1	101.4	7.5	93493	1669	6737	2328	2.24	2.95
"	4. Upper ring / thick closure plate / vane end plate	"	-118.8	14.4	7.5	85994	4272	5850	439	2.36	15.6
SR-a	1. Middle hood (near reinforcement strip)	No	-90.0	69.3	29.1	36721	1401	3755	3541	7.31	3.49
SR-a	**1. Middle hood / reinforcement strip**	**Yes**	**-98.0**	**69.3**	**29.9**	**84521**	**1196**	**5345**	**5147**	**2.82**	**1.33**
"	2. Middle hood / reinforcement strip	"	-98.4	-68.4	41.7	84399	843	3773	3496	4.00	1.96
"	3. Middle hood / thin closure plate	"	84.7	59.3	95.0	92526	3246	5038	3244	3.00	2.12
"	4. Middle hood / reinforcement strip	"	97.7	-69.8	18.0	84319	1112	2867	2785	5.27	2.47
"	5. Thin closure plate, top cover / outer vane bank side plate	"	-84.7	-77.4	96.1	82694	905	2847	2658	5.30	2.58

Rev 1

See Table 6a for locations nomenclature.

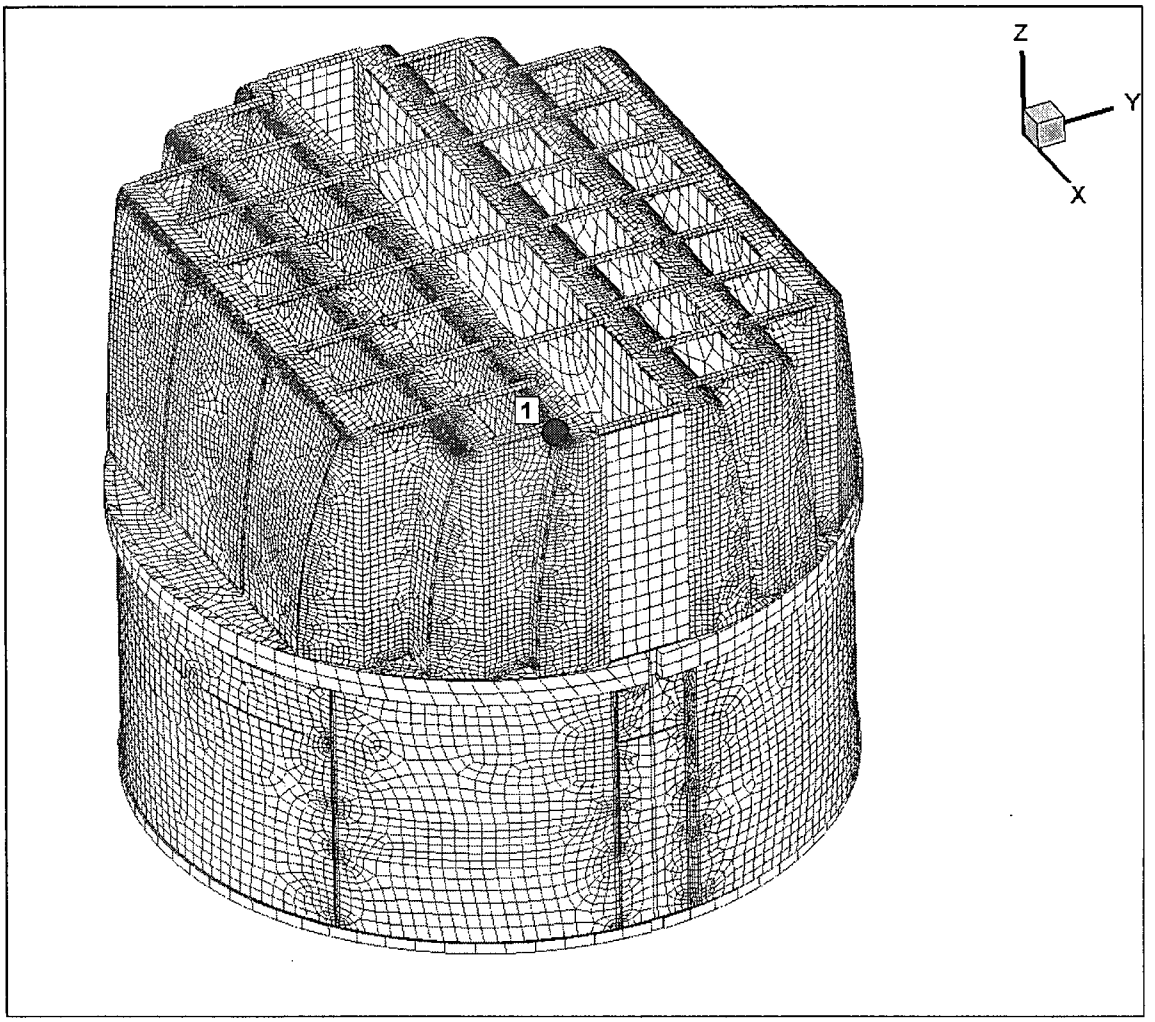

Figure 19a. Locations of minimum peak stress ratios, SR-P, at non-welds for 115% CLTP operation. Numbers refer to the enumerated locations for SR-P values at welds in Table 7a.

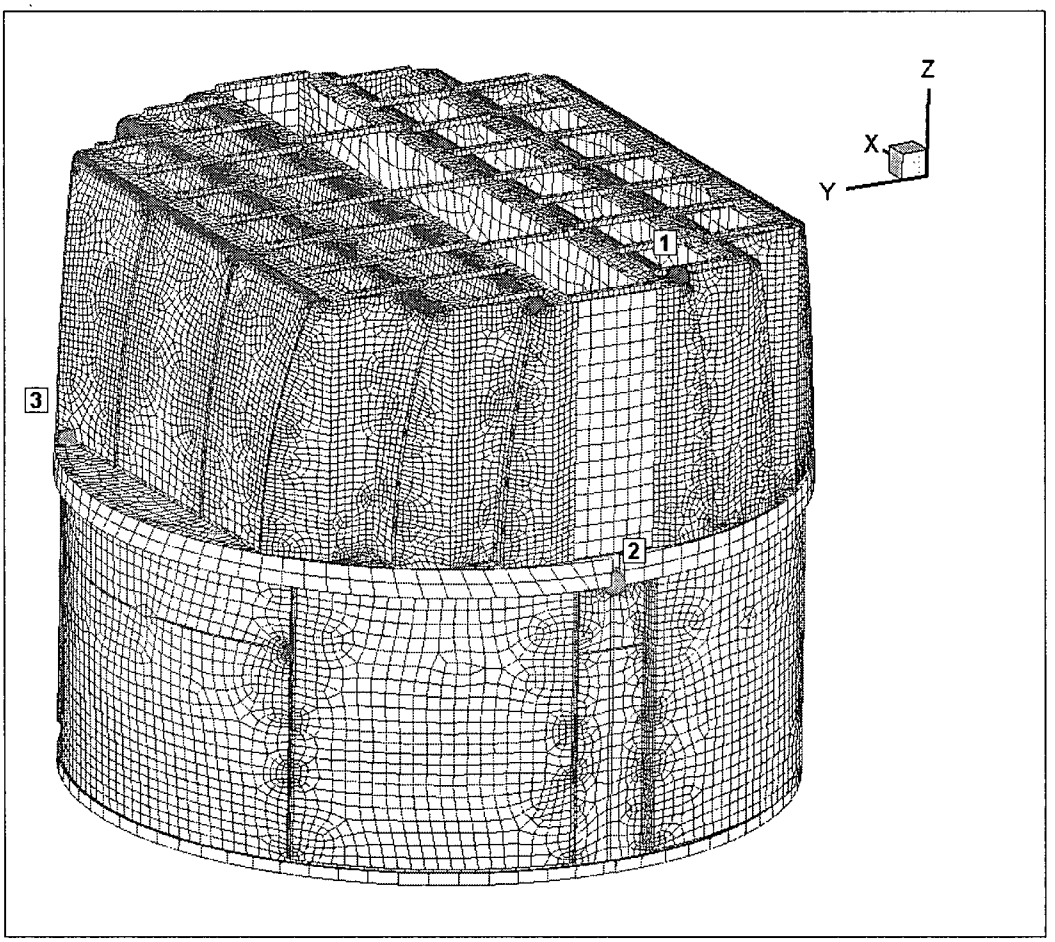

Figure 19b. Locations of minimum peak stress ratios, SR-P, at welds for 115% CLTP operation. Numbers refer to the enumerated locations for SR-P values at welds in Table 7a.

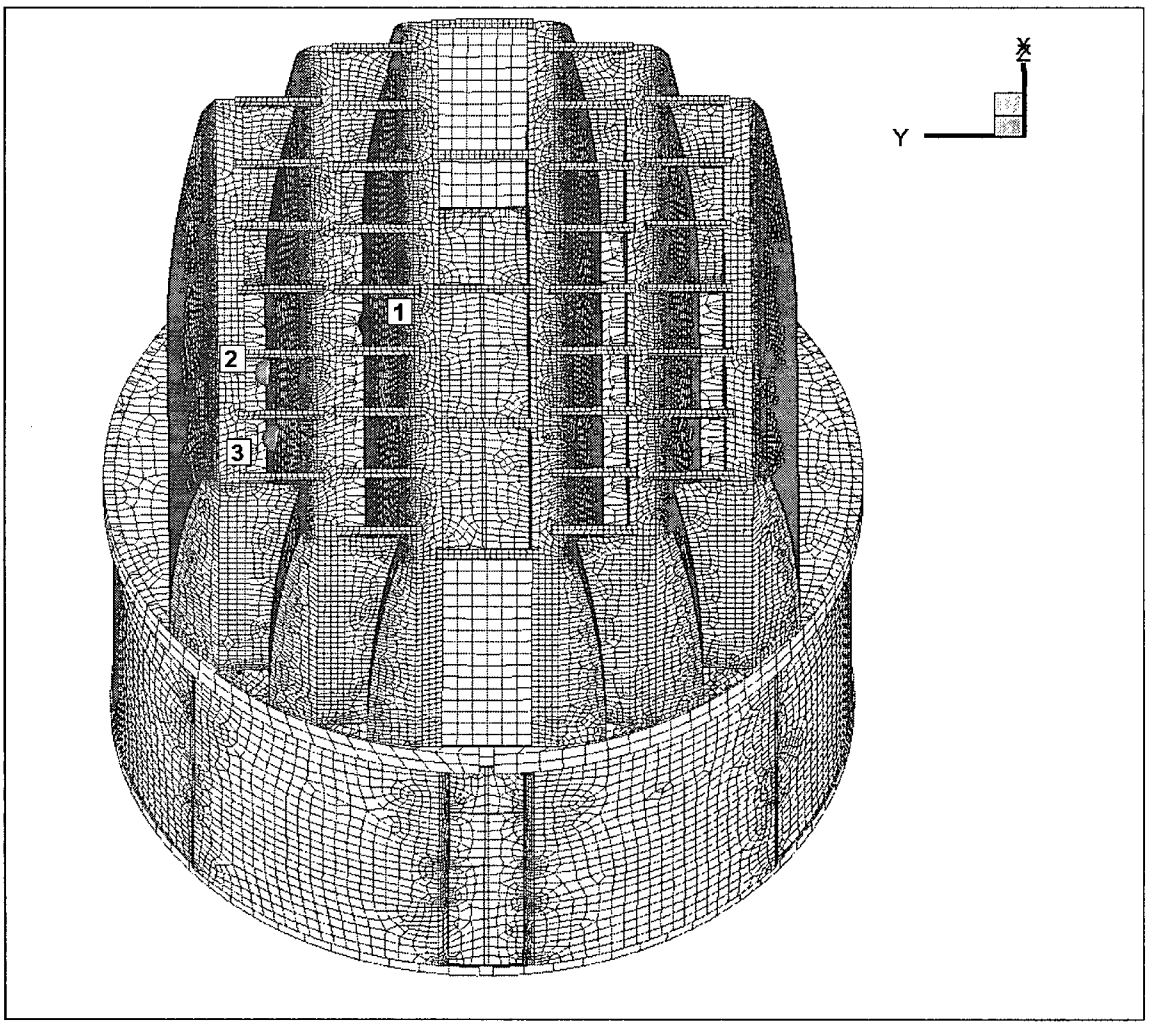

Figure 19c. Locations of minimum alternating stress ratios, SR-a, at non-welds for 115% CLTP operation. Numbers refer to the enumerated locations for SR-a values at non-welds in Table 7a.

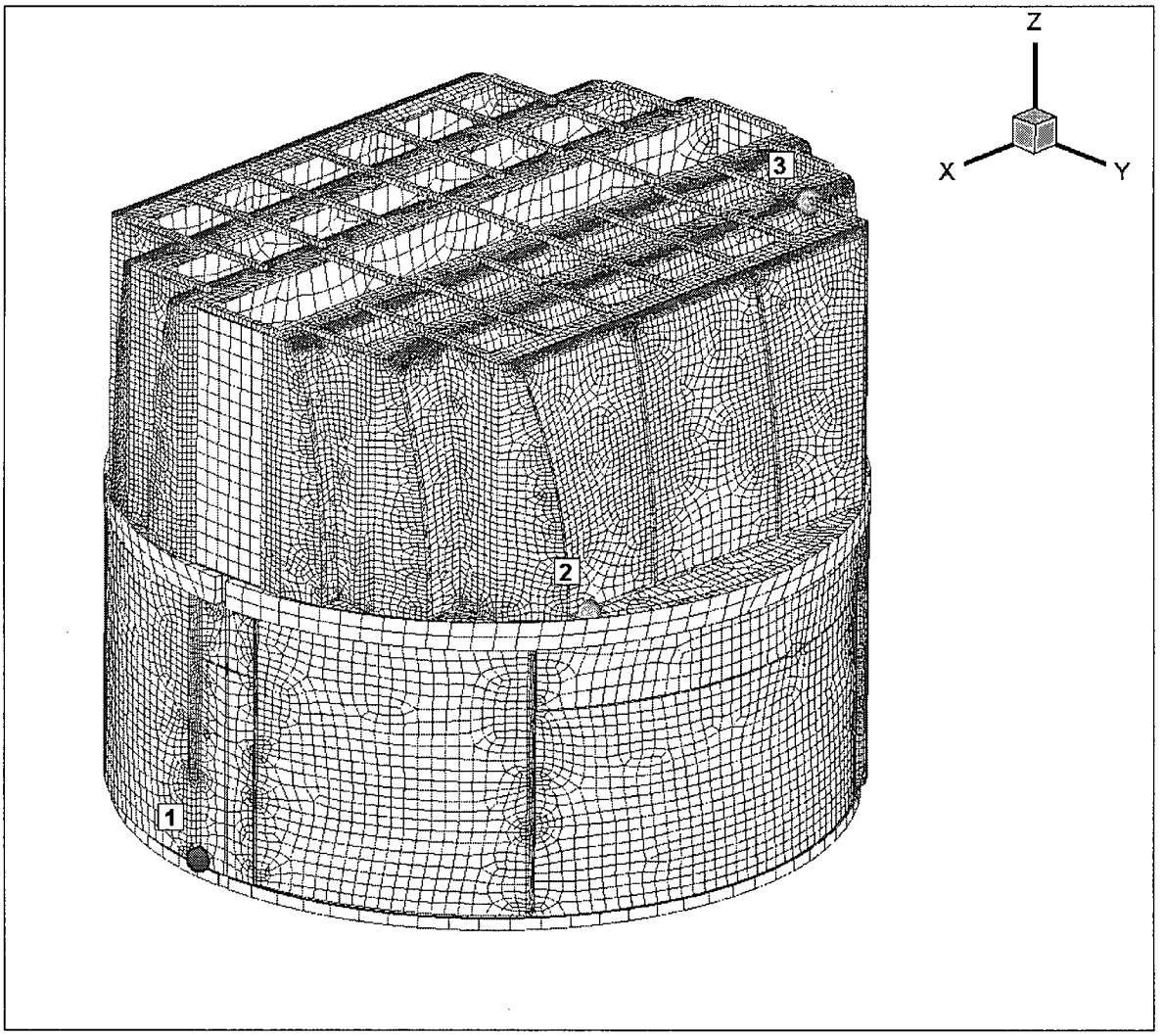

Figure 19d. Locations of minimum alternating stress ratios, SR-a, at welds for 115% CLTP operation. Numbers refer to the enumerated locations for SR-a values at welds in Table 7a.

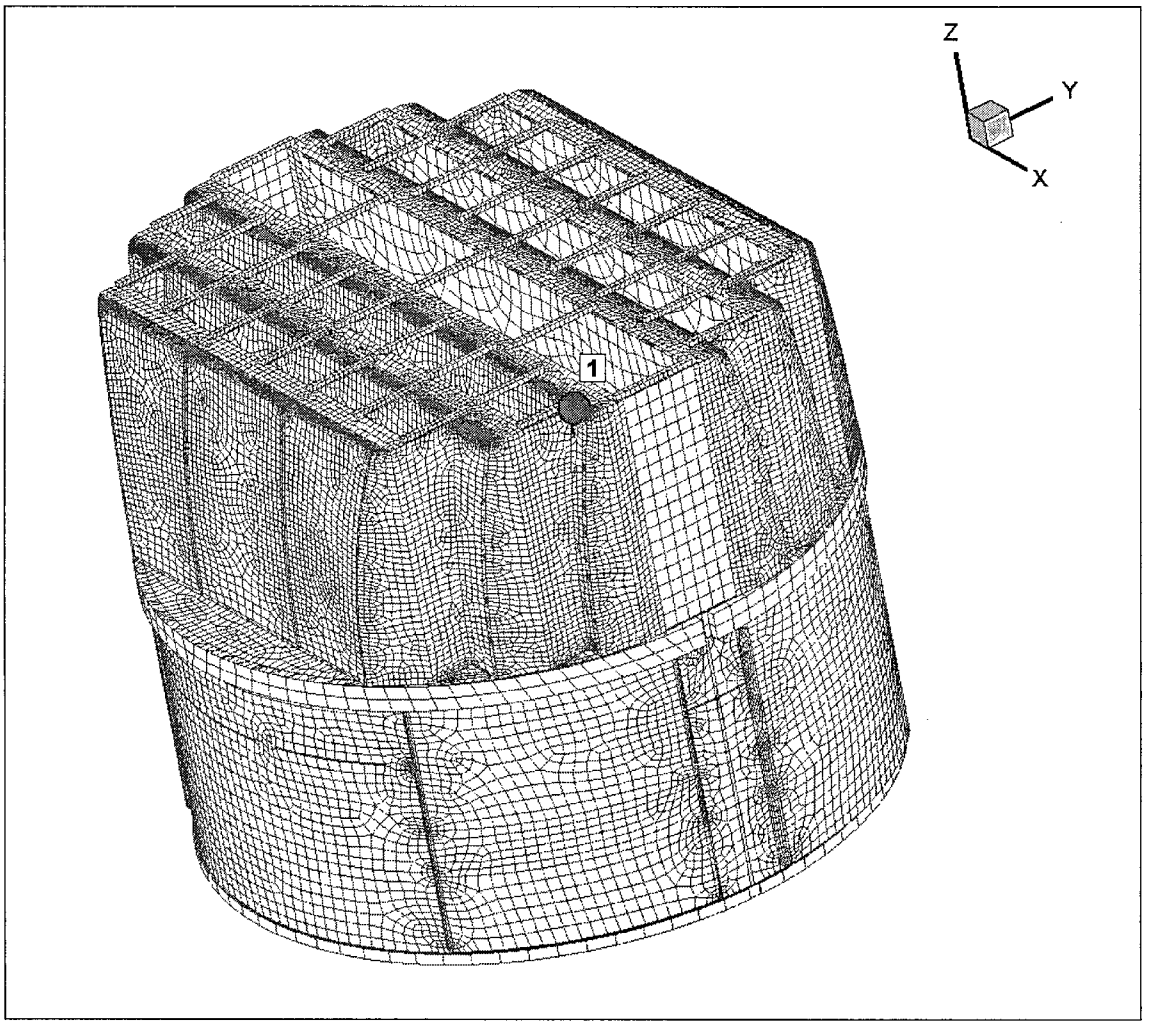

Rev 1

Figure 20a. Location of minimum peak stress ratio, SR-P, at non-welds for 115% CLTP operation with frequency shifts. The recorded stress ratio is the minimum value taken over all frequency shifts. The number refers to the enumerated location for SR-P values at welds in Table 7b.

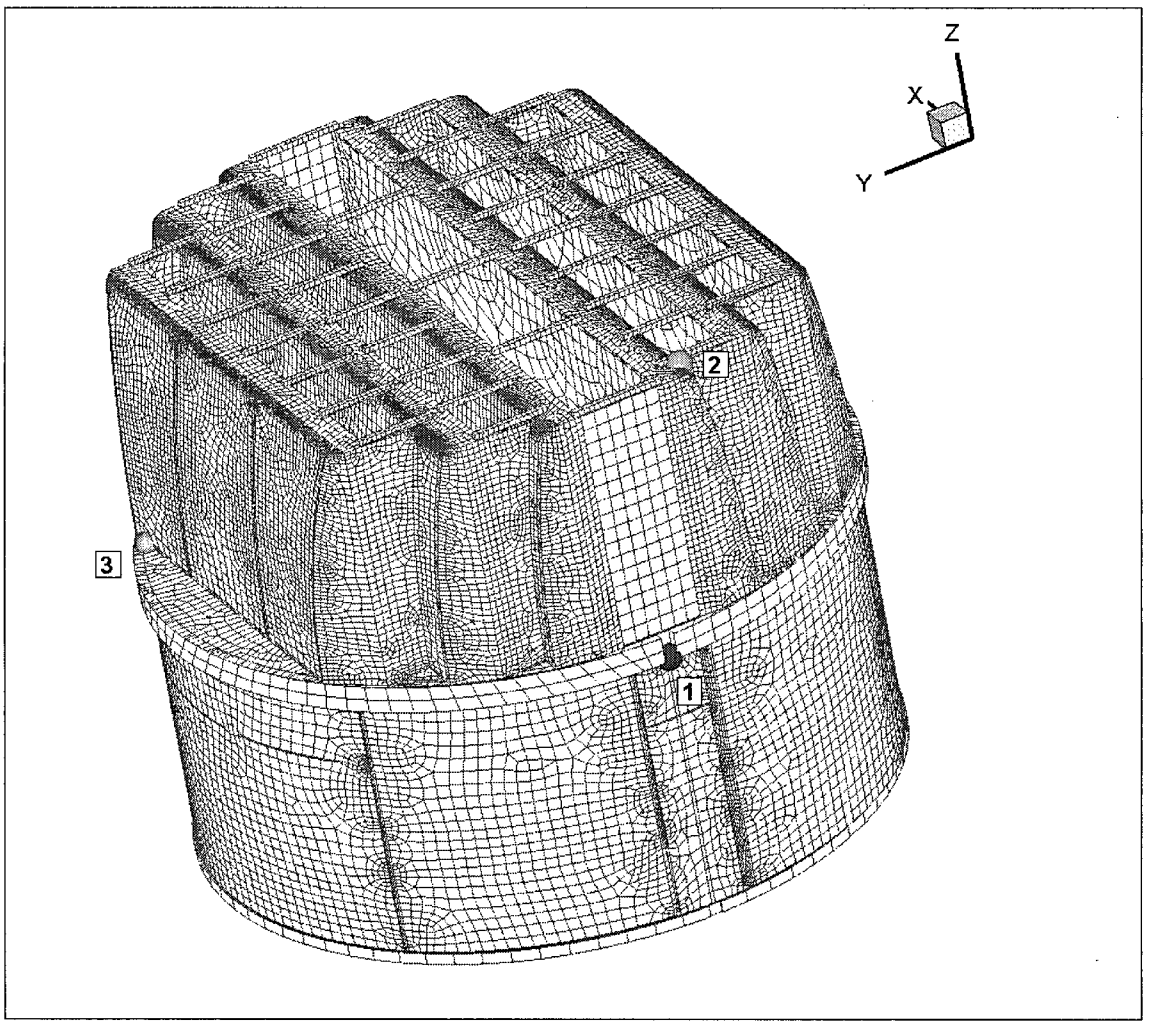

Rev 1

Figure 20b. Locations of minimum peak stress ratios, SR-P, at welds for 115% CLTP operation with frequency shifts. The recorded stress ratio at a node is the minimum value taken over all frequency shifts. Numbers refer to the enumerated locations for SR-P values at welds in Table 7b.

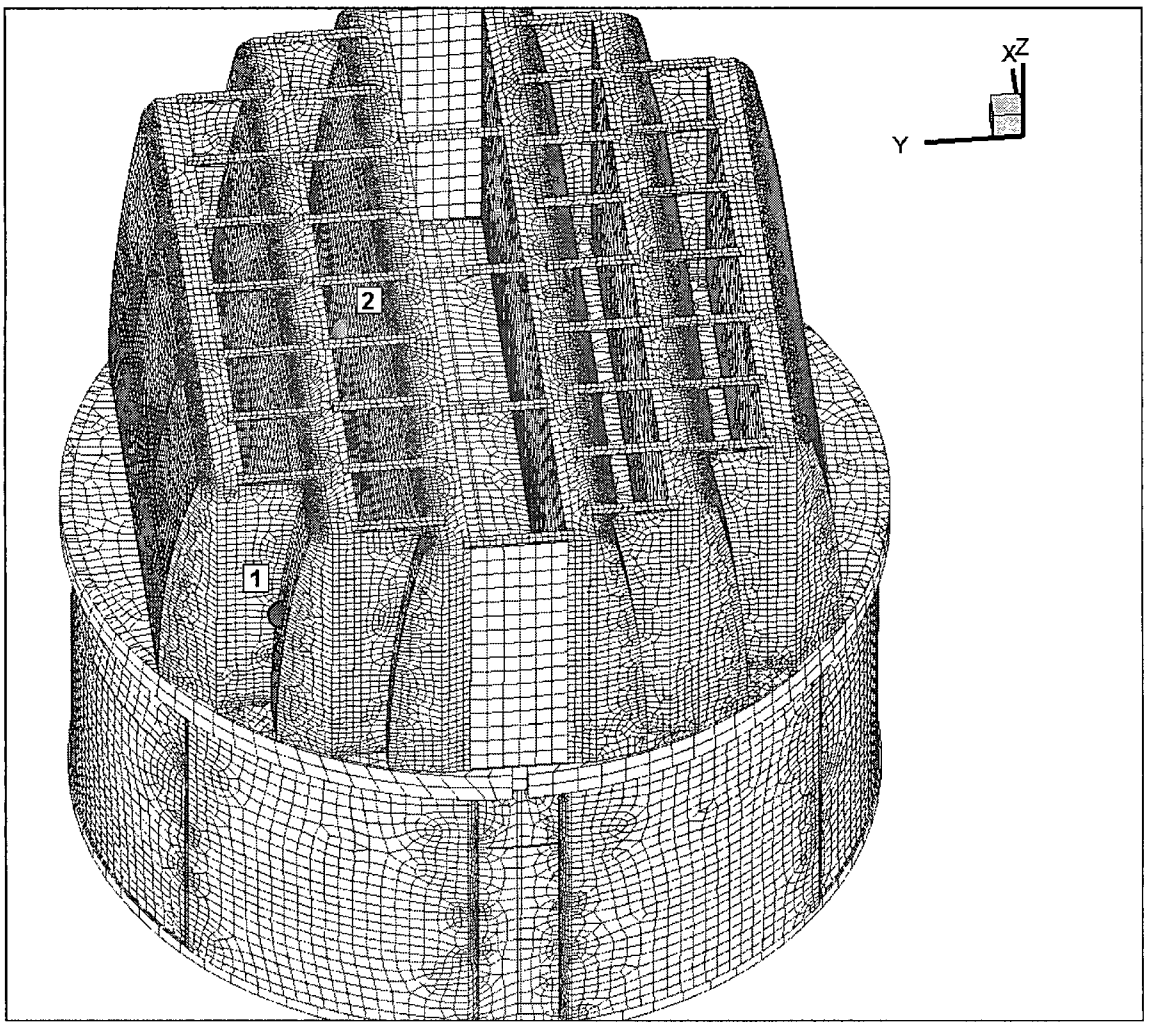

Rev 1

Figure 20c. Locations of minimum alternating stress ratios, SR-a, at non-welds for 115% CLTP operation with frequency shifts. The recorded stress ratio at a node is the minimum value taken over all frequency shifts. Numbers refer to the enumerated locations for SR-a values at non-welds in Table 7b.

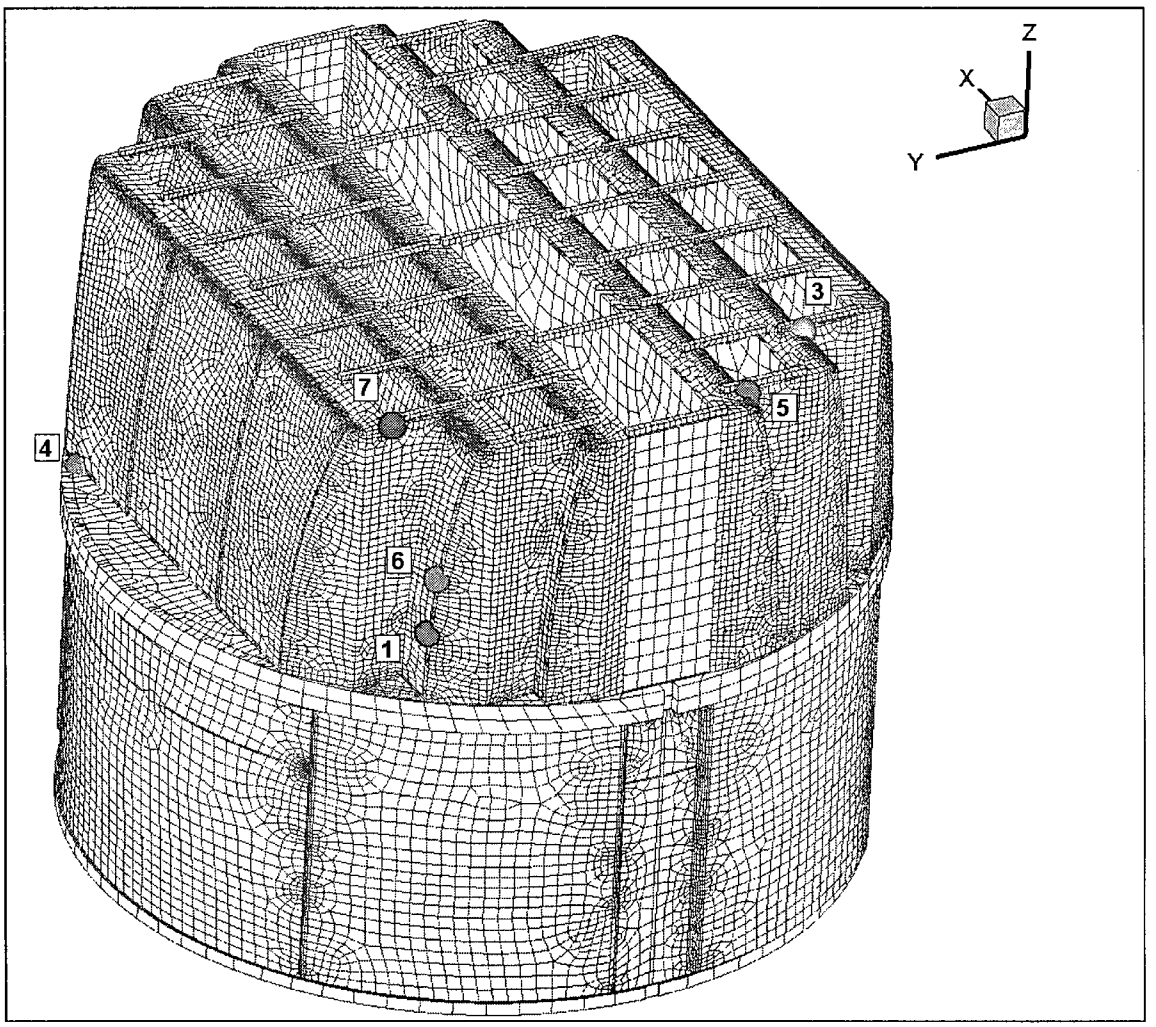

Rev 1

Figure 20d. Locations of minimum alternating stress ratios, SR-a, at welds for 115% CLTP operation with frequency shifts. The recorded stress ratio at a node is the minimum value taken over all frequency shifts. Numbers refer to the enumerated locations for SR-a values at welds in Table 7b. First view showing enumerated locations 1 and 3-7.

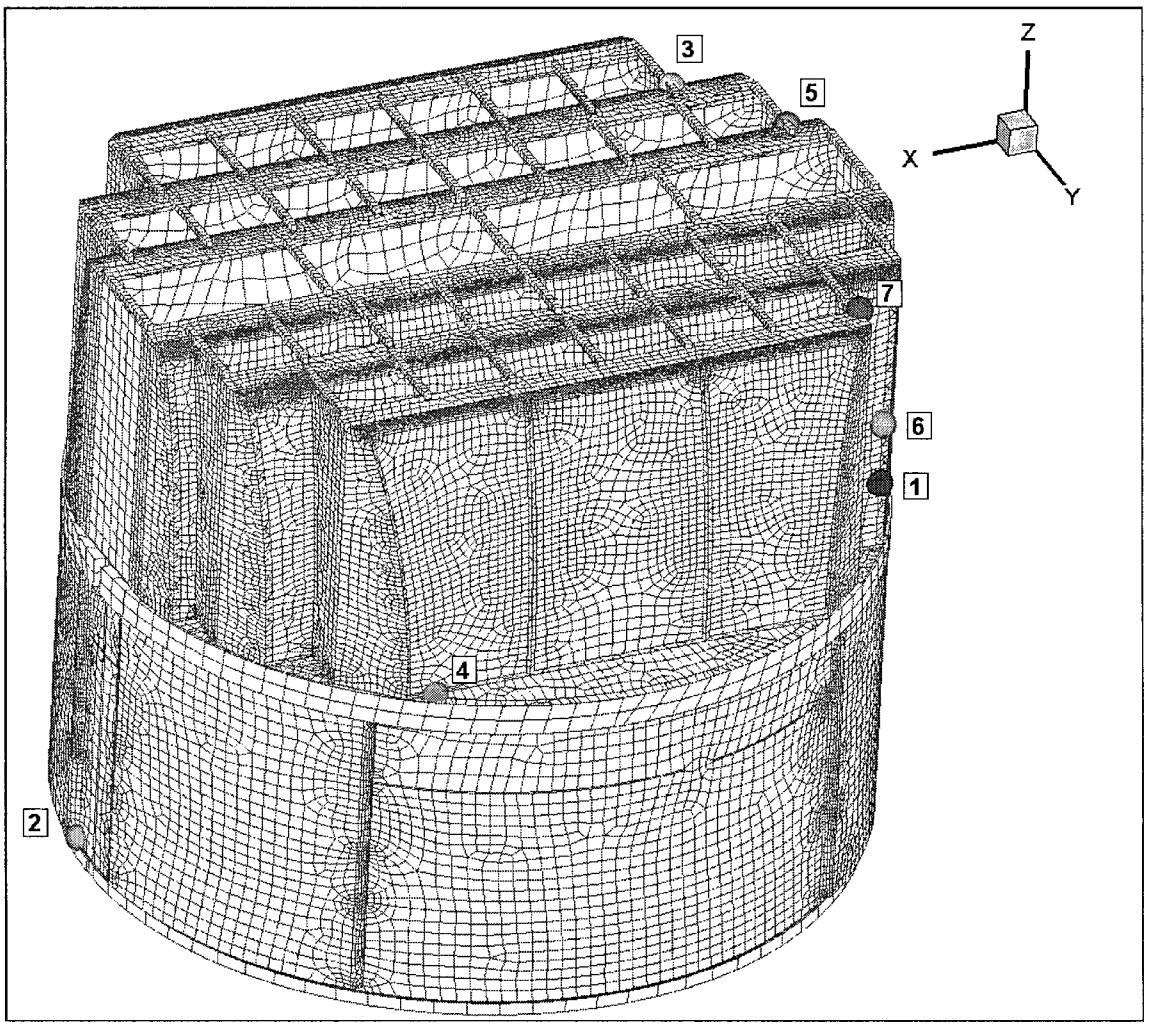

Rev 1

Figure 20e. Locations of minimum alternating stress ratios, SR-a, at welds for 115% CLTP operation with frequency shifts. The recorded stress ratio at a node is the minimum value taken over all frequency shifts. Numbers refer to the enumerated locations for SR-a values at welds in Table 7b.

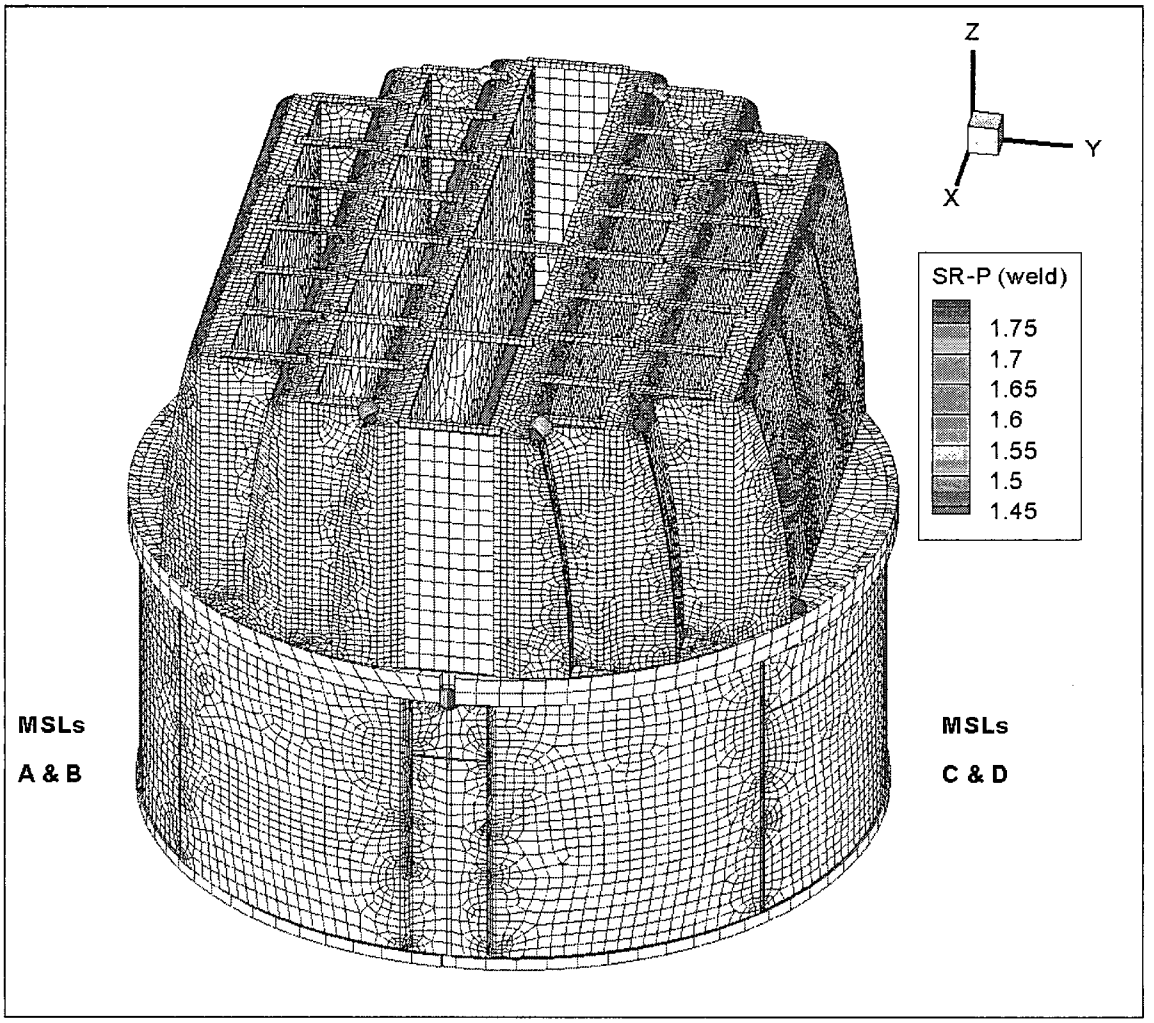

Rev 1

Figure 20f. Locations of minimum peak stress ratios, SR-P, at welds for 115% CLTP operation with frequency shifts. The recorded stress ratio at a node is the minimum value taken over all frequency shifts. This figure shows *all* nodes with SR-P<1.8. View 1, essentially along –X axis.

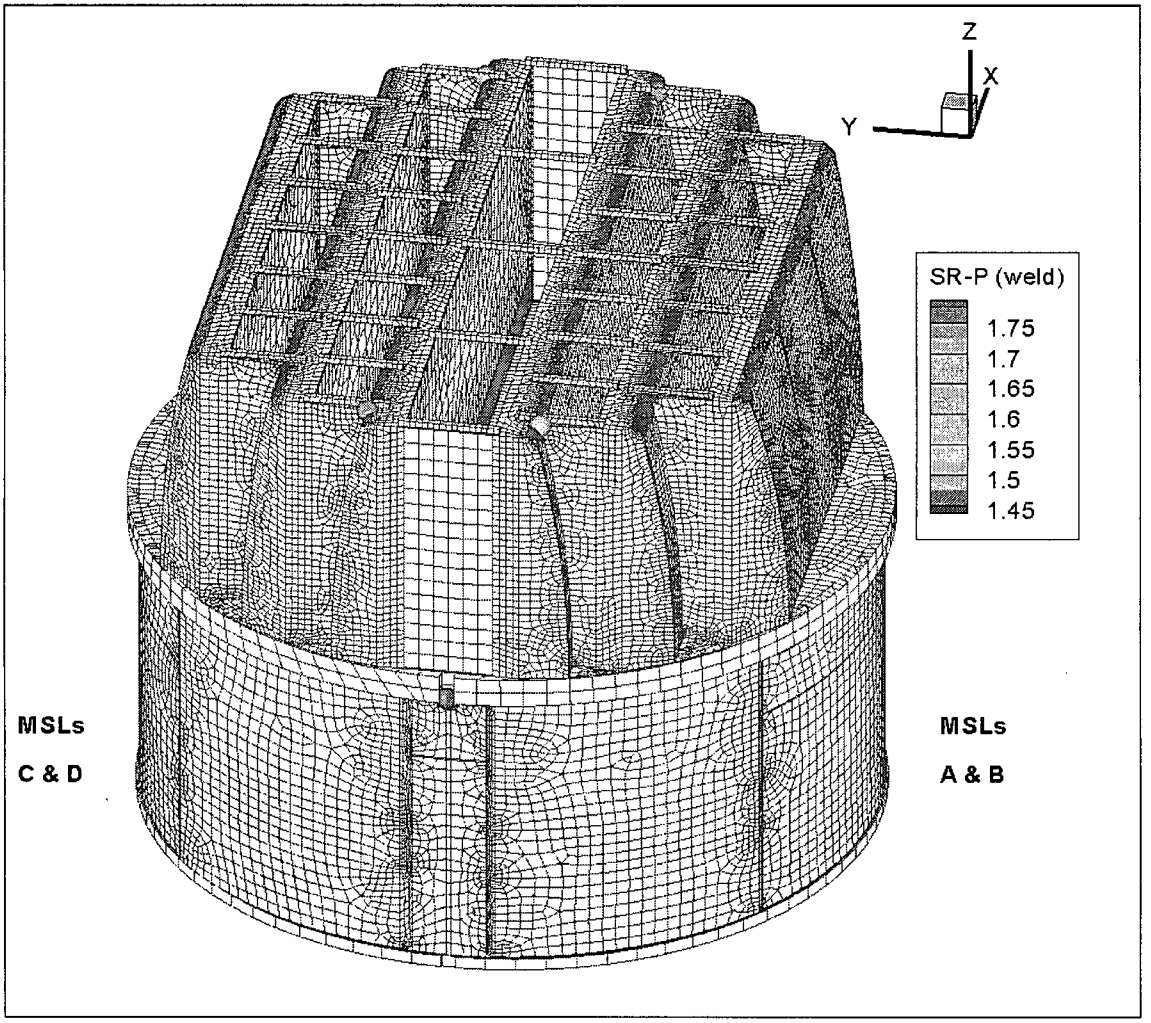

Rev 1

Figure 20g. Locations of minimum peak stress ratios, SR-P, at welds for 115% CLTP operation with frequency shifts. The recorded stress ratio at a node is the minimum value taken over all frequency shifts. This figure shows *all* nodes with SR-P<1.8. View 2, essentially along +X axis.

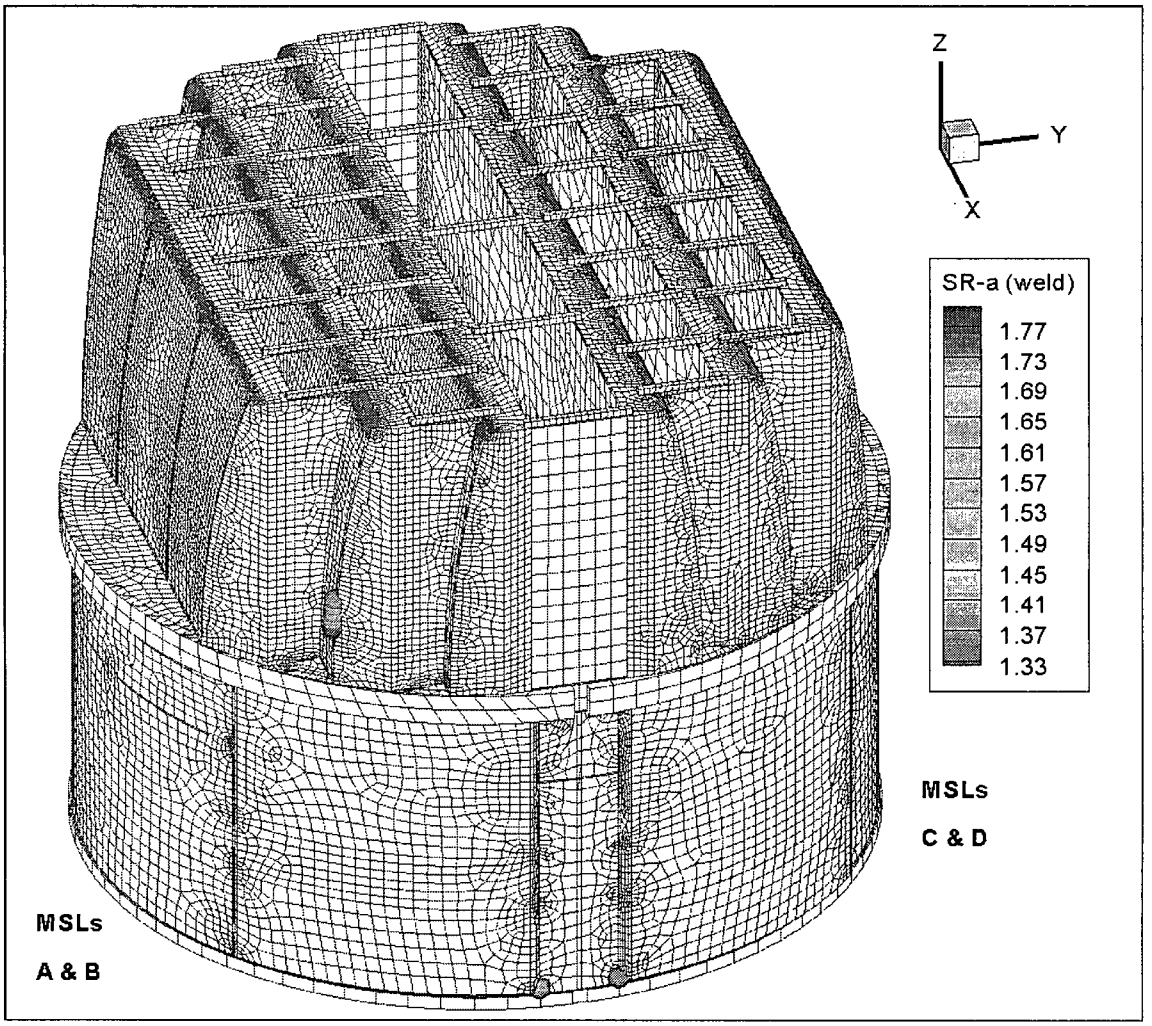

Rev 1

Figure 20h. Locations of minimum alternating stress ratios, SR-a, at welds for 115% CLTP operation with frequency shifts. The recorded stress ratio at a node is the minimum value taken over all frequency shifts. This figure shows *all* nodes with SR-a<1.8. View 1, essentially along –X axis.

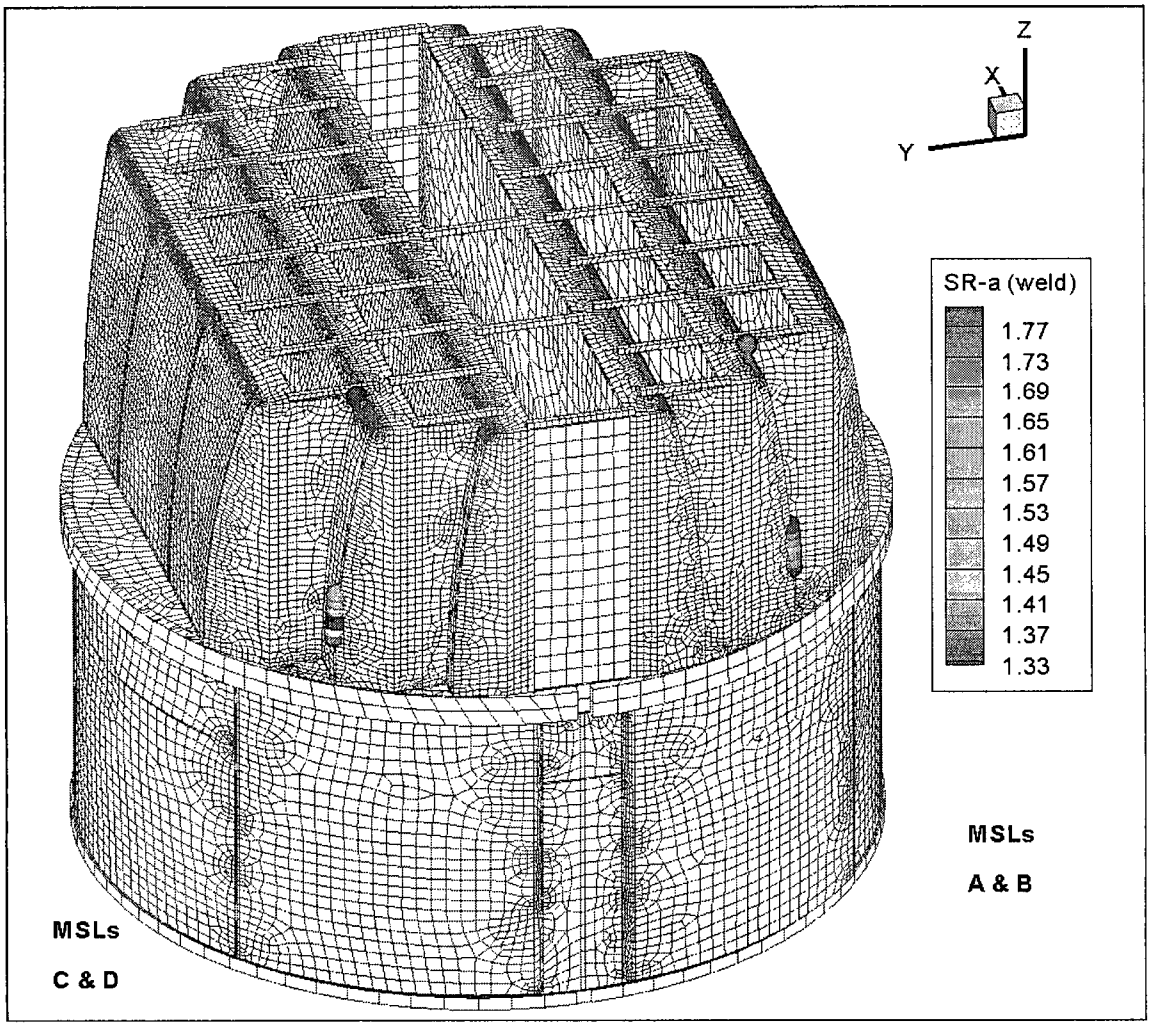

Rev 1

Figure 20i. Locations of minimum alternating stress ratios, SR-a, at welds for 115% CLTP operation with frequency shifts. The recorded stress ratio at a node is the minimum value taken over all frequency shifts. This figure shows *all* nodes with SR-a<1.8. View 1, essentially along +X axis.

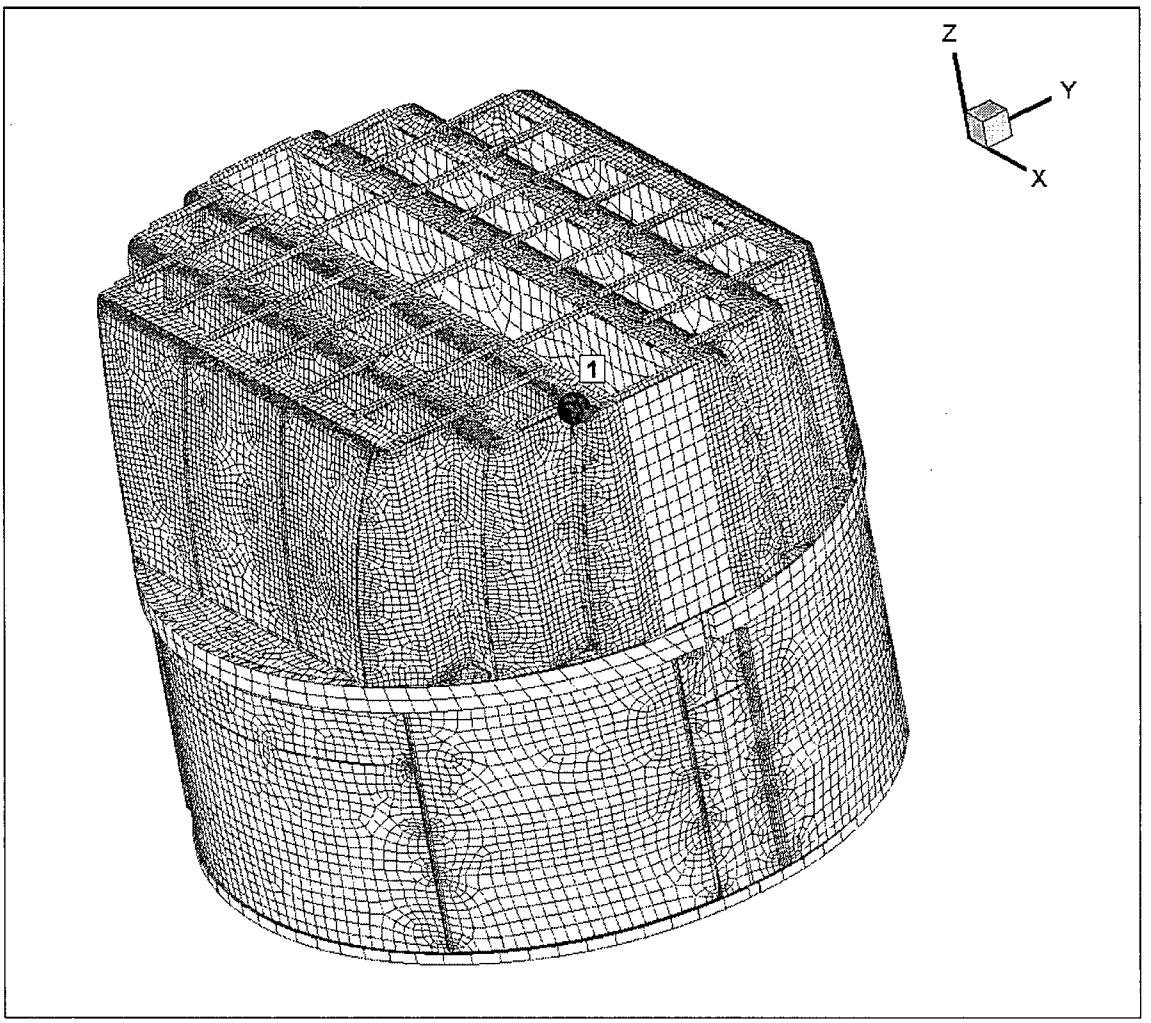

Rev 1

Figure 21a. Locations of minimum peak stress ratios, SR-P, at non-welds for 115% CLTP operation with -10% frequency shift. Numbers refer to the enumerated locations for SR-P values at welds in Table 7c.

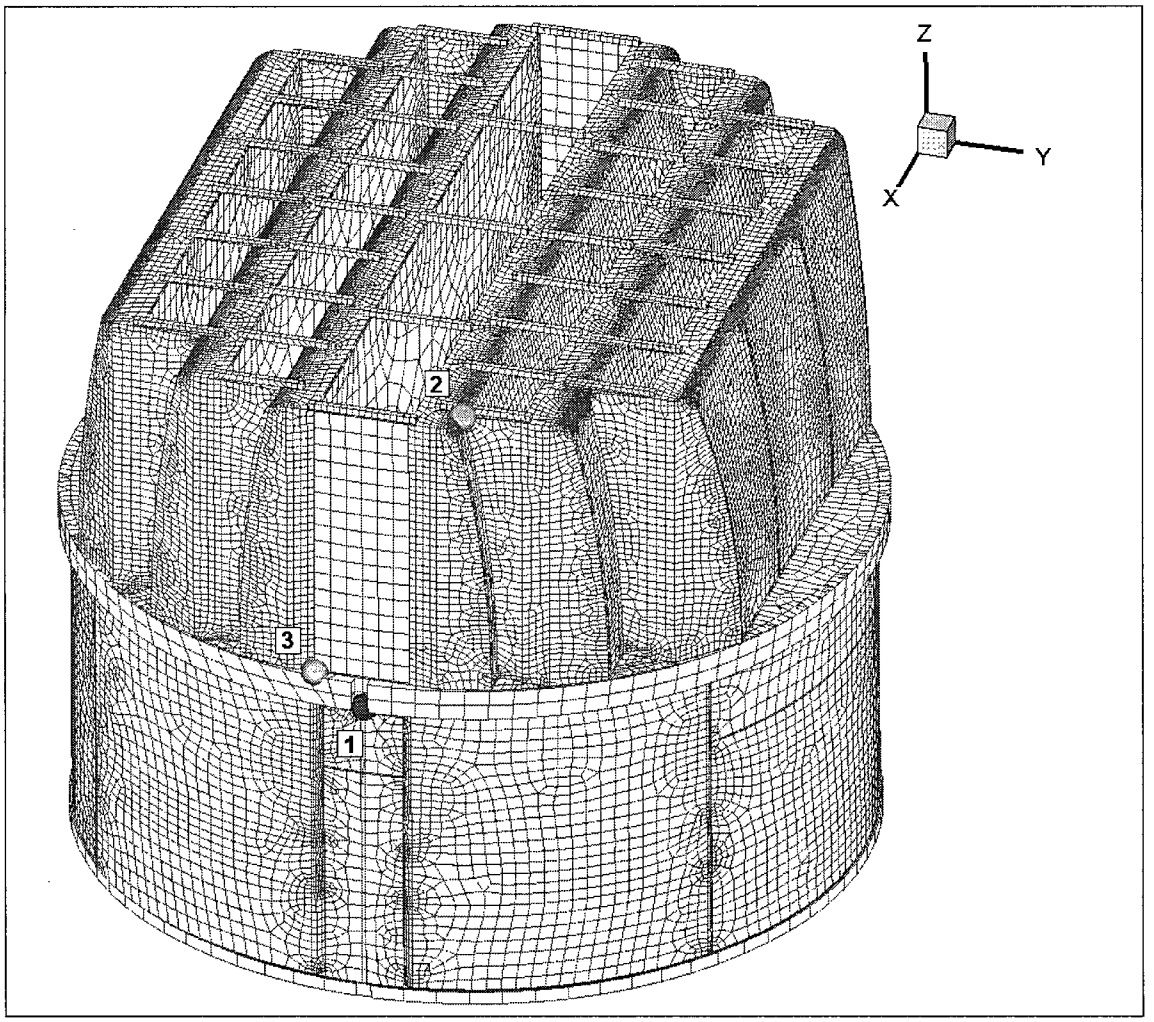

Rev 1

Figure 21b. Locations of minimum peak stress ratios, SR-P, at welds for 115% CLTP operation with -10% frequency shift. Numbers refer to the enumerated locations for SR-P values at welds in Table 7c.

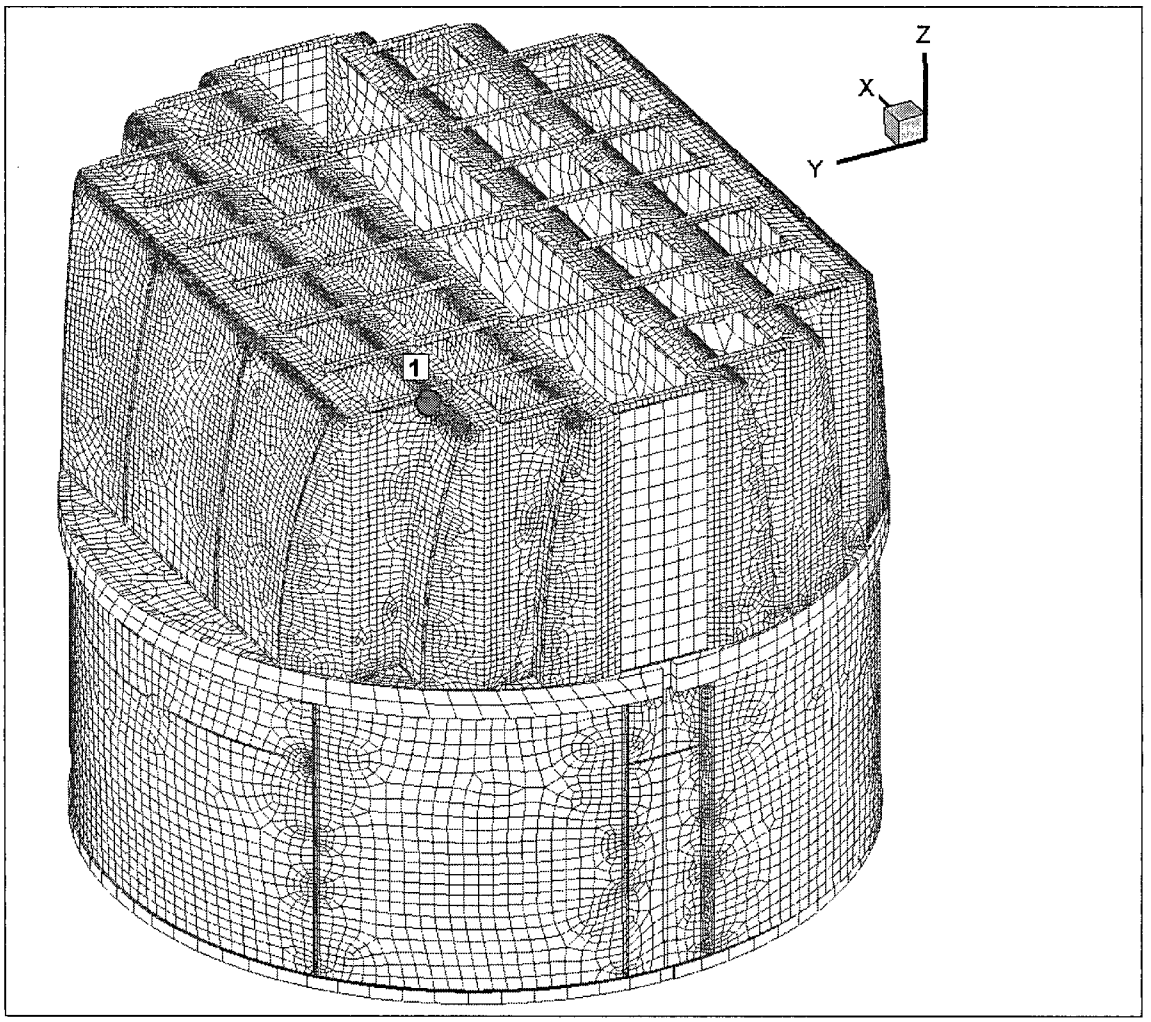

Rev 1

Figure 21c. Locations of minimum alternating stress ratios, SR-a, at non-welds for 115% CLTP operation with -10% frequency shift. Numbers refer to the enumerated locations for SR-a values at non-welds in Table 7c.

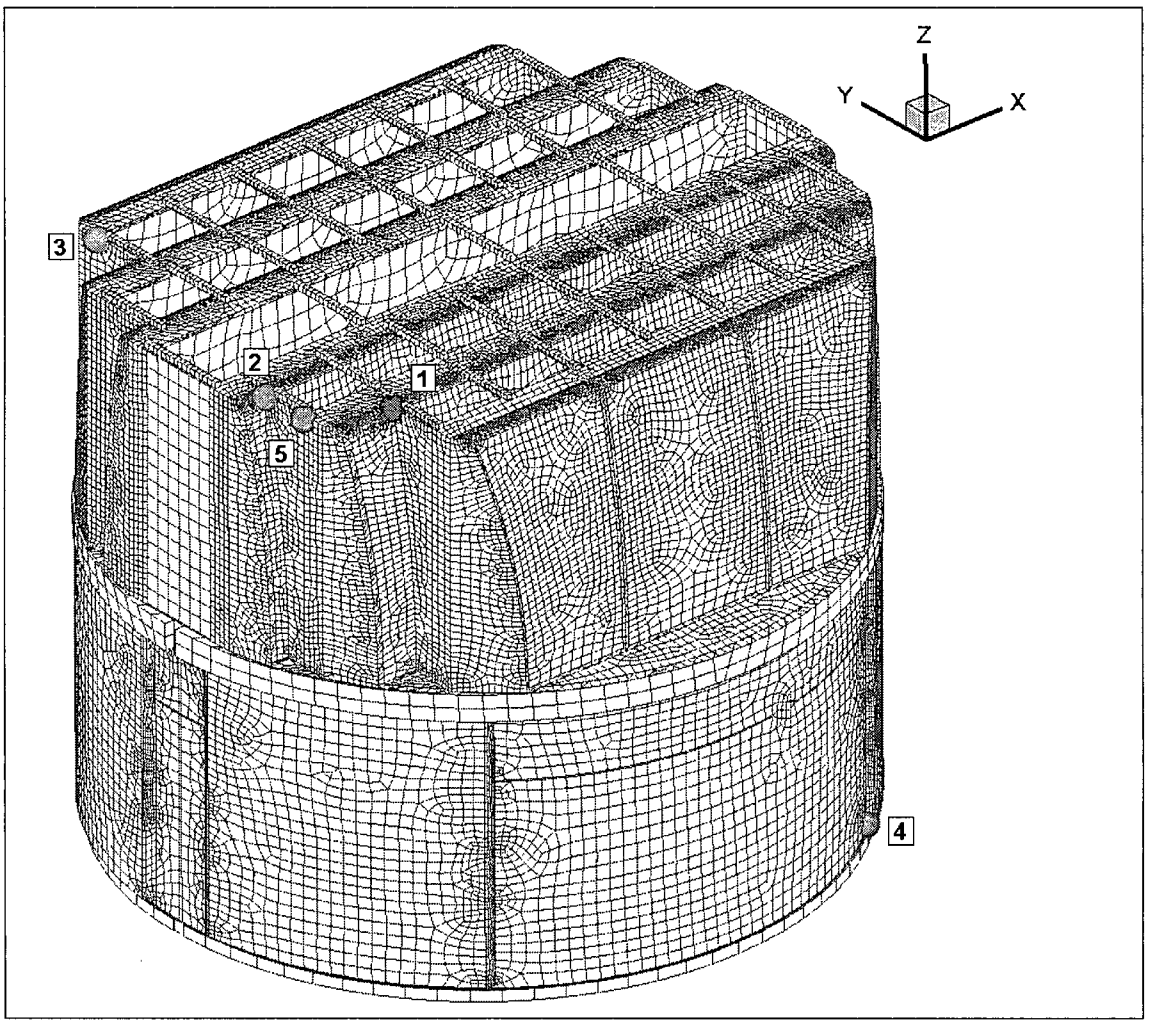

Rev 1

Figure 21d. Locations of minimum alternating stress ratios, SR-a, at welds for 115% CLTP operation with -10% frequency shift. Numbers refer to the enumerated locations for SR-a values at welds in Table 7c.

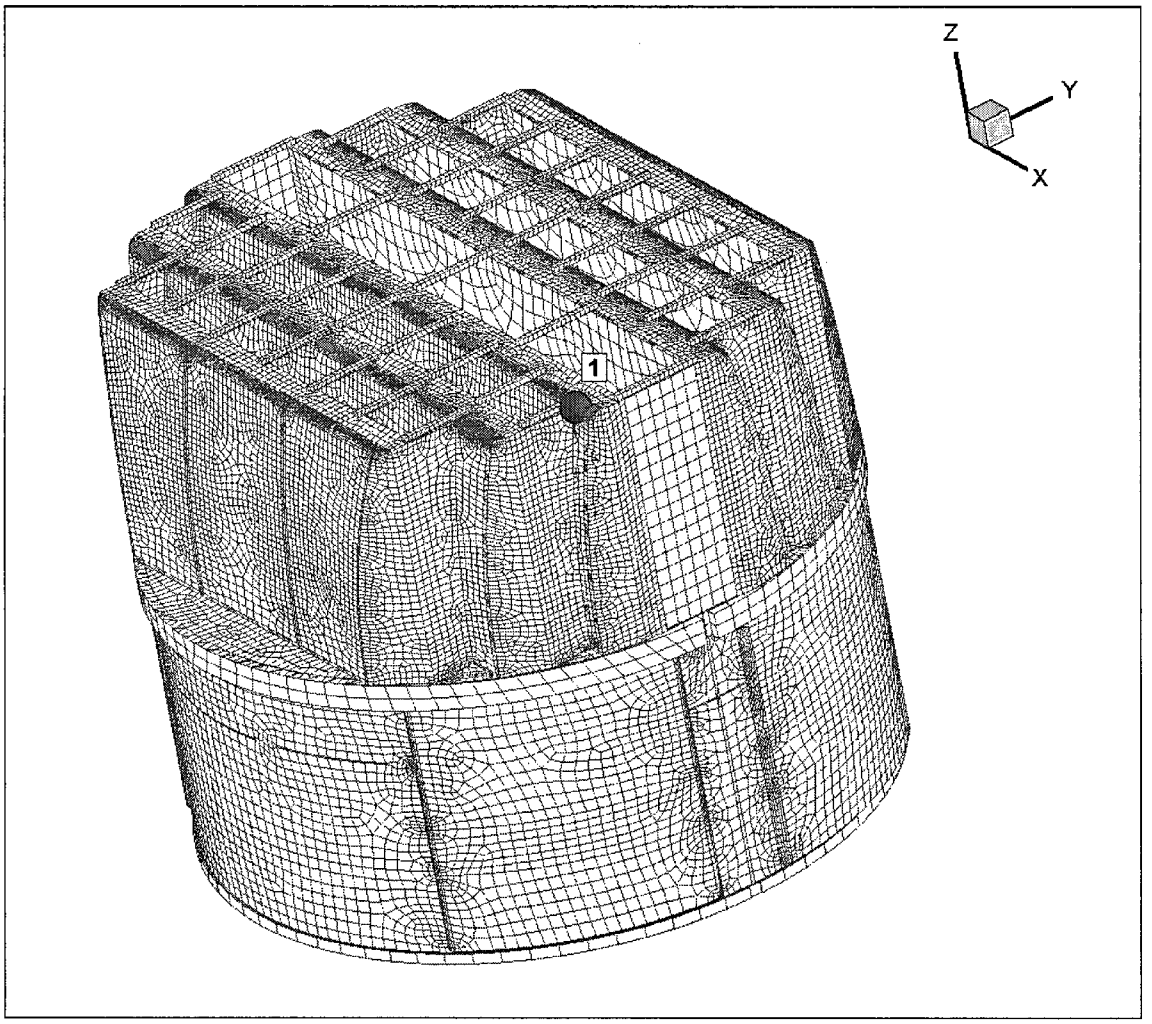

Rev 1

Figure 22a. Locations of minimum peak stress ratios, SR-P, at non-welds for 115% CLTP operation with +10% frequency shift. Numbers refer to the enumerated locations for SR-P values at welds in Table 7d.

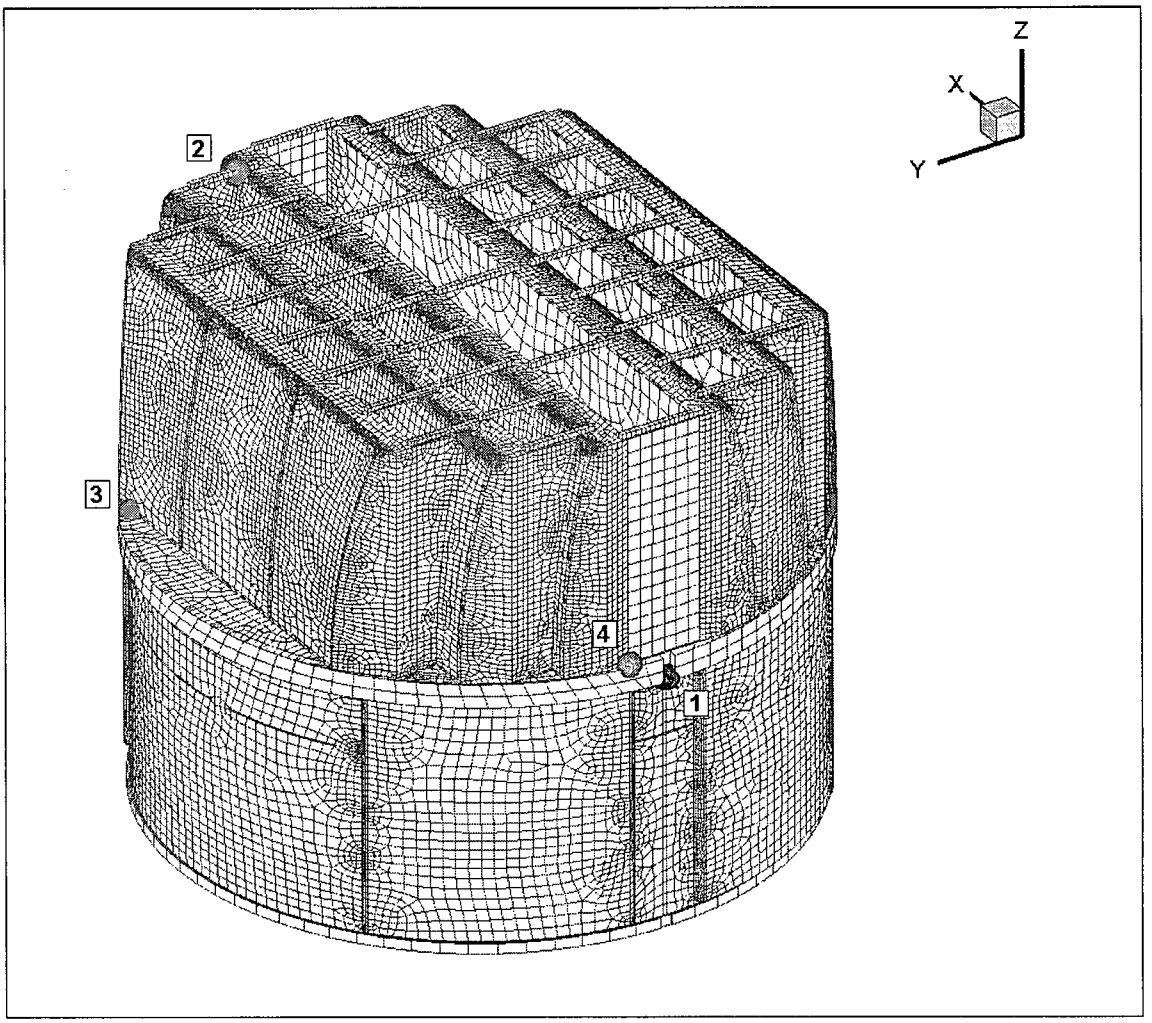

Rev 1

Figure 22b. Locations of minimum peak stress ratios, SR-P, at welds for 115% CLTP operation with +10% frequency shift. Numbers refer to the enumerated locations for SR-P values at welds in Table 7d.

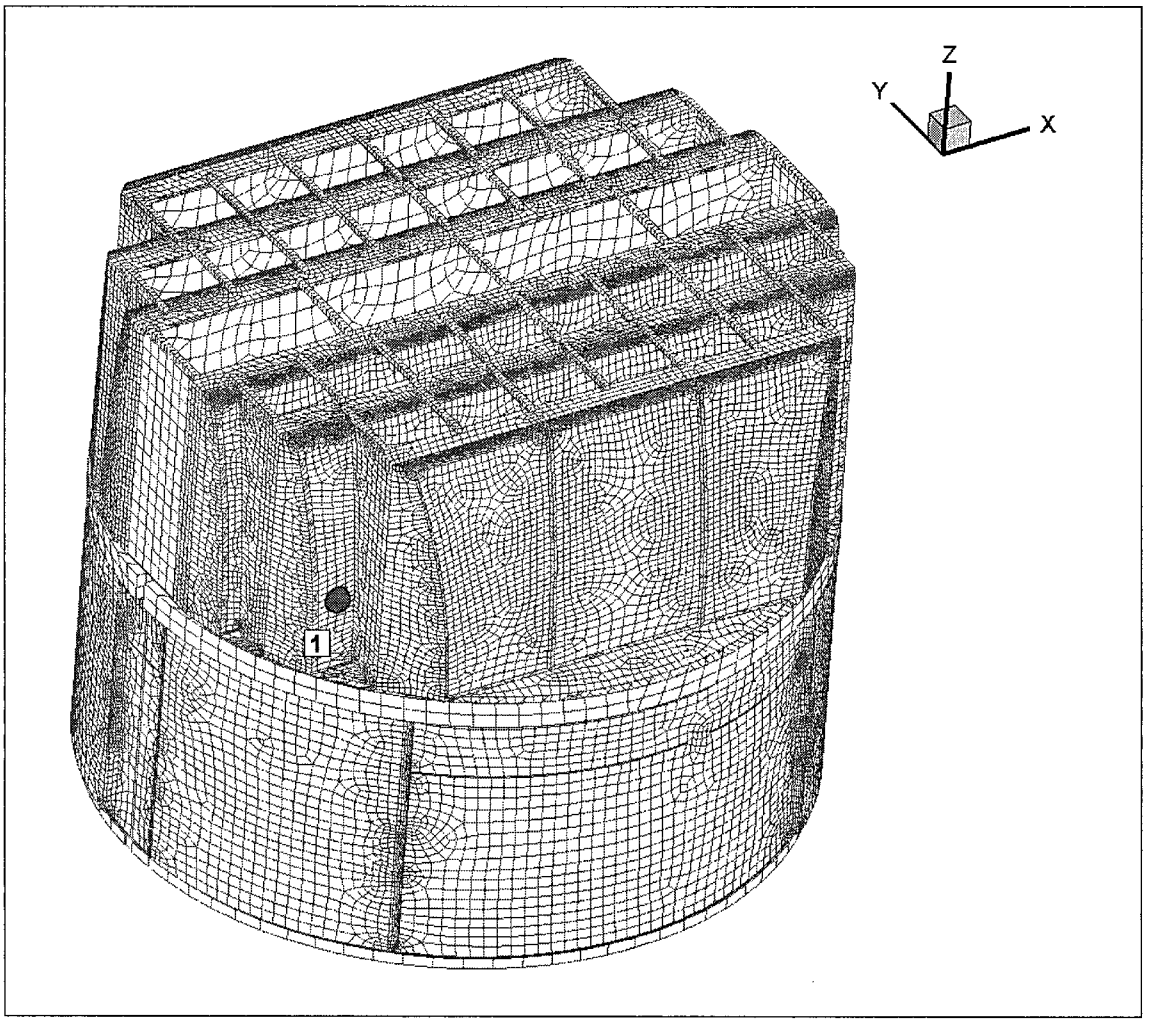

Rev 1

Figure 22c. Locations of minimum alternating stress ratios, SR-a, at non-welds for 115% CLTP operation with +10% frequency shift. Numbers refer to the enumerated locations for SR-a values at non-welds in Table 7d.

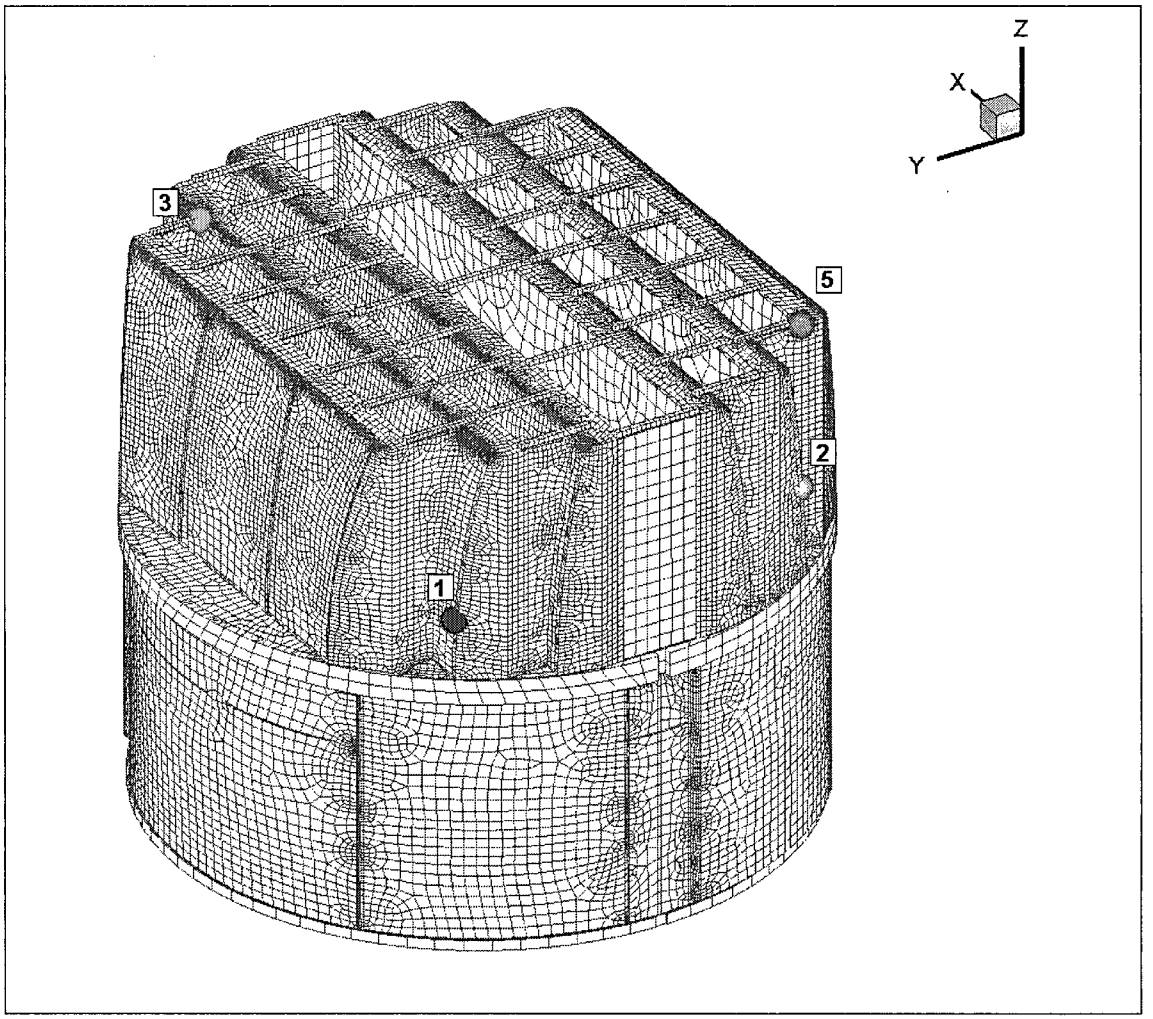

Rev 1

Figure 22d. Locations of minimum alternating stress ratios, SR-a, at welds for 115% CLTP operation with +10% frequency shift. Numbers refer to the enumerated locations for SR-a values at welds in Table 7d. First view showing enumerated locations 1-3 and 5.

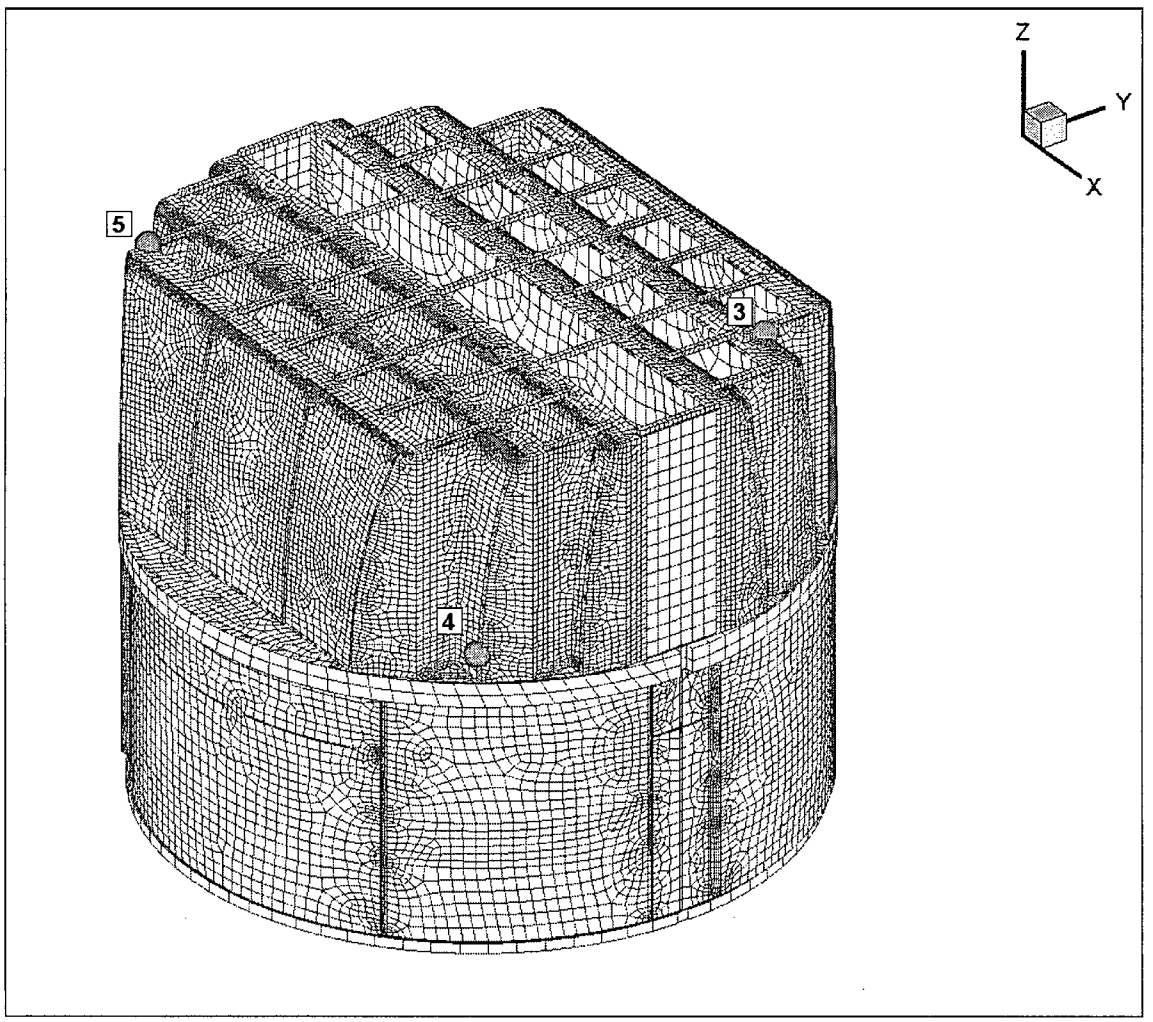

Rev 1

Figure 22e. Locations of minimum alternating stress ratios, SR-a, at welds for 115% CLTP operation with +10% frequency shift. Numbers refer to the enumerated locations for SR-a values at welds in Table 7d. Second view showing enumerated locations 3-5.

5.3 PSD of Stress Time History

One way to assess the sensitivity of the analysis to uncertainty in frequency domain is to compare the stress responses obtained for the same load history with different time steps, corresponding to the frequency shift. In this section therefore, the PSDs are presented for nodes identified as having the lowest stress ratios, according to Table 7b. Stresses are evaluated at the structural parts and shell element locations (top/bottom) with the highest stresses for a given node. The stress PSDs are estimated from FFTs of the last 1024 time steps with approximately 0.7 Hz resolution. As mentioned above the 80 Hz component was filtered from the results in the nominal, no frequency shift, case. The corresponding shifted component was filtered in all other cases. In the figures below, stress histories obtained with no frequency shift and at the frequency shift yielding the highest stress intensities, are compared. Rev 1

The selected nodes are:

Node 79487 - located on the junction of skirt and upper support ring (minimum SR-P). The associated PSDs are shown in Figure 23.

Node 88252 - located on the junction of inner hood and thin closure plate (second minimum SR-P). The associated PSDs are shown in Figure 24. Rev 1

Node 84521 - located on the junction of middle hood and reinforcement strip (minimum SR-a). The associated PSDs are shown in Figure 25.

Node 93818 - located on the junction of skirt and drain channel (second minimum SR-a). The associated PSDs are shown in Figure 26.

The 115% CLTP response at these locations has significant peaks approximately at 65 Hz and 119 Hz. When the frequencies are shifted these dominant peaks are shifted accordingly. The PSD value at the peak can change depending on how close it is to a structural resonant mode.

To ensure that there are no significant structural modes at frequency shifts other than considered, the behavior of stresses with respect to frequency shift was analyzed. In Figure 27 the stress intensities (peak, SR-P, or alternating, SR-a, as indicated) for the nodes having the minimum SR-P or SR-a values are plotted as a function of frequency shift. Overall, stresses vary smoothly and do not indicate the presence of interior maxima over the frequency shift range considered. In particular, the trend for node 84521, which yielded the smallest overall stress ratio, appears monotonic with steady increase towards the +10% frequency shift. Rev 1

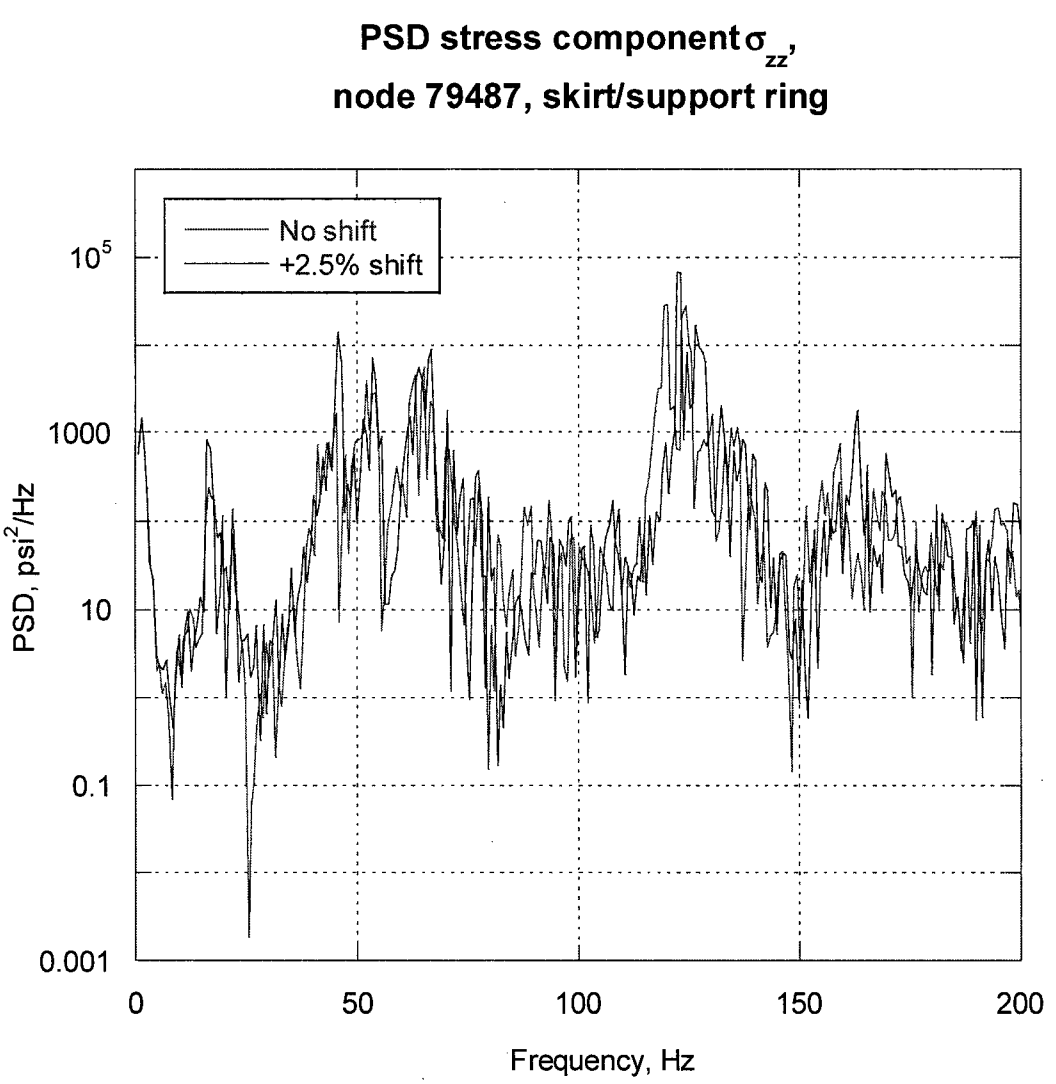

Figure 23. PSD of the σ_{ZZ} stress response at node 79487 for 115% CLTP operation. Red curve – no frequency shift; blue curve – frequency shift +2.5%.

Rev 1

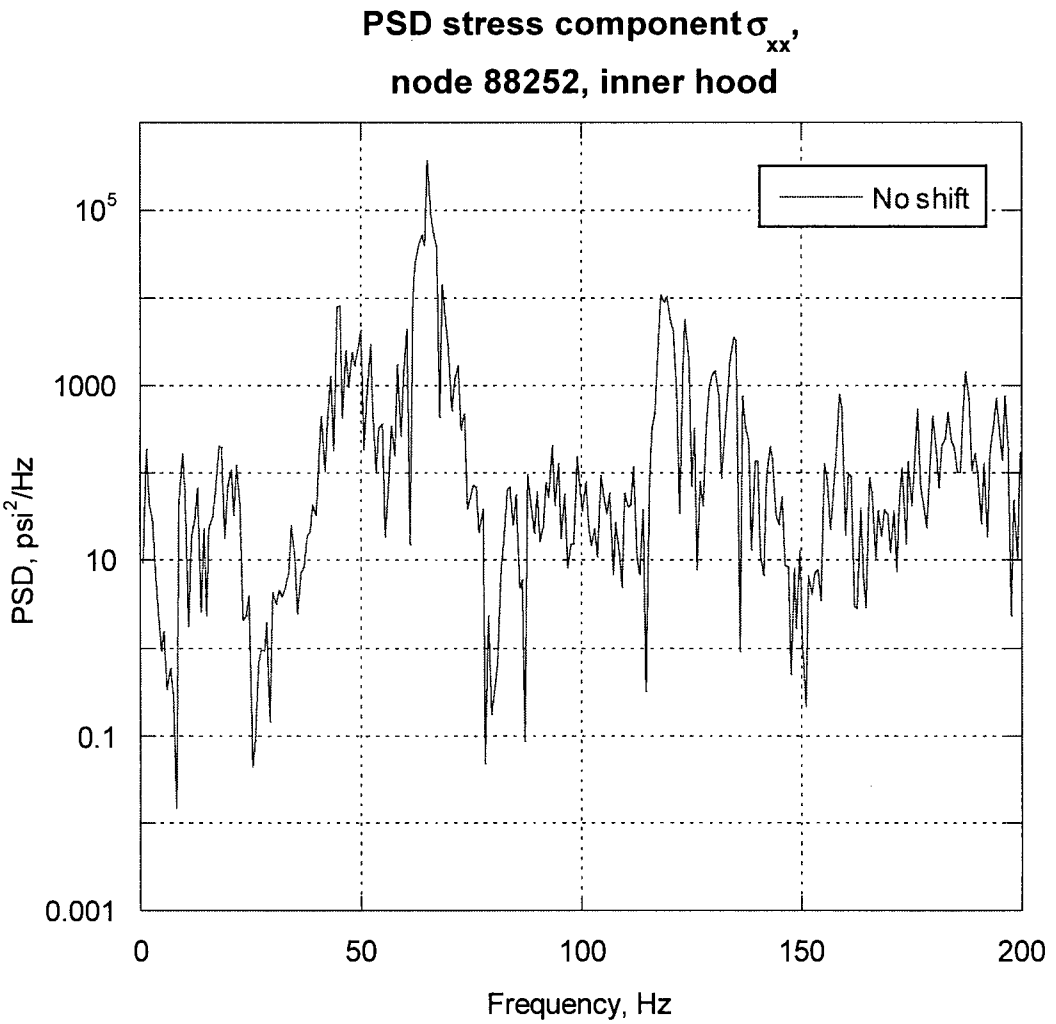

Figure 24. PSD of the σ_{xx} stress response at node 88252 for 115% CLTP operation.

Rev 1

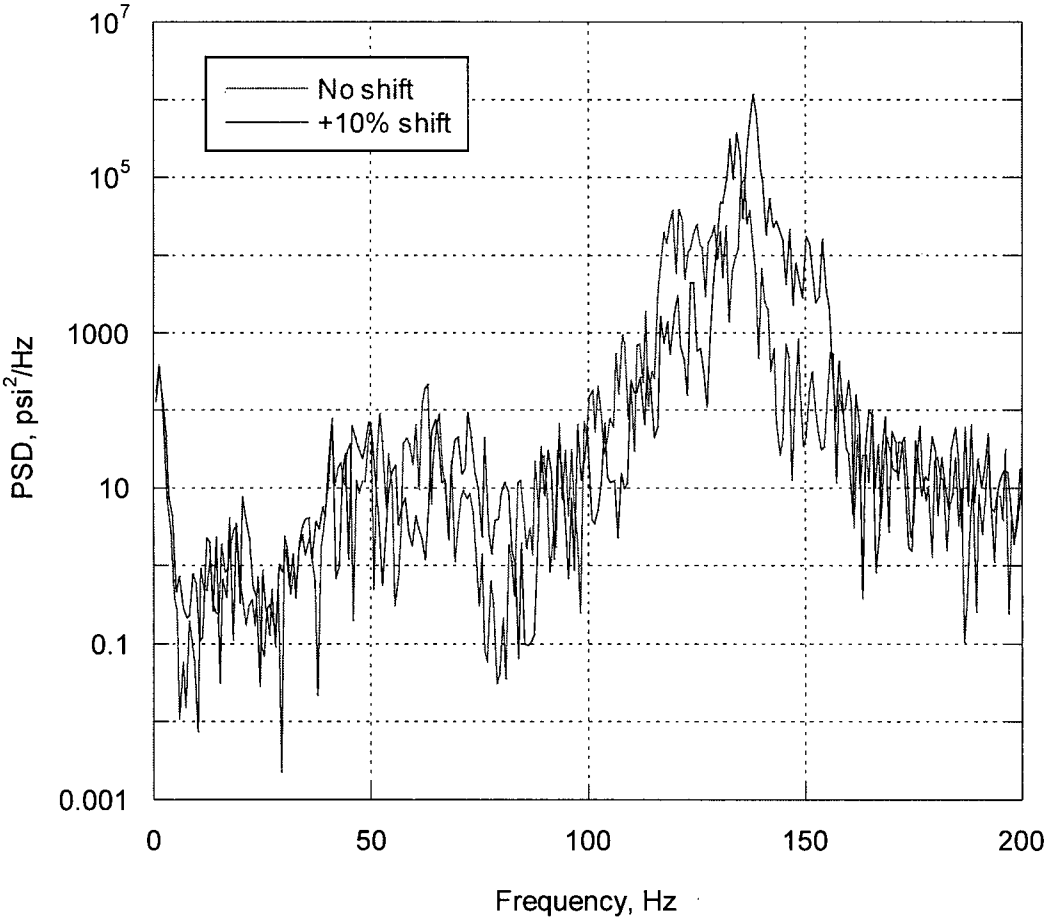

Rev 1

Figure 25. PSD of the σ_{XX} stress response at node 84521 for 115% CLTP operation. Red curve – no frequency shift; blue curve – frequency shift +10%.

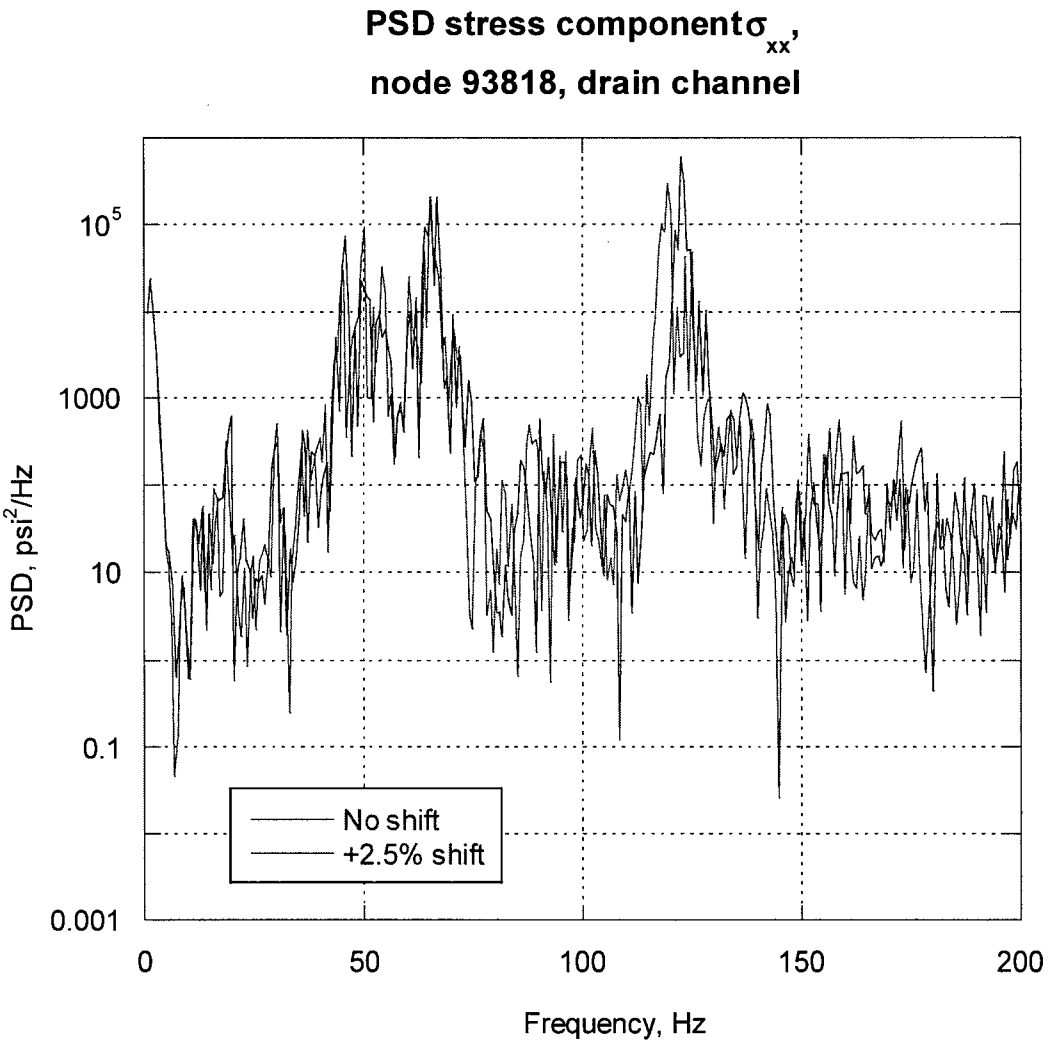

Rev 1

Figure 26. PSD of the σ_{yy} stress response at node 93818 for 115% CLTP operation. Red curve – no frequency shift; blue curve – frequency shift +2.5%.

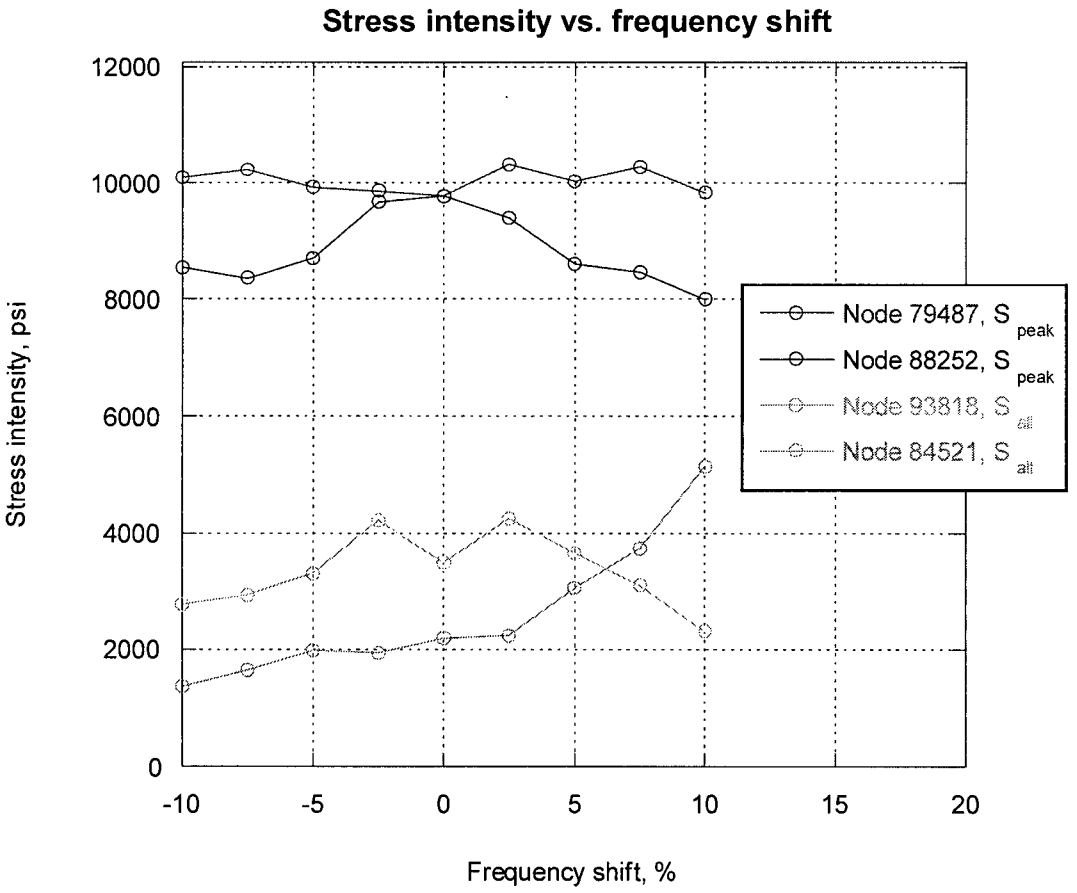

Figure 27. Stress intensity versus frequency shift for selected nodes.

Rev 1

6. Conclusions

Maximum points of stress and calculated / allowable stress ratios have been obtained for the Hope Creek Unit 1 steam dryer at 115% CLTP load conditions using 1/8th scale measurement data. The 115% CLTP loads obtained in a separate acoustic circuit model [1] were applied to a finite element model of the steam dryer consisting mainly of the ANSYS Shell 63 elements and brick continuum elements, for a duration of 2 seconds. The unsteady pressure loads contain a strong 80 Hz component which is not present in the plant [2]; therefore, this frequency component was removed during post-processing. The resulting stress histories were analyzed to obtain peak and alternating stresses at all nodes for comparison against allowable levels. These results are tabulated in Table 7 of this report. Rev 1

On the basis of these 1/8th scale loads, the dynamic analysis of the steam dryer shows that the steam flow and gravity loads produce the following minimum stress ratios:

Frequency Shift	Minimum Stress Ratio	
	Peak Stress, SR-P	Alternating Stress, SR-a
0% (nominal)	1.53	1.96
-10%	1.46	1.76
-7.5%	1.46	1.83
-5%	1.48	1.77
-2.5%	1.52	1.63
+2.5%	1.46	1.62
+5%	1.50	1.88
+7.5%	1.47	1.79
+10%	1.54	1.33
All shifts	1.46 – 1.54	1.33 – 1.96

Rev 1

It is important to note that the minimum stress ratio, SR-a=1.33, occurs only at one weld location and only at the +10% frequency shift. If the +10% frequency shift is excluded from the results then the alternating stress ratio jumps to SR-a=1.62 so that the minimum stress ratio is associated with a peak stress, SR-P=1.46. Relative to all of the other data, SR-a=1.33 value is clearly an outlier.

After removal of the 80 Hz signal, the dominant component in the load is approximately 120 Hz. Examination of the PSDs for the nodes exhibiting the minimum stress ratios, reveals that the main effect of frequency shifting is to excite the structural modes in the vicinity of the suitably shifted 120 Hz peak.

It is important to recognize that the results presented above <u>do not</u> account for any factors of conservatism and uncertainty in the applied loads. Rev 1

7. References

1. Continuum Dynamics, Inc. 2006. Estimating High Frequency Flow Induced Vibration in the Main Steam Lines at Hope Creek Unit 1: A Subscale Four Line Investigation of Standpipe Behavior (Rev. 1). C.D.I. Report No. 06-16.

2. Continuum Dynamics, Inc. 2006. High and Low Frequency Steam Dryer Loads by Acoustic Circuit Methodology (Draft). C.D.I. Technical Memorandum No. 06-25P.

3. Meijers, P. 1985. Refined Theory for Bending and Torsion of Perforated Plates. *Journal of Pressure Vessel Technology* 108: 423-429. Rev 2

4. Hechmer, J. L. and E. J. Kuhn, E. J. 1999. Fatigue Strength Reduction Factors for Welds Based on Nondestructive Examination. *Journal of Pressure Vessel Technology* 121: 6-10. Rev 1

5. Continuum Dynamics, Inc. 2006. Stress Analysis of the Hope Creek Unit 1 Steam Dryer at CLTP and EPU Conditions Using 1/8th Scale Model Pressure Measurement Data Rev. 0). C.D.I. Report No. 06-27.

6. Bednar, H. H. 1986. Pressure Vessel Design Handbook. Van Nostrand Reinhold: New York.

7. Faires, V. M. 1965. Design of Machine Elements. Macmillan: New York. Rev 1

8. Blodgett, O. W. 1963. Design of Weldments. James F. Lincoln Arc Welding Foundation: Cleveland.

9. Continuum Dynamics, Inc. 2005. Onset of High Frequency Flow Induced Vibration in the Main Steam Lines at Hope Creek Unit 1: A Subscale Investigation of Standpipe Behavior (Rev. 0). C.D.I. Report No. 05-31. Rev 2

Appendix A. Correction of Weld Fatigue Factor and Stress Ratio for Multi-Component Weld Between Inner Hood and Side Panel

In the original stress calculations no distinction between weld types or geometry was made. Instead, at every weld a weld factor of 1.8 was used to conservatively account for weld stress amplification as described in Section 4.4. This factor corresponds to the weakest fillet weld, with surface/visual nondestructive examination performed with progressive liquid penetrant testing. In [4] Table 1, p. 7, the recommended value for such welds and inspection methods is 1.7 for as-welded and 1.5 for machined or ground surface conditions with no distinction between weld types, thus, 1.8 is a conservative factor.

In previous computations [5], the welds along the junction between the inner hood and side panels were found to experience high stresses yielding stress ratios below unity. It was therefore decided to examine these welds in more detail in order to establish whether these predictions were overly conservative and, if so, to revise these estimates using more accurate, but still conservative, values. This Appendix reviews the approaches considered to update the weld factors for these welds.

As depicted in the figure below, the cross-section of the welds under consideration consists of three parts: the original groove weld connecting two plates under the approximately 120° angle (weld A), a fillet weld connecting the reinforcement strip to the plates (weld B) having a minimum throat of approximately 0.11", and an additional reinforcement fillet weld (weld C) with a throat of 0.19". Weld C was added based on PSE&G uncovering additional records from pre-commercial operations modifications. These were HC1-KTI-415-3 and HC1-KTI-415-5. Rev 1

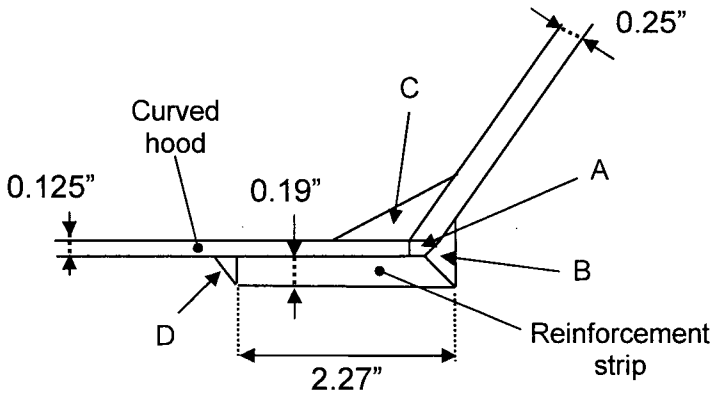

A direct analysis of the welded joint using continuum finite elements can, in principle, be performed. However, this is neither computationally attractive (high storage and CPU cost) nor likely to eliminate important sources of error. For example, the stress at a loaded re-entrant corner becomes theoretically infinite, so that numerical discretizations of such geometries do not necessarily converge with mesh resolution. Another source of error is incomplete knowledge regarding details of the weld geometry. Small features such as defects or cracks, filet radii, variations in throat thickness, etc. are difficult to obtain and can deviate significantly from the

ideal weld geometries listed in the specifications. Hence, even with the advent of advanced computational modeling methods, the use of weld factors and industrial experience in their application, remains a practically useful, accurate and cost-effective approach for assessing weld stresses. Here, three methods were applied to the particular weld geometry considered here and the most conservative approach retained in the stress ratio evaluations of this report. To describe each method, first note the following definitions:

Weld fatigue factor (WFF) –the ratio, Sa(nom)/ Sa(weld), where Sa(nom) is the allowable alternating stress for a weld-free component and Sa(weld) is the allowable alternating stress with welds included. This factor accounts for weld quality and inspection technique and corresponds to the factor (1.8) used in this report to adjust alternating stresses corresponding, nominally, to fillet welds.

Stress concentration factor (SCF) – the ratio, $\sigma_{max}/\sigma_{nom}$ where σ_{max} is the maximum stress at a weld or discontinuity and σ_{nom} is the nominal stress (bending+membrane) predicted by classical methods without accounting for structural discontinuities.

Joint efficiency (also referred to as 'reduction' or 'reliability factor') – engineering factor used to adjust allowable stress to compensate for variations in weld quality and approximations in stress computations.

Method 1. Stress Concentration Factor Ratio

The simplest (and most conservative) method is to ratio the stress concentration factors corresponding to a fillet weld (the default weld type assumed for analysis of the steam dryer) and a reinforced full-penetration groove-weld butt joint which most closely corresponds to the weld combination under consideration here. References [6], Table 10.6, p. 280, and [7], p. 515, provide the following stress concentration factors: Rev 1

- Fillet welds, $SCF_1 = 1.5$.
- Reinforced full-penetration groove-weld butt joint, $SCF_2 = 1.2$.

This means that the fatigue stress concentration factor can be conservatively reduced by $SCF_2/SCF_1=0.8$. Equivalently, the stress ratios obtained by assuming simple fillet welds can be increased by a factor of $f_{sw}=1.0/(0.8)=1.25$. This result implicitly assumes that: (i) The weld combination can be classified as full-penetration groove weld. (ii) The weld fatigue factor and SCF ratio in the same way. Both assumptions are reasonable from an engineering point of view.

Method 2. Ratio of Joint Efficiency Factors

The stress ratios can also be adjusted by considering the joint efficiencies for the different weld types. Reference [6], p. 279, provides the following joint efficiencies:

- For *fillet welds* the joint efficiency is 0.45 - 0.55, based on leg area, with the upper value corresponding to welds subjected to liquid penetrant examination. The value 0.55 was used in the original calculations for the reduction in peak stress allowables at welds.

- For *groove welds* the recommended joint efficiency is 0.8 – 1.0.

A conservative estimate of the adjustment to the weld fatigue factor is obtained by using the upper estimate of the joint efficiency value for the fillet weld (0.55) and the lower estimate for groove welds (0.8) resulting in the ratio, f_{SW}=0.8/0.55=1.45. Again, this estimate rests upon the following reasonable assumptions: (i) The weld combination can be classified as a full-penetration groove weld. (ii) Weld fatigue factor ratios are inversely proportional to joint efficiency ratios.

Method 3. Weld Critical Area Adjustment

This approach assumes that the weld fatigue factor ratios scale inversely with critical resisting areas. The representative thickness of each weld is:

- Weld A: smallest thickness of the connected plates, i.e. 0.125".
- Weld B: minimum throat, or approximately 0.11".
- Weld C: minimum throat, or approximately 0.19".

Then, direct calculations of the increase in critical resisting area [8], Ch. 6.3, [6], p. 263, produce the following:

Critical resisting area of assumed (fillet) weld A+B: (0.125 + 0.11) = 0.235"
Critical resisting area of actual weld A+B+C: (0.125 + 0.11+0.19) = 0.425"

Implying that the stress ratios for these welds can be increased by the factor, f_{SW}=0.425/0.235=1.81.

Summary & Application

The increase in stress ratio indicated by the three methods are:

Method 1: f_{SW}=1.25
Method 2: f_{SW}=1.45
Method 3: f_{SW}=1.81

Rev 1

The most conservative prediction, f_{SW}=1.25, is used to modify the stress ratios for the welds joining the inner and middle curved hoods with the side panels. The stress ratios on the corresponding outer hood welds were not modified because the curved hood is thicker (½ inch) and stress ratios were well within margins on these welds.

Finally, the stress ratios were only modified on that portion of the weld that is less than 60" above the cover plates (HC1-KTI-415-3 and HC1-KTI-415-5). The reason is that because of the small interior spatial confines near the top of the hoods, it was not possible to reinforce the welds along the entire curved hood/end-plate junction. Therefore stress ratios are readjusted only for those FE nodes that located on the weld and below the 60" height.

Localization of Weld Effects

From a computational standpoint, the effects of weld alterations are completely localized. Thus increasing a weld thickness or reclassifying a weld as, say, a groove weld rather than a fillet weld, does not redistribute stresses on other portions of the structure. This is because the finite element computation treats welds as any other connection between elements by equating displacements and rotations between adjacent elements. Welds are accounted for after the finite element calculation has completed during post-processing using weld factors. These weld-based stress adjustments are entirely local and are applied on a per-node basis. From a physical perspective, this representation is consistent with the St. Venant's principle underlying beam and shell theories which states that stress-predictions are accurate at locations that are 1-2 thicknesses away from structural discontinuities (e.g., welded junctions, mounts or restraints). To accurately predict stresses at structural discontinuities it is necessary to model the detailed geometry and employ a full 3D stress description, or to adopt a correction factor such as the weld fatigue factors used here. Note that for the welded reinforcement strip considered here, the effective increase in thickness due to the strip itself will affect stresses at other locations and modify the local mode shapes. These effects will be reflected in the finite element calculation since it accounts for the additional thickness of the modified strip and corresponding increase in structural stiffness.

Rev 1

Appendix B. EPU Conditions in the Main Steam Lines at Hope Creek Unit 1: Additional Subscale Four Line Tests

As part of the engineering effort in support of power uprate at Hope Creek Unit 1 (HC1), Continuum Dynamics, Inc. (C.D.I.) undertook a subscale examination of the standpipe/valve geometry on two of the four main steam lines, in an effort to validate the frequency onset at which flow induced vibration, resulting from standpipe/valve flow resonance, could potentially impact steam dryer loads. In this study [9] C.D.I. constructed a nominal one-fifth scale model of a single main steam line (prototypical of main steam lines A and D) at HC1, from the reactor vessel main steam line nozzle to beyond the standpipes, using seamless steel pipe with full penetration welds. This rig was used to test the as-built configuration of standpipes and Target Rock valves, and did not predict SRV standpipe resonance at Current Licensed Thermal Power (CLTP), as confirmed by in-plant data. These data suggested that EPU conditions would be past excitation onset, and that this loading should receive further evaluation, and possible mitigation.

As part of a subsequent effort [1], C.D.I. constructed a nominal one-eighth scale model of the complete steam delivery system at HC1, from the steam dome to the turbine, with PVC pipe, with the objective of estimating the steam dryer loads at higher power. Simulations were conducted for a wide range of main steam line flow velocities, from below CLTP conditions to well above Extended Power Uprate (EPU) conditions. The results of this testing showed no SRV standpipe resonance at 0.8 x CLTP but SRV resonance at 0.9 x CLTP, with increasing values for CLTP and 1.15 x CLTP. Rev 2

In the present effort, additional tests were run in the one-eighth scale test facility, in an effort to compare with the previous one-fifth scale test results and refine the flow speed at CLTP conditions. These results confirmed that flow conditions run during the one-eighth scale tests, as reported in [1], were higher by 14% at the SRV standpipe. This high reading resulted from non-prototypical frictional losses in the one-eighth scale rig. The additional testing established new CLTP and EPU flow rates in the one-eighth scale test facility, from which steam dryer loads may be obtained. The added testing demonstrated the following corrections:

Power Level Based on [1]	% CLTP	86%	100%	115%
Power Level Revised	% Revised CLTP	100%	116%	133%

With these corrections, the one-eighth scale test facility no longer includes SRV resonance at CLTP, which agrees with plant data and the one-fifth scale tests. But, it retains the prediction from the one-fifth scale model that resonance starts immediately above CLTP.

The previous loads for CLTP conditions in [1] bound the proposed power uprate to 115% of CLTP conditions. Consequently, the structural analysis labeled as CLTP in [5] can be used as the structural analysis for EPU conditions. Further, when comparing the previously assumed CLTP loads against the revised CLTP loads, peak subscale differential pressure (corrected to full scale) are reduced by 32%.

Hope Creek Generating Station
Facility Operating License NPF-57
Docket No. 50-354

Supplement to Request for License Amendment
Extended Power Uprate

CDI Technical Memorandum 06-23NP
Comparison of the Hope Creek and Quad Cities Steam Dryer
Loads at EPU Conditions
Revision 1
January 2007